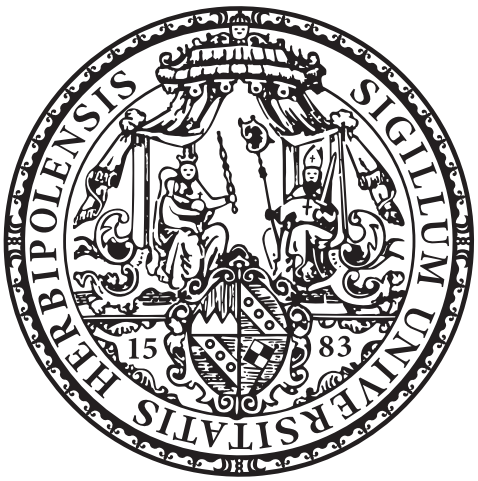

Investigation of dynamic processes of prototypical class A GPCRs by single-molecule microscopy

Untersuchung von dynamischen Prozessen von prototypischen Klasse A GPCR's durch Einzelmolekülmikroskopie

Doctoral thesis for a doctoral degree

at the Graduate School of Life Sciences,

Julius-Maximilians-Universität Würzburg,
Section Biomedicine

submitted by

Kerstin Seier

from

Luckenwalde

Würzburg 2019

Submitted on: .....

Office stamp

Members of the *Promotionskomitee*:

Chairperson:	Prof. Georg Gasteiger
Primary Supervisor:	Prof. Davide Calebiro
Supervisor (Second):	Prof. Markus Sauer
Supervisor (Third):	Prof. Kristina Lorenz

Date of Public Defence: .....

Date of Receipt of Certificates: .....

Summary

In this work, two projects were pursued.

In the first project, I investigated two different subtypes of opioid receptors, which play a key role as target for analgesia. A set of subtype specific fluorescent ligands for μ opioid receptor (MOR) and δ opioid receptor (DOR) was characterised and used to gain insights into the diffusion behaviour of those receptors. It was shown that the novel ligands hold photophysical and pharmacological properties making them suitable for single-molecule microscopy. Applying them to wild-type receptors expressed in living cells revealed that both sub-types possess a heterogeneous diffusion behaviour. Furthermore, the fluorescent ligands for the MOR were used to investigate homodomerisation, a highly debated topic. The results reveal that only $\approx 5\,\%$ of the receptors are present as homodimers, and thus the majority is monomeric.

G-protein coupled receptors (GPCRs) play a major role as drug targets. Accordingly, understanding the activation process is very important. For a long time GPCRs have been believed to be either active or inactive. In recent years several studies have shown, that the reality is more complex, involving more substates. [1, 2, 3, 4] In this work the α_{2A}AR was chosen to investigate the activation process on a single-molecule level, thus being able to distinguish also rare or short-lived events that are hidden in ensemble measurements. With this aim, the receptor was labelled intracellular with two fluorophores using supported membranes. Thus it was possible to acquire movies showing qualitatively smFRET events. Unfortunately, the functionality of the used construct could not be demonstrated. To recover the functionality the CLIP-tag in the third intracellular loop was replaced successfully with an amber codon. This stop codon was used to insert an unnatural amino acid. Five different mutants were created and tested and the most promising candidate could be identified. First ensemble FRET measurements indicated that the functionality might be recovered but further improvements would be needed.

Overall, I could show that single-molecule microscopy is a versatile tool to investigate the behaviour of typical class A GPCRs. I was able to show that MOR are mostly monomeric under physiological expression levels. Furthermore, I could establish intracellular labelling with supported membranes and acquire qualitative smFRET events.

Zusammenfassung

In dieser Arbeit wurden zwei Projekte verfolgt.

Im ersten Projekt wurden zwei Subtypen der Opioidrezeptoren untersucht, die eine wichtige Rolle für die Wirksamkeit von Analgetika spielen. Ein Set von subtypspezifischen fluoreszierenden Liganden für den MOR und den DOR wurde charakterisiert und eingesetzt, um Einblicke in das Diffuionsverhalten der Rezeptoren zu gewinnen. Es konnte gezeigt werden, dass die neuartigen Liganden sowohl photophysikalische als auch pharmakologische Eigenschaften besitzen, die sie für die Einzelmolekülmikroskopie interessant machen. Versuche mit Opioidrezeptoren, die in lebenden Zellen exprimiert werden, zeigten, dass beide Subtypen heterogenes Diffuionsverhalten aufweisen. Des Weiteren wurden die fluoreszierenden Liganden für den MOR genutzt um Homodimerisierung zu untersuchen, da dies ein kontrovers diskutiertes Thema ist. Die Ergebnisse zeigen, dass lediglich $\approx 5\,\%$ der Rezeptoren als Homodimere vorliegen und der Großteil monomerisch ist.

GPCRs sind besonderem Interesse, weil sie Angriffspunkt vieler Medikamente sind. Deshalb ist es wichtig ihren Aktivierungsmechanismus besser zu verstehen. Lange Zeit wurde angenommen, dass GPCRs entweder aktiv oder inaktiv sind. Neuere Studien zeigten jedoch, dass die Realität komplexer ist und der Prozess Zwischenschritte involviert. [1, 2, 3, 4] In dieser Arbeit wurde der α_{2A} Adrenorezeptor als prototypischer Klasse A GPCR gewählt, um den Aktivierungsprozess auf Einzelmoleküllevel zu untersuchen. Durch die Betrachtung einzelner Rezeptoren ist es möglich auch seltene oder sehr kurzlebige Ereignisse zu unterscheiden, die in Kollektivmessungen untergehen. Um dies zu erreichen wurde der Rezeptor erfolgreich intrazellulär mit zwei Fluorophoren markiert. Dies gelang durch die Herstellung von “supported membranes”, also Zellmembranen die auf einem Objektträger fixiert wurden. Dadurch war es möglich Videos aufzunehmen, die Einzelmolekül-FRET-Ereignisse zeigen. Jedoch gelang es nicht zu zeigen, dass der

Rezeptor als Ganzes noch funktional war. Um einen funktionalen Rezeptor zu erhalten, wurde das CLIP-Tag in der dritten intrazellulären Schleife erfolgreich durch ein Stopcodon ersetzt, welches für eine nicht kanonische Aminosäure kodierte. Fünf verschiedene Mutanten wurden kloniert und getestet, wobei der vielversprechendste Mutant identifiziert werden konnte. Erste FRET-Kollektivmessungen deuten darauf hin, dass dieser Mutant funktional sein könnte. Jedoch sind weitere Verbesserungen nötig.

Insgesamt konnte ich zeigen, dass Einzelmolekülmikroskopie vielseitige Möglichkeiten bietet um das Verhalten von GPCRs zu untersuchen. Ich konnte nachweisen, dass MOR unter physiologischen Bedingungen hauptsächlich als Monomere vorliegen. Des Weiteren konnte ich Dank supported membranes die Markierung durch Farbstoffe im Intrazellularbereich etablieren und qualitative smFRET Ereignisse aufnehmen.

Contents

List of abbreviations

AA amino acid

AGT O^6-alkylguanine-DNA alkyltransferase

amp ampicillin

AMPAR α-amino-3-hydroxy-5-methyl-4-isoxazolepropionic acid receptor

BC O^2-benzylcytosin

BES N,N-Bis(2-hydroxyethyl)-2-aminoethanesulfonic acid

BG O^6-benzylguanine

BRET bioluminscence resonance energy transfer

BSA Bovine Serum Albumin

CACO 14β-(p-nitro-cinnamoylamino)-7,8-dihydrocodeinone

cAMP cyclic adenosine monophosphate

CCP clathrin coated pit

CFP cyan fluorescent protein

CG coarse-grained

CHO chinese hamster ovary

CMOS complementary metal-oxide-semiconductor

DAMGO [D-Ala^2, *N*-MePhe^4, Gly-ol]-enkephalin

DNA deoxyribonucleic acid

DOR δ opioid receptor

EDTA Ethylenediaminetetraacetic acid

EM electron microscopy

EMCCD electron-multiplying charge-coupled device

Epac exchange proteins activated by cAMP

FBS fetal bovine serum

FCS fluorescence correlation spectroscopy

FIJI Fiji is just ImageJ

FP fluorescent protein

FRAP fluorescence recovery after photobleaching

FRET fluorescence resonance energy transfer

FWHM full-width at half maximum

GABA$_B$ γ-aminobutyric acid type B

GDP guanosine diphosphate

GEF guanine nucleotide exchange factor

GFP green fluorescent protein

GPCR G-protein coupled receptor

GTP guanosine triphosphate

HA human influenza hemagglutinin

HEK human embryonic kidney

HEPES 4-(2-Hydroxyethyl)piperazine-1-ethanesulfonic acid

ICL intracellular loop

kan kanamycin

KOR κ opioid receptor

LB Luria Bertani

LBD ligand binding domain

MD molecular dynamics

mGluR metabotropic glutamate receptor

MHT Multiple-hypothesis tracking

MOR μ opioid receptor

MSD mean squared displacement

NE norepinephrin

NOR nociception receptor

NTS1 neurotensin receptor 1

PBS phosphate-buffered saline

PCR polymerase chain reaction

PLL Poly-L-Lysine

POI protein of interest

PSF point spread function

PTHR parathyroid hormone receptor

ROI region of interest

RT room temperature

SDS Sodium dodecyl sulfate

SEM standard error of the mean

SiR silicon-rhodamine

SPAAC strain-promoted alkyne-azide cycloaddition

SPIEDAC strain-promoted inverse electron-demand Diels-Alder cycloaddition

SPT single-particle tracking

STORM stochastic optical reconstruction microscopy

smFRET single-molecule fluorescence resonance energy transfer

TAMRA tetramethylrhodamine

TAMSD time-averaged mean squared displacement

TCO trans-Cyclooctene

Temed N,N,N',N'-Tetramethyl ethylenediamine

TIRF total internal reflection fluorescence

TM transmembrane

TM6 transmembrane segment 6

TM7 transmembrane segment 7

Tris Tris(hydroxymethyl)aminomethane

tRNA transfer ribonucleic acid

unAA unnatural amino acid

VDCC Voltage-gated dependent calcium channel

YFP yellow fluorescent protein

List of Figures

1. Introduction

1.1. GPCR's and their physiological role

GPCRs constitute the largest super family of membrane receptor and are encoded by over 800 genes in the human genome. They are implicated in the sensation of light, taste and smell and they are the receptors for several hormones and neurotransmitters. Furthermore, they play a crucial role in many physiological processes, like pain transmission, and are implicated in several diseases like Alzheimer and schizophrenia amongst others. For this reason, 34 % of all drugs on the market act on GPCRs. These comprise 475 drugs acting on just 108 of the non-olfactory GPCRs. [5] This implies there is an ample market and large need for more research on GPCRs to improve existing drugs and to find and develop new compounds as well.
All GPCRs share major common structural features: they comprise seven transmembrane helices linked by three extracellular loops and three intracellular loops (ICLs). The N-terminus is located extracellularly, whereas the C-terminus is in the cytosol, both differing in length depending on the receptor. Recently, more and more structures were solved especially using x-ray crystallography, and even more recently cryo electron microscopy (EM). [6, 7, 8] The structure is closely linked to the receptor function. Thus, more insights in the structure can provide a better understanding of the functionality, especially with structures of the same receptor in different conformation states. The structure of a prototypical class A GPCR is shown in figure 1.1.

GPCRs are grouped into 6 different classes based on similarities among their structures. The first and biggest class, class A, is formed by rhodopsin-like receptors (over 700 members). The secretin family, class B, contains 15 members whereas the adhesion family has 24 members. Class C, the glutamate family, is formed by 15 members. The last class present in vertebrates is class F, containing frizzled and taste receptors (24 members). [10, 11] Class D and E do not occur in vertebrates.

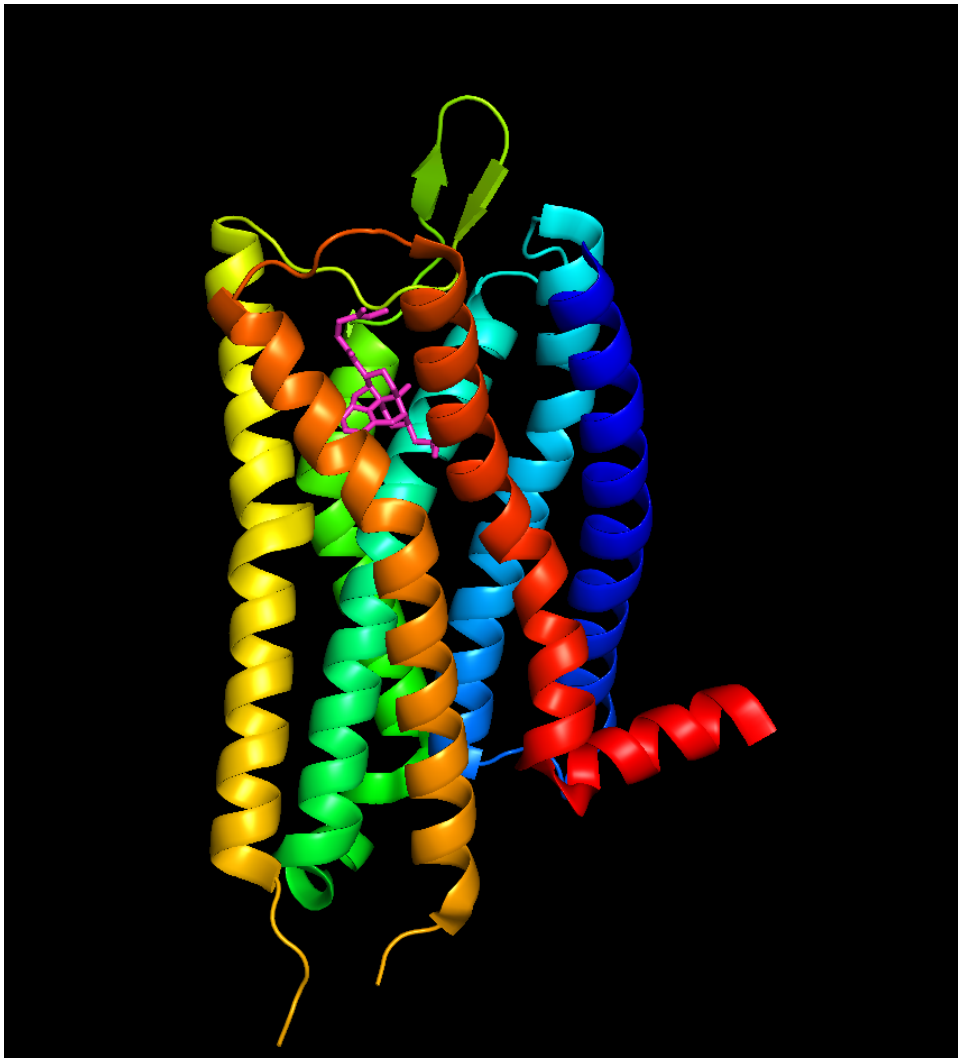

Figure 1.1.: Molecular structure of the μ opioid receptor. Shown is the molecular structure of the μ opioid receptor bound to an antagonist (pink) as representative for the general structure of GPCRs. The seven helices spanning the membrane are characteristic for GPCRs. Based on the crystal structure from Manglik et al. [9] (PDB: 4DKL)

1.2. The activation mechanism of GPCRs

For a long time, it was thought that GPCRs essentially exist in two distinct states: active and inactive. [12, 13] In recent years, however, more and more evidence accumulated that the nature of GPCRs is more complex. It is hypothesised that GPCRs have several conformational substates between which they are switching back and forth. [1, 2, 3, 4] Upon ligand binding to the orthosteric site, which is extracellular, a conformational re-arrangement is triggered. Depending on the receptor and the ligand, the first conformational changes are rather slight, e.g. a small turn of a side chain or a twist of a transmembrane helix. Those re-arrangements at the extracellular side cause movements within the receptor, propagating to its centre and further to the intracellular side, where the half of transmembrane segment 6 (TM6) facing the intracellular side, is moving outwards by about 14 Å. [6] A smaller movement in form of a rotation is observed for the intracellular end of transmembrane segment 7 (TM7), involving the conserved NPxxY motif. [14] This re-arrangement leads to the formation of a binding pocket for the G protein is. The binding of the G protein stabilises the active conformation of the receptor by lowering the free energy of this state in comparison to the inactive state. [14, 15, 16]

The receptor can freely switch between different substates ranging from fully inactive to inactive through partially active to fully activated, or even more substates. [4, 17, 14] This can explain why a basal activity can be observed for several receptors. In absence of a ligand and nucleotides the inactive states are more likely to be found as their free energy is lower than that of active conformations (as shown in figure 1.2). [14, 4] Ligands have the ability to modulate the free energy levels of the different substates through chemical interactions and, thereby, change the probabilities of finding the receptor in the different substates. [14, 4, 18] For example, an agonist lowers the free energy of the activated state in comparison to the inactive conformations. An inverse agonist on the other hand would lower the free energy of the inactive state further and/or increase the one of the activated states and in consequence decrease the probability of activated receptors. [19]

Lamichhane et al. ([17]) used single-molecule fluorescence imaging on the β_2AR embedded in phospholipid nanodiscs. [17] They showed that the receptor spontaneously switches between two distinct conformational states, which they assigned to an inactive

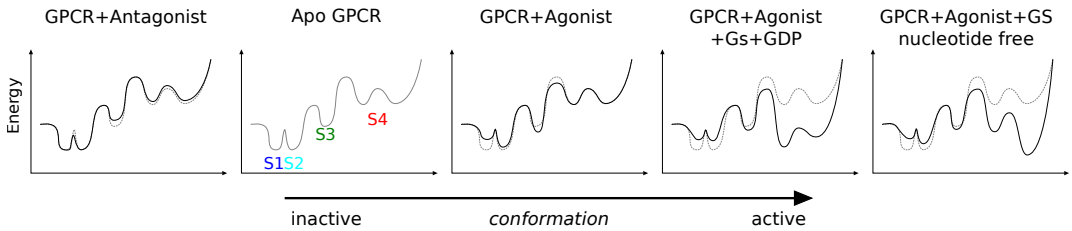

Figure 1.2.: Energy landscape of different substates. A schematic representation of the effects of different ligands and nucleotides on the free energy of the receptor and how this leads to different probabilities to find the receptor in certain conformations. Adapted from [14]

and active-like receptor conformation. Under basal condition, the inactive form was more likely to be present whereas after treatment with a full agonist the receptor favoured the active conformation. In line with this, an inverse agonist changed the probability in favour of the inactive conformation. [17]

The activation process of GPCRs can be monitored with different biophysical methods and/or biochemical essays. The most direct way is to look at the conformational changes at the intracellular side of the receptor itself, while most of the assays focus on downstream changes and signals following the activation (e.g. radioactive GTPγS binding assay, calcium assay [12, 20]). With direct approaches, it is not only possible to investigate the amplitude of the conformational changes necessary for the activation, but also to determine the activation speed. The fastest known activated GPCR is rhodopsin, which is activated within milliseconds. [21] For this prototypical GPCR the conformational changes are triggered by the absorption of a photon which causes an isomerisation of the retinal from 11-cis to all-trans. [22] In comparison to rhodopsin, Vilardaga et al. ([23]) investigated two GPCRs that are activated by binding of ligands: the α_{2A}AR, a class A GPCR, and the parathyroid hormone receptor (PTHR), belonging to class B. [23] In this study, cyan fluorescent protein (CFP) and yellow fluorescent protein (YFP) were cloned into the third ICL and the C-terminus, respectively, using the fluorophores as FRET pair. After stimulation with the respective ligand, an activation time constant of $\sim$ 40 ms was observed for the α_{2A} adrenergic receptor (α_{2A}AR) and $\sim 1\,s$ for the PTHR. [23] Further studies by different groups showed that various class A GPCRs have an activation speed in the range of $30 - 50$ ms. [24, 25, 26]

The ligand induced conformational changes enable the receptor to function as a guanine nucleotide exchange factor (GEF) for the G protein. More precisely, the receptor stimulates the exchange of guanosine diphosphate (GDP) for guanosine triphosphate (GTP) on the G_α subunit. This exchange triggers the dissociation of the G protein complex from the active receptor and the dissociation of the G_α subunit from the $G_{\beta\gamma}$ dimer. The G_α and $G_{\beta\gamma}$ subunits then act as effectors for intracellular second messenger cascades and therefore continue the signal transmission from an extracellular stimulus to an intracellular signal. The bound GTP is hydrolysed to GDP. This hydrolysation inactivates the G_α subunit, causing it to re-associate again with the $G_{\beta\gamma}$ dimer. The inactive trimeric G protein can in turn bind to a receptor awaiting a new activation round. A scheme of the activation cycle is shown in figure 1.3. [27, 28, 29, 13]

Still a highly debated question in the field of GPCR research is whether the G protein just binds when a ligand has bound to the receptor, or if the receptor and the G protein can pre-couple without ligand binding. The latter is also known as the 'ternary complex model'. [30, 31, 32, 33] The ternary complex model is in good agreement with the idea that the free receptor can switch between an active and inactive conformation. Only if the receptor is present in the active conformation, i.e. the TM6 is moved outwards, pre-coupling can occur and thus might lead to basal activity of some receptors.

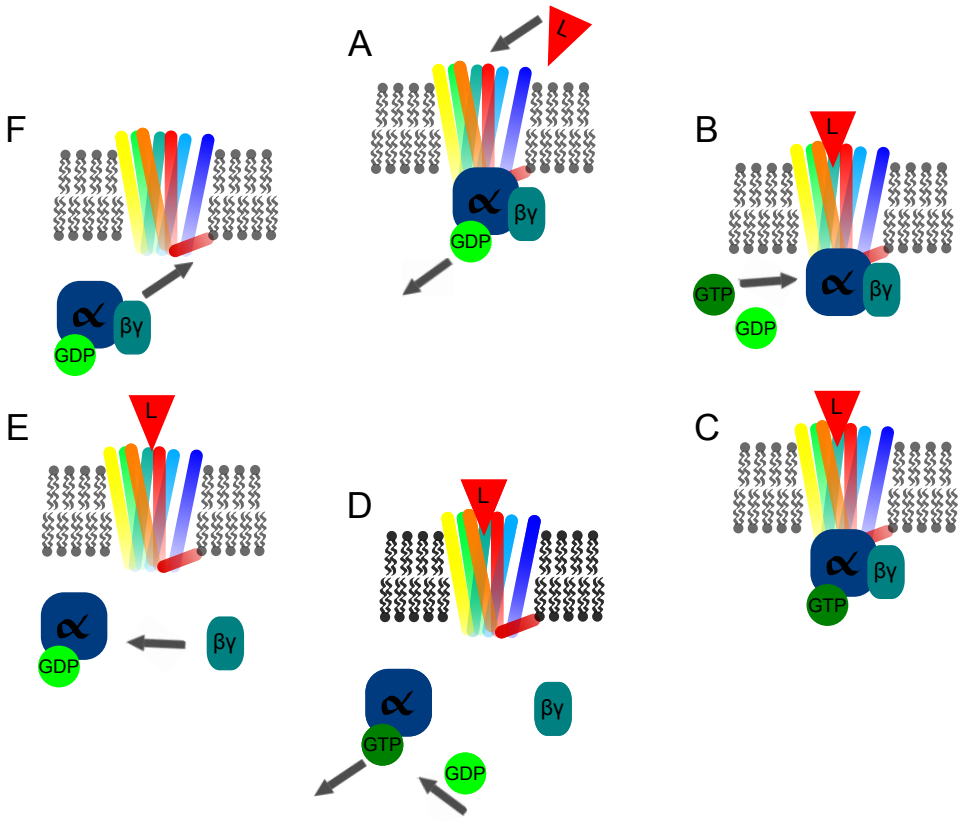

Figure 1.3.: Scheme of the GPCR activation cycle. Depicted is the activation cycle of a prototypical GPCR. A) Unbound GPCR pre-coupled to the heterotrimeric G-protein. The TM6 (orange helix) is inside. In B), the ligand (red triangle) is bound and the TM6 is moving outward. GDP is released and thus the nucleotide free high affinity ternary complex is present. C) The high amount of available GTP leads to the binding the G_α subunit and sub-sequentially to the dissociation of the G-protein itself (D). The activated G_α subunit and the $G_{\beta\gamma}$ can now interact with further effectors. E) the GTP will be hydrolysed to GDP, giving way to the re-association of the $G_{\beta\gamma}$ with the G_α subunit (F).

1.3. GPCR dimerisation

GPCRs interact with a multitude of other molecules like ligands, G-proteins, β-arrestins and other effectors. An abundance of studies has shown that GPCRs can also interact with each other and form dimers or even higher order oligomers. [34, 35, 36, 37, 38] For class C GPCRs, like the γ-aminobutyric acid type B ($GABA_B$), it was even shown that they can be obligatory heterodimers. [39, 40, 41] Class A GPCRs seem to be more heterogeneous as there are controversial findings regarding their prevalence as monomer or dimers. [37, 42, 38, 36, 43] The differences between studies, even for the same receptor, could be explained by the variety of methods that are applied for the investigation of dimerisation ranging from co-immunoprecipitation to FRET and bioluminscence resonance energy transfer (BRET) assays, to single-molecule fluorescence microscopy techniques and fluorescence correlation spectroscopy (FCS), or even computational simulations. [44, 45, 46, 43, 47] In addition, the studies often differ in the system they use, like transiently transfected cells (with different expression levels), purified receptors or native tissues. [48, 49, 50]

The investigation of dimerisation could give more insights into the underlying mechanism of how one ligand can trigger different signal responses. It has already been shown that dimerisation influences the pharmacological properties of receptors and ligands for example for the opioid receptors. [51, 49, 52] The heterodimerisation of MOR and DOR has been suggested to lead to a faster internalisation of both receptors, whereas the MOR does not internalise upon morphin stimulation. [53] Furthermore, the stoichiometry of monomers and dimers can be influenced by the application of different ligands. Tabor et al. could show an increase in dimer formation upon agonist binding for the dopamine receptor, while the application of an antagonist did not differ the fraction of dimers in comparison to ligand free receptors. [37] A better understanding on how the receptors interact, and how the downstream signalling is affected could help to develop drugs that act more specifically and may reduce side effects.

1.4. Opioid receptors

The group of opioid receptors consists of four members: the MOR and κ opioid receptor (KOR) were the first ones to be found and named after their prototypical ligands morphin and ketocyclazocine, respectively. [54] The DOR and nociception receptor (NOR) were discovered later. [54] All four belong to the rhodopsin-like class A of GPCRs. Overall the MOR, DOR and KOR show more homology towards each other than to the NOR. [55, 56] This is reflected in the ligand affinity of the NOR, which appears to be very limited for morphine-like compounds and opioid peptides. [57] On the other hand, the classical group of opioid receptors (MOR, DOR and KOR) show low affinities for the endogenous ligand of NOR, nociceptin.
Opioid receptors are widely expressed in the brain, spinal cord, digestive tract and in peripheral sensory neurons. They are widely known for their analgesic effect and therefore play a major role as a drug target for pain killers. Furthermore, opioid receptors are well known for their recreational effects. The opium poppy, *papaver somniferum*, has been used for thousands of years as agricultural crop. The first written report of the production of pharmaceutical compounds out of the seeds dates back to 4000 b.c.. [58] In modern medicine, opioids still play a big role with drugs on the market like Oxycodon, Codeine and Tilidin to name just a few. On the illegal drug market, Heroin proves to be a big problem. [59] Since the 90's, North America is struggling with the so termed 'opioid crisis', which causes more and more deaths by overdose. [60] Often addictions start with a prescription of opioids for medical reasons, leading to craving of more opioids as a side effect. To prevent addictions and overdoses safer and better opioid drugs are needed. [61, 62, 60] Hence, it is no surprise that opioid receptors and especially the MOR are subject of intense research ranging from the synthesis of new ligands over structural analysis to pharmacological studies and computational simulations.

Opioid receptors are coupled to the inhibitory G-protein (G_i) and after activation of the receptor, the $\beta\gamma$-complex of the G-protein binds to the Voltage-gated dependent calcium channel (VDCC). This causes an inhibition of the calcium channels and thus decreases the influx of calcium ions into the neuron. The calcium influx is required for the fusion of synaptic vesicles and the release of neurotransmitter. In addition, the $\beta\gamma$-complex binds to potassium channels as well, causing their opening, which leads to an increase of potassium ions. Taken together, these modifications of ion input to the

neuron causes a hyperpolarisation leading to the reduction of neurotransmitter release. The release of neurotransmitters from the pre-synaptic site, such as glutamate, causes the activation of AMPARs and other receptors at the post-synaptic site. In this way the sensation of pain can be transmitted from the primary neuron to the secondary neuron. By reducing the release of neurotransmitter, opioids can act as effective analgesia as the pain transmission is reduced directly. A schematic representation of pain transmission is shown in figure 1.4.

The first crystal structure of MOR was published by Manglik et al. in 2012 bound to β-funal- trexamine (β-FNA), which is an irreversible morphinan antagonist. [9] The receptor crystallized in parallel dimers, with contacts through transmembrane (TM) helices 5 and 6, and in a more limited way through TM helix 1, 2 and 8.
The question whether opioid receptors exists in monomers, hetero- or homodimers is still under debate, with some studies favouring monomers [63, 64] whereas in other studies dimers are observed [65, 66, 51, 67, 45, 68, 69]. In 1997, Cvejic and Devi could show that the DOR forms dimers and the ratio of homodimers to monomers can be alternated by agonist stimulation, leading to a decrease of dimers. [65] Two years later, Jordan and Devi published biochemical and pharmacological results for the heterodimerisation of the δ and κ opioid receptors. They also found evidence for different pharmacological behaviour of the heterodimer in comparison to the monomers. [35] This was further confirmed by a follow-up study from the same group in 2000, showing that for MOR and DOR heterodimers, δ subtype-specific ligands can lead to an increase in binding of μ agonist. [66, 51] The levels of $\mu - \delta$ heterodimers at the cell surface can be regulated by a Golgi chaperone (RTP4). [70] Furthermore, Gomes et al. confirmed the presence of homodimers of the μ subtype using BRET assays in living cells. [67]

Wang et al. also used BRET to investigate hetero- and homodimerisation of all three classical subtypes of opioid receptors, e.g. MOR, DOR and KOR. [45] They showed that the dimerisation happens before trafficking of the receptors to the membrane occurs and that all sub-types have similar affinities for the formation of dimers, regardless if the same sub-type (homodimers) or with a different sub-type (heterodimers). In addition to BRET, they also performed co-immunoprecipitation, receptor binding, and G protein coupling assays in their comprehensive study. [45] In 2002, He et al. investigated the effects of oligomerisation on the trafficking of MOR using a wild-type MOR receptor

with FLAG-tag and a human influenza hemagglutinin (HA)-tagged D MOR, which is a chimera of MOR where the tail is replaced by the tail of the DOR. [53] Upon stimulation with morphine they observed internalisation of both receptors. Wild-type MOR alone does not internalise upon morphine stimulation, hence they concluded that the D MOR is dragging the wild-type MOR into the endocytosis. This effect was shown in human embryonic kidney (HEK) 293 cells as well as in cultured neurons [53]

In 2009 Kuszak et al. expressed a MOR variant fused to a YFP in insect cells. [63] Single-particle imaging suggested that MOR function as monomers, which was also confirmed by using fluorescent ligands, labelled with Cy3, as well as for single-particle imaging giving the same result. Hence they claimed that oligomerisation is not needed for receptor function. [63] By performing coarse-grained (CG) molecular dynamics (MD) simulations with opioid receptors, Provasi et al. showed the formation of homo- as well as heterodimers for all three sub-types. [68] Once they observed a dimer formation there were just minor adjustments at the interfaces but no dissociation events within their 10 μs simulations. [68] Another study using CG MD simulations was published by Zhang et al.. [69] They looked at the role of the different conformational states of the two MOR protomers forming a homodimer. The simulations gave hints for both, positive and negative, co-operativity for the activation of the protomers. The dimerisation also influences the structural communication pathways from the ligand binding region to the G-protein binding site of the inactive protomer. The influence and importance of dimerisation on downstream signalling still needs to be investigated. [69] In a very recent study, Meral et. al used MD simulations to look at the dynamics of MOR homodimers and verified their findings with FRET acceptor photobleaching experiments both giving way for negligible fractions of homodimers at physiological conditions. [64]

These controversial findings obtained with various methods indicate that the answer to the question whether opioid receptors form dimers is rather complex. Nevertheless the answer can give important insights into the functionality of the receptors and especially whether the pharmacological function is alternated upon homo- or heterodimerisation. Better knowledge about this mechanism could pave the way for the development of improved drugs.

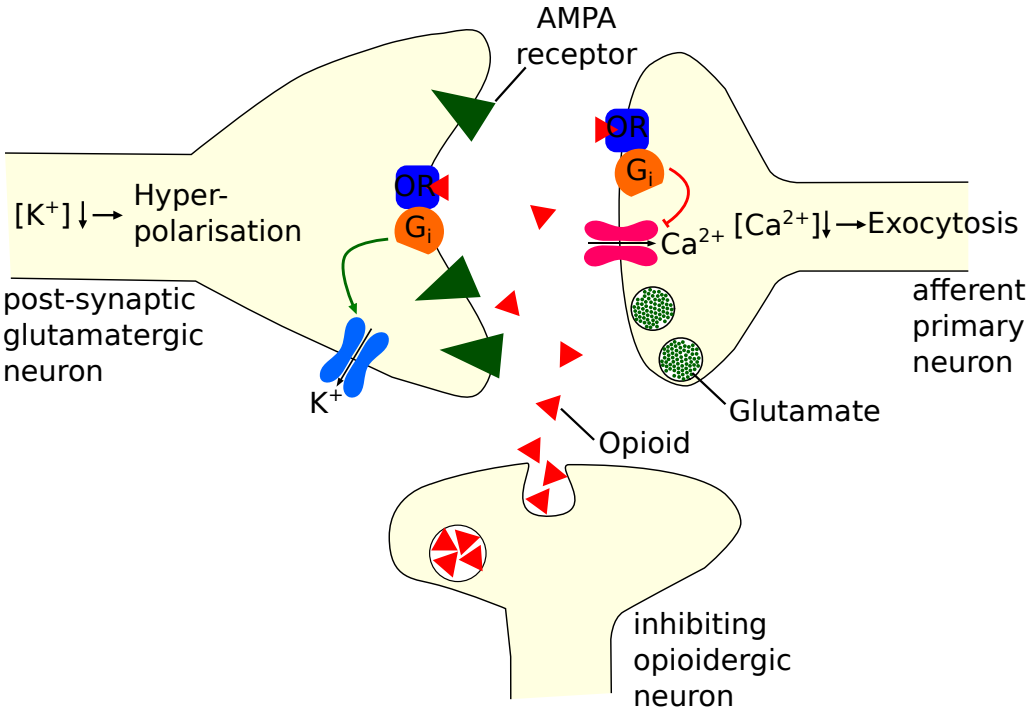

Figure 1.4.: Schematic representation of pain transmission. The afferent primary neuron transmits the nociceptive stimuli to the post-synaptic glutamatergic neuron by releasing glutamate activating AMPARs on post-synaptic neurons. If opioids are released by an efferent opioidergic neuron they cause the activation of the inhibiting G-protein, leading to an outflux of potassium in the post-synaptic side causing a hyperpolarisation. At the pre-synaptic side Ca-channels are inhibited, leading to a decrease of calcium influx and thus inhibits the fusion of synaptic vesicles and neurotransmitter release. Adapted from Graefe, Duale Reihe Pharmakologie und Toxikologie.

1.5. Single-molecule microscopy and its applications

1.5.1. Single-molecule microscopy and its requirements

For decades GPCRs have been investigated using ensemble measurements averaging over hundreds to thousands of receptors. Notwithstanding this brought a lot of knowledge and insights into the field, those ensemble measurements also have their drawbacks. Rare events and heterogeneous behaviours might be obscured, short-lived states averaged out by longer ones. Single-molecule approaches help to overcome those limitations. As they allow to study each single event individually there is no need for averaging and therefore making rare and transient events visible. Furthermore, there is no need of synchronisation, as it is for ensemble measurements with ligand stimulation, for example. [71, 72] In the case of single-molecule imaging, the resolution in time and space is approaching the millisecond and nanometer scale respectively, allowing to investigate heterogeneous diffusion behaviour. [73] The size of molecule complexes is another question that can be addressed by single-molecule imaging, even in living cells as there is no need to break down the cell and therefore the methods are less prone to artefacts. [38] Maybe most importantly they give way to studies of the dynamics of protein-protein and protein-ligand interactions, for example to calculate association and dissociation rates. [73, 38, 74]

To achieve single-molecule imaging, the protein of interest (POI) is normally fluorescently labelled (see section 1.6). The so attached fluorophore needs good photophysical properties like a) efficient absorption of light, b) a high quantum yield so that there are enough photons to be detected, c) having a high photostability to allow long observations before photobleaching occurs and d) rare blinking, so that the fluorophore does not go into a dark state. The latter is crucial for example in single-particle tracking (SPT) experiments. In this case, the blinking would lead to an interruption of detection and therefore break a long trajectory into two shorter ones. In other approaches the blinking behaviour of fluorescent probes can also be taken as an advantage, which is done for example in stochastic optical reconstruction microscopy (STORM).

Furthermore, the receptors need to be sufficiently separated in space for single-molecule microscopy. That means the separation needs to be higher than the Abbe diffraction limit which is about 200 nm for visible light and defined by:

$$d = \frac{\lambda}{2n \sin \Omega} = \frac{\lambda}{\mathrm{NA}} \tag{1.1}$$

where λ is the wavelength and NA the numerical aperture. Due to this diffraction limit the single fluorophore will appear as a blurry disc. By fitting it with a two-dimensional Gaussian distribution the localisation of the centre of the spot can be accurately determined in a range of $10 - 30\,\mathrm{nm}$, as shown in figure 1.5 B. [71] The localisation precision depends on the number of collected photons, N:

$$\sigma = \sqrt{\frac{s^2 + \frac{a^2}{12}}{N} \left(\frac{16}{9} + \frac{8\pi s^2 b^2}{a^2 N} \right)} \tag{1.2}$$

where a^2 is the pixel area of the detector, b^2 is the average number of photons of the background and s is the standard deviation of the point spread function (PSF). This correlation shows that there are two ways of improving the localisation precision. One was already mentioned above, to use fluorophores with a high quantum yield, thus increasing the number of photons that can be detected. Another way is to improve the signal-to-noise ratio, e.g. minimising the background.

Fluorescence from the background can be reduced by using TIRF microscopy. In this case, the excitation light, typically a laser beam with a specific excitation wavelength, is entered in an over-critical angle into a prism, causing the effect of total internal reflection. The thus reflected light creates an evanescent wave, penetrating the specimen/probe (see scheme in figure 1.5 A). The electromagnetic field of the evanescent wave decays exponentially, leading to a penetration depth of just about 100 nm. This allows to image everything that is close to the objective, where the evanescent wave is created, with high precision, while everything beyond this area appears dark and does not contribute to the background. In the range of the evanescent wave typically lies the basal membrane of cells, allowing imaging of receptors on and within the membrane with high precision.

In combination with high speed electron-multiplying charge-coupled device (EMCCD) or complementary metal-oxide-semiconductor (CMOS) sensors as detectors, the temporal resolution can also be improved up to a few μs only, which is crucial for the investigation of dynamic processes.

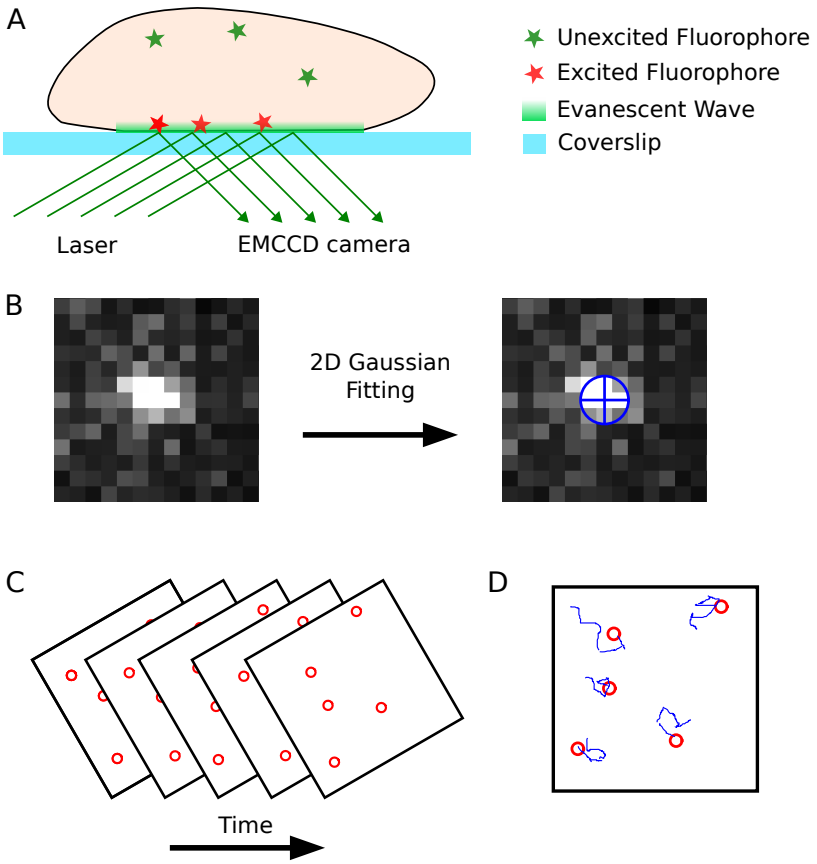

Figure 1.5.: TIRF, single-particle detection and tracking. A) shows the principle of total internal reflection fluorescence (TIRF) microscopy. In B) a representative blurred fluorescent spot from TIRF imaging is shown and how a 2D Gaussian fitting is applied. C) depicts the detection of single-particles over time in consecutive frames. The following tracking and linking is shown in D).

1.5.2. Single-particle detection and tracking

Employing those single-molecule microscopy techniques generates a tremendous amount of data, which needs to be analysed accordingly. This lead to the development of automated SPT algorithms. The first step in SPT is always the detection of the single-particles. As mentioned before, a two-dimensional Gaussian is fitted to the fluorescent spot and the centre is thus localised. This is done for each single frame of the movie. The next step is to determine which detected particle in frame f is the same particle in frame $f + 1$. With the assumption that the particle can just travel a certain distance within Δt, the time between two frames, a search radius is defined and adjusted

according to the experimental parameters. The particle trajectories are built by linking the localised particles from one frame to the other, a schematic representation of detection and tracking is shown in figure 1.5 C and D. The algorithms have to take into account particle splitting and merging events like in complex formation, dissociation and in protein-protein interactions. In addition, particles can be dark for a few frames, for example because of blinking, despite this the algorithm should be capable of linking the trajectories correctly. Aside from those difficulties, receptors in living cells show heterogeneous diffusion behaviour. The expression level of receptors can also be challenging, as higher densities make the correct assignment and tracking more difficult.

To address all those issues, Jaqaman et al. developed a robust single-particle tracking algorithm which calculates the overall cost of each linkage to approach the optimal solution, which would be Multiple-hypothesis tracking (MHT). [75, 76] The problem with MHT is, that it would be too greedy for computational analysis even for a small number of particles. Therefore it can only be approached by either searching the temporal, or the locally optimal solution for tracking. Jaqaman et al. tackled all challenges of SPT at once with their algorithm by using the linear assignment problem. The initially detected particles are linked between consecutive frames and afterwards the so obtained trajectory fractions are linked, also taking merging and splitting events and the closure of gaps into account. In their algorithm, a 'cost' is calculated for each linkage and event, and the overall cost is then optimised, resulting in a solution with the lowest cost, which represents the most likely tracking. This leads to a global optimisation in space and time comparable to MHT. [75]

1.5.3. The quest of explaining diffusion

The single trajectories can then be further investigated for example to obtain insights into the diffusion behaviour of particles in and on the cell surface. To determine the form of motion present, the mean squared displacement (MSD) is calculated.

$$\mathrm{MSD} = \left\langle \big[x(t) - x(0)\big]^2 \right\rangle = \frac{1}{N}\sum_{n=1}^{N} \big[x_n(t) - x_n(0)\big]^2 \tag{1.3}$$

where N is the number of particles, over which the average is taken, $x_n(0) = x_0$ is

the initial position of each particle and $x_n(t)$ is the position of each particle at time t. Thus it is possible to calculate the average diffusion behaviour of particles in a cell, for example. In case of single-particles the MSD is averaged over time, therefore it is called time-averaged mean squared displacement (TAMSD), making it possible to get information about the diffusion behaviour of single trajectories. By applying TAMSD, different groups were able to show very heterogeneous diffusion behaviour ranging from virtually immobile particles, to sub-diffusive motion, to normal diffusion or even super-diffusive behaviour. To distinguish between these different forms of motion it has been shown to be advantageous to look at the anomalous diffusion factor α as schematically shown in figure 1.6, but also other methods for classification have been used. [77] In contrast to normal diffusion, anomalous diffusion follows a power law dependence

$$\text{MSD} \simeq D \cdot t^{\alpha} \tag{1.4}$$

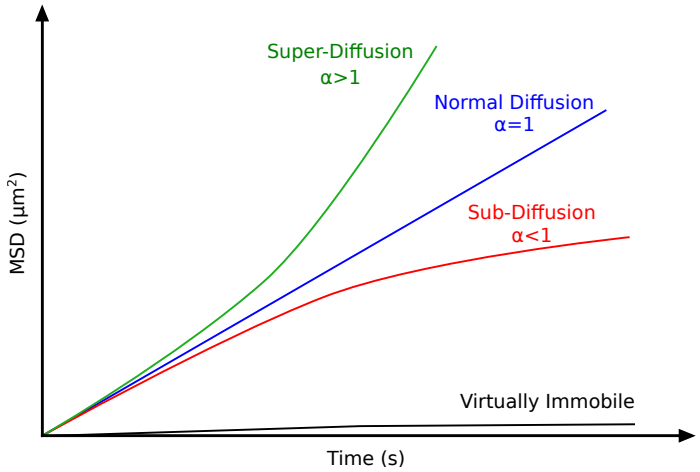

Figure 1.6.: MSD and diffusion categories. Schematic graph of mean squared displacements (MSD) for different types of motion: virtually immobile (black), sub-diffusion (red), normal diffusion (blue) and super-diffusion (green).

with D as diffusion coefficient. If $\alpha = 1$ it is normal diffusion. Every trajectory with $\alpha > 1$ is called super-diffusion, which requires more then just random forces. Trajectories with $\alpha < 1$ are called accordingly sub-diffusion, in which case the membrane is crowded and the receptor faces some obstacles which makes it more difficult to explore the space. [78] The reasons for the deviation from normal diffusion can be numerous, ranging from the lipid environment of the particles to protein-protein interactions, to

physical barriers like the cytoskeleton. In 2005 Suzuki et al. showed that MORs labelled with gold spheres in living cells can jump between neighbouring compartments. [73] Within the compartments the receptors were confined until they overcame the barrier to the next compartment. This led to the formulation of the 'fence-and-picket' model. The cytoskeleton, like actin fibers, is represented as fences, and the membrane proteins, anchored to the cytoskeleton, are acting like pickets. Together these structures act as barriers limiting the diffusion and leading to an observed confinement. [73, 71].

1.5.4. Investigating protein complexes using single-molecule imaging

Single-molecule imaging techniques can also be used to investigate the size of complexes, e.g. how many molecules the complex comprises and the dimerisation of receptors (see section 1.3). [38, 37, 79] Therefore the fluorescent intensity of the detected spots is analysed and compared to the intensity of single fluorophores. As expected, monomers have the same intensity profile as a single fluorophore, dimers have double the intensity etc.. Furthermore, it is possible for long enough observations to simply count the bleaching steps. By looking at the fluorescent intensity of complexes it was possible to compare three different prototypical GPCRs: β_1 adrenergic receptor (β_1AR), β_2 adrenergic receptor (β_2AR) and $GABA_B$. The β_1AR showed the least degree of dimerisation and mostly stayed monomeric whereas $GABA_B$ showed a high degree of oligomerisation, which can be expected as it is a constitutive dimer. [38, 11, 40, 41]
In the case of the dopamine receptor, Tabor et al. were able to show that the binding of ligands can change the ratio between monomeric and dimeric receptors, whereas the application of an antagonist did not change the ratio in comparison to unbound receptors. [37] As discussed earlier, the formation of dimers can play an important role for the pharmacology of GPCRs. Using single-molecule approaches to study the formation and the size of receptor complexes can give new and more insights in the dynamics, and is less prone to artefacts as there is no need of cell disruption as for example in co-immunoprecipitation.

1.5.5. Single-molecule FRET

Single-molecule imaging techniques can be combined with Förster resonance energy transfer (FRET), which is also known as 'molecular ruler'. [80, 81] It is a fluorescence-based technique with two fluorophores, a donor and an acceptor. The latter is red-shifted in comparison to the donor and can be used for measuring distances in the range of $1 - 10\,\mathrm{nm}$. [81] The so called FRET-pair has to be chosen wisely, as the donor emission and acceptor excitation spectrum need to have some overlap to give efficient FRET ratios (see figure 1.7). On the other hand, both fluorophores need to be spectrally separated so that effects like bleed-through and cross-excitation are minimized. [82, 83]

FRET is a dipole-dipole coupling mechanism and its efficiency E is sensitive to the distance r between the two fluorophores:

$$E = \frac{1}{1 + (r/R_0)^6} \tag{1.5}$$

where R_0 is called the Förster distance, which is specific for each donor-acceptor-pair and the orientation they have towards each other and is defined by:

$$R_0 = 0.211\big(\kappa^2 n^{-4} Q_\mathrm{D} J(\lambda)\big)^{1/6} \tag{1.6}$$

with Q_D, the fluorescence quantum yield of the donor, κ^2 is the dipole orientation factor, n the refractive index of the medium and $J(\lambda)$ is given by the spectral overlap of the donor emission and the acceptor excitation spectrum. [84, 85, 82]

As shown in eq. (1.6), FRET is highly sensitive to even subtle distance changes (inverse 6th power law) and this in a range that cannot be resolved by common single-molecule imaging approaches. Thus the combination of both methods can give more insights into dynamic processes for intra- as well as for inter-molecular complexes. In recent years, this approach was also used for the investigation of GPCRs. Vafabakhsh et al. used single-molecule fluorescence resonance energy transfer (smFRET) on metabotropic glutamate receptors (mGluRs), dimeric class C GPCRs which have a large extracellular ligand binding domain (LBD). They showed that the LBD switches between three conformations: resting, a short-lived intermediate, and an active state. The transitions between those conformations can be alternated by ligands and in case of mGluR3 also by Ca^{2+}. [86]

Gregorio et al. applied smFRET on immobilised β_2AR mutants in a comprehensive

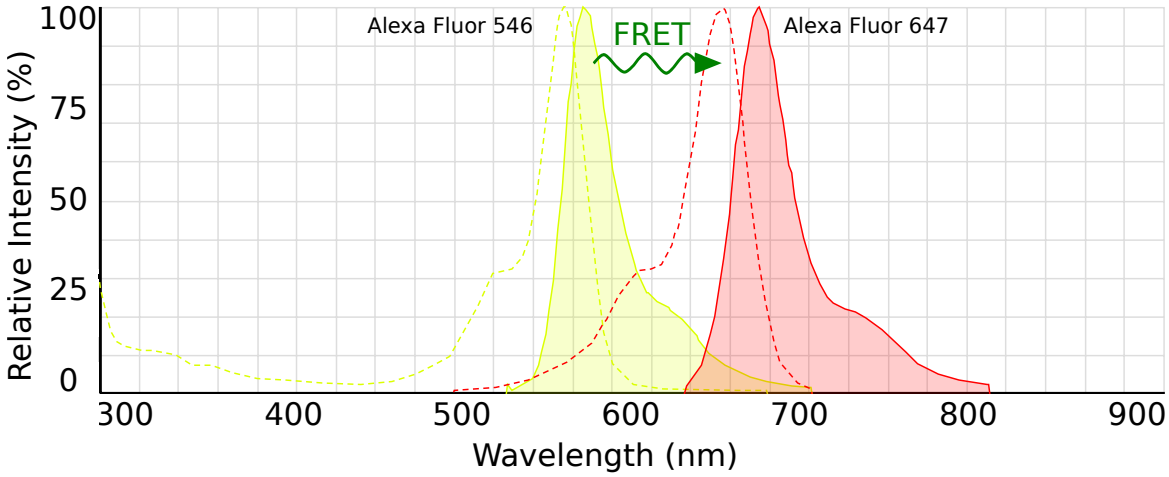

Figure 1.7.: FRET spectra. Shown are the excitation (dashed line) and emission (filled) spectra of Alexa Fluorophore 546 (left) and Alexa Fluorophore 647 (right).

study. The receptors were labelled with optimised Cy3B and Cy7 as FRET-pair to compare the efficacy of different ligands ranging from neutral antagonist and inverse agonist to partial agonist and full agonist. They observed shifts in the FRET efficiencies as well as in the full-width at half maximum (FWHM) values for the different conditions. Furthermore, they were able to investigate the formation of $\beta_2\mathrm{AR}-\mathrm{G_s}$ complexes and to show that the presence in a low FRET state, which is interpreted as activated and G_s bound, is correlated with the efficacy of the ligand. In addition, Gregorio et al. measured the effect of nucleotides on the dissociation of the $\beta_2\mathrm{AR}-\mathrm{G_s}$ complexes. In the presence of nucleotides the complexes stay for multiple seconds whereas they dissociate ca. twofold faster in the presence of GTP. [18]

Dijkman et al. combined smFRET with other methods to get more insights into the dynamics of dimer formation. They studied purified neurotensin receptor 1 (NTS1), labelled with Cy3 and Cy5, and reconstituted them into DPhPC droplet interface bilayers with a receptor density similar to physiological conditions. Thus, they were able to visualise the formation of individual dimers, and in combination with the results from other techniques, proposed a 'rolling-dime' interface model, meaning that different dimer conformations can exist and interchange. [44]

These recent studies show that smFRET can serve as a helpful addition to more established methods and give more insights into dynamic processes like receptor activation and dimerisation, but it can also be used for pharmacological studies about efficacies,

for example. As all previous described studies were performed on purified receptors, an important and missing step forward for smFRET is its application in living cells.

1.6. Different labelling strategies

As described earlier (section 1.5.1) it is necessary for the application of imaging techniques, to make the POI visible. This is usually achieved by introducing a fluorescent reporter probe. Over the past decades different approaches have been reported. [72, 87] Out of those, three were used in this work and are depicted in figure 1.8.
Crucial questions for the introduction of fluorescent probes are where it is located within the receptor, the kind of probe used and also how it should be introduced. All these factors could have an impact on the functionality and/ or expression of the receptor and lead to significant differences in comparison to the wild-type receptor. [88, 72]

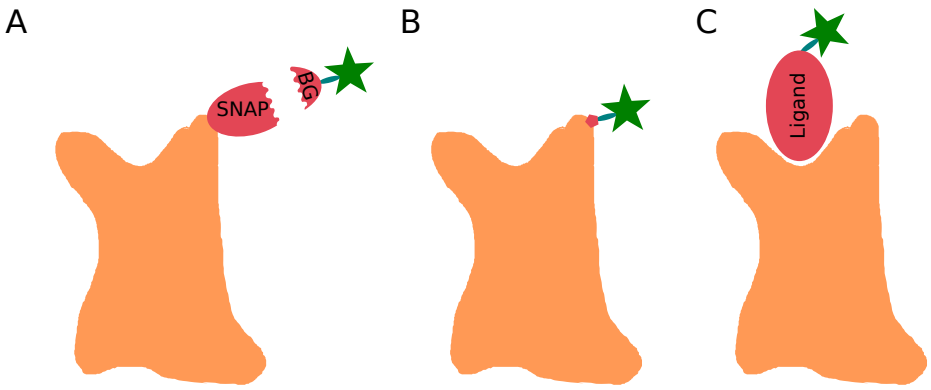

Figure 1.8.: Schemes of different labelling techniques. A) shows the SNAP-tag technique, where the fluorophore is bound to a BG substrate. B) depicts the usage of unAA for click labelling. In C) the labelling via a fluorescent ligand is shown.

1.6.1. Labelling via SNAP- and CLIP-tag

Site-specific labelling is crucial for the investigation of dynamic processes in GPCRs or other POIs. Using gen-editing it is possible to insert a fluorescent protein (FP) at specific sites, such as green fluorescent protein (GFP) derivatives. This technology has shown to be versatile in different applications and also lead to the development of biosensors/FRET-sensors like Epac1. [20, 89, 90, 91] Nevertheless FPs have some limitations. One disadvantage of FPs is that not all become fluorescent or are even correctly folded but for single-molecule studies of interactions or oligomerisation it is necessary to have a high labelling efficiency. [38, 92, 72] Small organic fluorophores are

also more photostable than FPs, giving way for longer observations. In addition, the insertion of a tag, which is labelled just before the experiments, allows for more flexibility in choosing the fluorophore. [92, 72, 93, 94] This requirement led to the development of self-labelling protein tags amongst which the SNAP-tag, CLIP-tag and Halo-tag are the most common one. [93, 95, 96]
Keppler et al. took advantage of the human deoxyribonucleic acid (DNA) repair protein O^6-alkylguanine-DNA alkyltransferase (AGT) which forms a covalent linkage with its substrate BG. [93] The SNAP-tag can be incorporated into the POI and be expressed in living cells. With a small organic fluorophore linked to BG a high labelling efficiency and specificity is achieved. Since the technique was developed in 2003, a lot of fluorescent probes have been engineered for the SNAP-tag technology, so that it is possible to select the suitable fluorophore from a wide range of wavelengths. [97] A few years later, the same lab developed a protein tag which can be labelled orthogonally to the SNAP-tag allowing for multi-colour staining – the CLIP-tag. [95] This new tag was also derived from the AGT, but in this case it has a substrate specificity with O^2-benzylcytosin (BC). With 19 kDa the SNAP- and CLIP-tag are smaller than GFP (27 kDa), for example, and can be used for *in vitro* and real-time experiments. As the choice of fluorophores is very flexible, it is possible to select those which fulfil the requirements for single-molecule experiments. With the development of different, orthogonal tags even multi-colour studies are in the realm of possibility. [38, 74, 98]

1.6.2. Labelling via unnatural amino acids

Even though the SNAP-tag is already smaller than FPs, an optimal protein tag would be even smaller, and in the best case just one amino acid (AA). The problem with site-specific labelling is that most of the amino acids are expressed on several sites, and for this reason the POI must be genetically modified to have, for example, only one cysteine left. The expanding of the genetic code by the use of unAA opens up a horizon of possibilities. By introducing a 21^{st} amino acid it is possible to choose nearly any site within the POI, creating just a minor deviation from the wild-type protein and still be very specific. As most of the codons are already translated to the 20 natural amino acids, one of the three stop codons must be used for the introduction of an artificial amino acid – opal or sometimes umber (UGA), ochre (UUA) or amber (UAG) (see figure 1.9). The amber codon is the least frequent stop codon and it was already shown in *E. coli* that

it can be suppressed efficiently. [99] Furthermore, the amber codon suppression is more readily read through in comparison to opal and ochre in mammalian cells. [100] The first successful incorporation of an unAA was achieved in 1989, when the amber codon was translated to phenylalanine analogues. [101]. To achieve the successful incorporation of an unAA, two different transfer ribonucleic acid (tRNA)s are required: one for the suppression of the amber codon and one for the recognition and transfer of the unAA. By applying a specific orthogonal aminoacyl-tRNA synthetase-tRNA it was achieved to introduce an unAA into GPCRs in the recent years. [102, 103, 104, 105] The unAA of choice needs to fulfil certain requirements for labelling. A promising approach is bioorthogonal chemistry or click chemistry. [106, 107] The unAA contains strained alkenes/alkynes which can then be labelled with an azide/tetrazine dye derivative. These reactions are called strain-promoted alkyne-azide cycloaddition (SPAAC) and strain-promoted inverse electron-demand Diels-Alder cycloaddition (SPIEDAC). They are biocompatible, non-toxic reagents, and hence applicable to living cells. They react specifically and fast in aqueous environments. [106, 108, 107]. As with SNAP- and CLIP-tag, several dyes are available bearing the reactive group for SPAAC and SPIEDAC. In addition, both are free of copper, which is commonly used for bioorthogonal labelling, but can be toxic for living cells. Furthermore, SPAAC and SPIEDAC are orthogonal to each other meaning they can be simultaneously used for two-colour labelling. [106, 109]

Figure 1.9.: The three stop codons in their colour representation: amber translated by UAG, ochre by UUA and umber by UGA.

1.6.3. Labelling via fluorescent ligands

An approach of labelling GPCRs without the need of modifications on the POI is offered by the use of fluorescent ligands. Here, endogenous or synthetic ligands are chemically modified to transform them into fluorescent probes. This is usually achieved by conjugat-

ing a dye via a linker to a known pharmacophore. The big advantage of this approach is the possibility to investigate wild-type receptors even in living tissue. [110, 111] Caution has to be taken as the chemical modifications can change the pharmacological properties of the pharmacopohore. Therefore tests and comparisons to the parent compound are advised. [72] Furthermore, the design and synthesis may not be straightforward, making this approach sometimes laborious. Nevertheless, fluorescent ligands were already successfully applied in different applications like binding assays, FRET-based binding studies in living cells and also for the investigation of receptor oligomerisation. [110, 111, 112] If the fluorescent ligand has a high binding affinity to the POI it is suitable for single-molecule imaging where high labelling efficacy is crucial. In addition it should have a high specificity and some level of wash-resistance to reduce the fluorescent background. It can then be used for studies of the receptor mobility on the membrane, oligomerisation and protein-protein interactions if the interaction partner is labelled as well. The use of fluorescent ligands comes with some limitations as it interacts with the receptor at the binding site. Depending on the ligand, it can act as an agonist or antagonist and thus influence the behaviour of the receptor and might lead to faster internalisation, for example. Furthermore, it limits the possibilities of dynamic interactions with other ligands as the binding pocket is already occupied. In comparison to technologies like SNAP-tag or the introduction of an unAA especially, the choice of binding site is limited as ligands can only bind to the orthosteric or allosteric binding site.

2. Aim

During this thesis two projects were pursued.
The aim of the first project was the characterisation of a set of novel subtype specific ligands for the μ and δ opioid receptors. This included their pharmacological characterisation as well as testing their applicability for single-molecule microscopy.
The new fluorescent ligands should be used to shed new lights on the dynamics of opioid receptors. Until now there are conflicting finding about whether they form homodimers or not. The dynamics of the receptors can have an impact on the downstream signalling, thus a better understanding can lead to better and safer pain killers.
The use of the fluorescent ligands as tools for single-molecule microscopy techniques will allow to investigate the dynamics of wild-type opioid receptors at the cell membrane. Furthermore, they will be applied to to clarify if μ opioid receptors stay as monomers or form homodimers, and if they form homodimers, to which extent.

The second project focused on understanding the activation process of α_{2A}AR as prototypical class A G-protein coupled receptor using single-molecule fluorescence resonance energy transfer (smFRET). The establishment of smFRET in living cells should allow the observation of short-lived and rare events and thus the investigation of heterogeneous dynamic processes. Thus it could serve to unravel the question if GPCRs exist in only two states, inactive and active, or in more substates depending on the presence and nature of ligands and coupling of G-proteins.
In order to succeed, first labelling of intracellular SNAP and CLIP-tags needs to be achieved. Next, smFRET needs to be established at the lab. Afterwards, the receptor could be tested in different environments, e.g. in the presence of different ligands or nucleotides to favour different substates. Furthermore, data processing needs to be established to draw conclusions from those types experiments. The findings should be confirmed by ensemble FRET measurements, showing the functionality of the receptor mutant bearing a SNAP- and CLIP-tag.

3. Material and Methods

3.1. Materials

,

3.1.1. Cell Lines

- Chinese hamster ovary (CHO)-K1 cells (#ACC 110 Leibnitz-Institut DSMZ)
- Human Embryonic Kidney (HEK)-293 A cells (ATCC)
- CHO α2A-CLIP-SNAP (Altair) cells (this work)
- CHO α2A-K327amb-SNAP (Bellatrix) cells (this work)
- CHO α2A-S347amb-SNAP (Capricorni) cells (this work)
- CHO α2A-S360amb-SNAP (Deneb) cells (this work)
- CHO α2A-K370amb-SNAP (Enif) cells (this work)
- CHO α2A-T373amb-SNAP (Fafnir) cells (this work)
- *E. coli* (TOP10) (#C404010 Thermo Fisher Scientific)

3.1.2. Cell Culture Media and Supplements

- Dulbecco's modifies Eagle's medium (DMEM)/F-12 without phenol red (#11039-021 Gibco)
- Dulbecco's modifies Eagle's medium (DMEM) with phenol red (#21969-035 Gibco)
- Dulbecco's phosphate buffered saline (DPBS) without Ca^{2+} and Mg^{2+} (#14190-094 Gibco)

- Reduced serum medium (Opti-MEM) (#11058-021 Gibco)
- Fetal bovine serum (FBS) (#S0115 Biochrom AG)
- Penicillin/Streptomycin (#P4333 Sigma-Aldrich)
- Trypsin/EDTA solution (#P10-023100 PAN Biotech)
- L-Glutamin (#P04-80100 PAN Biotech)

3.1.3. Dyes

- SNAP-Cell 430 (#S9109S New England BioLabs (NEB))
- SNAP-Surface 488 (#S9124S New England BioLabs (NEB))
- SNAP-Cell 505-Star (#S9103S New England BioLabs (NEB))
- SNAP-Cell TMR-Star (#S9105S New England BioLabs (NEB))
- SNAP-Surface Alexa Fluor 546 (#S9132S New England BioLabs (NEB))
- SNAP-Surface 549 (#S9112S New England BioLabs (NEB))
- SNAP-Surface Alexa Fluor 647 (#S9136S New England BioLabs (NEB))
- SNAP-Cell 647-SiR (#S9102S New England BioLabs (NEB))
- SNAP-Surface 649 (#S9159S New England BioLabs (NEB))
- CLIP-Surface 488 (#S9232S New England BioLabs (NEB))
- CLIP-Cell 505 (#S9217S New England BioLabs (NEB))
- CLIP-Cell TMR-Star (#S9219S New England BioLabs (NEB))
- CLIP-Surface 547 (#S9233S New England BioLabs (NEB))
- CLIP-Surface 647 (#S9234S New England BioLabs (NEB))

3.1.4. Plasmids

Table 3.1.: Plasmids used

construct	description	resistance
α2A-AR-wt	α2A-AR wild-type with HA-tag	amp
α2A-AR-YFP-CFP	α2A-AR with HA-tag, YFP in 3ICL and CFP c-tail	amp
α2A-AR-CLIP-SNAP	α2A-AR with HA-tag, CLIP-tag in 3ICL and SNAP-tag c-tail	amp
α2A-AR-SNAP-CLIP	α2A-AR with HA-tag, SNAP-tag in 3ICL and CLIP-tag c-tail	amp
α2A-K327amb-SNAP	α2A-AR with HA-tag, K327amb mutation and SNAP-tag c-tail	amp
α2A-S347amb-SNAP	α2A-AR with HA-tag, S347amb mutation and SNAP-tag c-tail	amp
α2A-S360amb-SNAP	α2A-AR with HA-tag, S360amb mutation and SNAP-tag c-tail	amp
α2A-K370amb-SNAP	α2A-AR with HA-tag, K370amb mutation and SNAP-tag c-tail	amp
α2A-T373amb-SNAP	α2A-AR with HA-tag, T373amb mutation and SNAP-tag c-tail	amp
CLIP-SNAP-CD86	CD86 with N-terminal FLAG-, CLIP- and SNAP-tag	amp
MOR-wt	μ opioid receptor wild-type	kan
DOR-wt	δ opioid receptor wild-type	kan
Galphai	$G_{\alpha i}$ PTX insensitive	amp
Gbeta-wt	G_{β} wild-type	amp
Ggamma-wt	G_{γ} wild-type	amp
pcDNA	empty pcDNA vector	amp
EYFP	enhanced YFP	kan
EYFPmem	membrane-tagged enhanced YFP	kan
clathrin-GFP	clathrin tagged with a GFP	amp
pcGi Trimer	pcGi Trimer mTq Venus (Gi sensor)	kan

3.1.5. Laboratory Equipment and Accessories

Adhesion microscope slides	SuperFrost Plus®, R. Langenbrinck
Attofluor cell chamber	Thermo Fisher Scientific
Agarose gel system	Agaget Standard, Whatman Biometra
Bio-Rad Gene Pulser II	#165-2077, Bio-Rad
Blotting chamber	Criterion Blotter, BioRad
Centrifuge EBA 12R	Hettich
Centrifuge Rotanta 96R	Hettich
Centrifuge 5810R	Eppendorf
Electrophoresis Power Supply	EPS 301, Amersham Biosciences
Electrophoresis Unit	SE600 Series, Hoefer
Electroporation cuvettes	#165-2088, BioRad
Glass fiber filters without binders	#APFF02500, Merck
Inverted Laboratory Microscope	Leica DM IL
Liquid Scintillation Analyzer	Tri-Carb® 2910 TR Perkin Elmer
Microscope cover glasses 24 mm	#0111640, Marienfeld superior
NanoDrop 2000 C Spectrophotometer	Thermo Fisher Scientific
Scintillation Vials 20 ml	#SZFL, Hartenstein
Shaker	Heidolph Reax 2000
Sonicator Tip	Sonopuls HD206, Bandelin
Ultracentrifuge LE-70	Beckman
Ultraturrax	T8, IKA Labortechnik

3.1.6. Chemicals and Reagents

Rotiszint® eco plus LSC Universalcocktail	#0016.3 Roth
Lipofectamine® 2000	#11668019 Thermo Fisher Scientific
Effectene Transfection Reagent	#301427 QIAGEN
jetPRIME®	#114-01 VWR™

3.1.7. Antibodies

Primary antibodies

- Mouse monoclonal anti-HA-tag (# 901513 Biolegend)
- Rabbit polyclonal anti-SNAP-tag (#CAB4255 Thermo Fisher)

Secondary antibodies

- Goat anti-mouse horseradish peroxidase conjugate (#115-035-003 Jackson ImmunoResearch)
- Goat anti-rabbit horseradish peroxidase conjugate (#111-035-144 Jackson ImmunoResearch)

3.1.8. Solutions

2x BBS

- 280 mM NaCl
- 1.5 mM Na_2HPO_4
- 50 mM BES

FRET buffer

- 5 mM KCl
- 137 mM NaCl
- 1 mM $MgCl_2$
- 2 mM $CaCl_2$
- 10 mM HEPES
- pH 7.3

smFRET buffer

- 10 mM Tris at pH 8.0
- 50 mM NaCl
- 1 %/v D-glucose
- 25 U/ml glucose oxidase[1]
- 250 U/ml catalase[1]

[1]GOCAT already as stock prepared, needs to be diluted 50 fold

- 1 mM chloramphenicol
- $1 - 2$ mM Trolox

10% separation gel

Recipe for two gel 14 loading chambers

- 7.2 *ml* Rotiphorese 30
- 5.6 *ml* 1.5 M Tris, 0.4% SDS
- 9.75 *ml* H_2O
- 300 μl 10% APS
- 22.5 μl Temed

Running buffer

- 25 mM Tris
- 190 mM glycine
- 1% SDS
- pH 8.3

TBS-T

- 10 mM Tris pH 7.4
- 100 mM NaCl
- 0.1% Tween20

Transfer buffer

- 25 mM Tris
- 150 mM glycine
- 10% methanol

Washing buffer

- 50 mM Tris pH 7.4
- 150 mM NaCl
- 0.2% BSA
- 0.2% NP-40

RIPA buffer

- 50 mM Tris pH 7.2
- 150 mM NaCl
- 1% NP40
- 0.5% sodium deoxycholate
- 0.1% SDS

Lysis Buffer GTPγS

- 5 mM Tris
- 2 mM EDTA
- pH 7.4

Binding buffer

- 20 mM HEPES
- 10 mM NaCl
- 10 mM $MgCl_2$
- pH 7.4

3.2. Methods

3.2.1. Transformation (Top 10)

For the amplification of plasmids, chemically competent *E. coli* (TOP10) were used. $20\,\mu l$ $5\times$ KCM buffer, $80\,\mu l$ ddH_2O and $0.75\,\mu g$ of plasmid DNA were mixed in a $1.5\,ml$ Eppendorf tube. After addition of $100\,\mu l$ of competent cells the mixture was incubated for 20 minutes on ice followed by 10 minutes incubation at room temperature. Then $1\,ml$ Luria Bertani (LB) medium was added followed by 50 minutes incubation at $37°\,C$ with horizontal shaking. From this mixture $100\,\mu l$ were taken and plated on agar plates by spreading with a sterilised instrument. The agar plates contained the appropriate antibiotic, namely either ampicillin at a final concentration of $0.1\,mg/ml$ or kanamycin at a final concentration of $0.04\,mg/ml$. The agar plates were incubated overnight for 14-16 hours at $37°\,C$ to obtain isolated colonies. The following day, a single colony was picked and used for the plasmid amplification (3.2.2).

3.2.2. Plasmid amplification

For plasmid DNA extraction and purification the Qiagen MIDI plus kit was used following the manufacturer's protocol with modifications. Either a single colony from the transformation from the previous day (section 3.2.1) or a swab from a gylcerol stock of transformed bacteria was used to inoculate in $2\,ml$ LB medium supplemented with the appropriate antibiotic. This mixture was incubated for $8\,h$ at $37°\,C$ with horizontal circular shaking at $180\,rpm$. Then, $50\,\mu l$ of this culture were taken to inoculate $50\,ml$ LB medium supplemented with either $50\,\mu l$ ampicillin or kanamycin. %TODO After incubating this culture overnight for 14-16 h at $37°\,C$ with horizontal circular shaking at $180\,rpm$, the culture was centrifuged at $4°\,C$ with $4000\,rpm$ for 15 minutes. The so obtained bacterial pellet was resuspended and homogenised with a pipette in $4\,ml$ resuspension buffer P1 containing LyseBlue. Then, $4\,ml$ of lysis buffer P2 were added and the mixture was gently mixed by inverting it 4 to 6 times and incubated at room temperature (RT) for 3 minutes. After this incubation, $4\,ml$ neutralisation buffer S3 were added and the mixture was gently mixed again by inverting it until all traces of blue were eliminated. The lysate was then centrifuged at $4000\,rpm$ at RT for 5 minutes before it was transferred into a QIAfilter cartridge. The lysate was incubated 5 minutes followed by a filtration into a $15\,ml$ tube and an addition of $2\,ml$ binding buffer BB.

The mixture was gently mixed by inverting the tube 4 to 6 times and then transferred to a vacuum pump assembly where the lysate ran through a column. The column was washed by adding 700 μl wash buffer PE and centrifugation with 10000 $\times g$ for 1 minute at RT. Next, 700 μl buffer ETR with ethanol were added followed by another 1 minute of centrifugation. To remove any buffer traces, the column was centrifuged again before the DNA was eluted. Afterwards, 100 μl ddH_2O were added on the column, incubated for 5 minutes at RT and then the DNA was collected in a sterile 1.5 ml tube by centrifugation with 10000 $\times g$ for 1 minute at RT. A NanoDrop 2000 (from Thermo Fisher Scientific) was used to measure the DNA concentration and purity. The DNA concentration was adjusted to 1 $\mu g/\mu l$ and the aliquot stored at $-20° C$.

3.2.3. Cloning

The insertion of unAA into our receptor of interest (α2A-AR) was performed by substituting amino acids in the third ICL. Serine and Lysine have been shown to be the most promising amino acids for the replacement with an unAA (Beliu et al. unpublished). 5 target amino acids were chosen: 2 Lysine, 2 Serine and 1 Threonine. The mutagenesis was performed on α2A-AR-wt. As an example, the cloning scheme for the K327amb mutant is described. First, two single cutting sites were chosen around the insertion side chain. In this case BspEI downstream and XbaI upstream and the respective primers were designed. A second set of primers was designed with the same sequence as the original receptor around the insertion side chain with a length of 30 bases. For the reverse primer the codon for lysine was replaced by 'ATC', which is the amber codon. Accordingly, the forward primer contained 'TAG' at the respective site. A polymerase chain reaction (PCR) was run with the forward primer containing BspEI and the reverse primer with the amber mutation. A second PCR was used for the forward primer with the amber mutation and the reverse primer containing XbaI. The products of those two PCRs were used as templates for a third PCR, giving a product that was then ready to be inserted via the two single cutting sites into the α2A-AR-CLIP-SNAP. The final product contained a substitution with an amber codon in the third ICL and a SNAP-tag at the C-tail. The PCRs were performed by Dr. Ulrike Zabel (Institute of Pharmacology, University of Würzburg).

3.2.4. Preparation of superclean coverslips

Glass coverslips with a diameter of $24\,mm$ were placed in a custom made holder, which was then placed into a beaker. The coverslips were covered with chloroform and the beaker was sealed with aluminium foil. The beaker containing chloroform and coverslips was sonificated for 30 minutes. Afterwards, the holder was taken out and left to dry before it was placed in a beaker containing $5\,M$ NaOH, covered with aluminium foil and sonificated for 30 minutes. Next, the coverslips were washed 3 times with super-pure water before being stored in 99.98 % ethanol.

3.2.5. Cell culture

CHO cells

chinese hamster ovary (CHO) cells were cultured in $10\,cm$ petri dishes in complete culture medium (DMEM/F-12 supplemented with $10\,V\%$ fetal bovine serum (FBS), $100\,U/ml$ penicillin and $100\,\mu g/ml$ streptomycin) at $37°\,C$ and 5% CO_2. The cells were routinely passaged at a confluence of $70 - 90\%$. The cells were washed gently with phosphate-buffered saline (PBS) and detached by an incubation of 2 minutes with $1\,ml$ Trypsin/EDTA. Trypsin was then inhibited with complete medium and the cells were detached, homogenised and collected. A fraction of the cell suspension was then cultured in a new plate containing fresh medium.
The stable clones derived from CHO cells were cultured with the same conditions, with the addition of $500\,nm/\mu l$ gentamicin.

HEK293 A cells

HEK293 A cells were cultured in complete culture medium (phenol red-free DMEM supplemented with $10\,V\%$ FBS, $2\,mM$ L-Glutamine, $100\,U/ml$ penicillin and $100\,\mu g/ml$ streptomycin) at $37°\,C$ and 5% CO_2. The cells were routinely passaged at a confluence of $70 - 90\%$. The cells were washed gently with PBS and detached by an incubation of 2 minutes with $1\,ml$ Trypsin/EDTA. Trypsin was then inhibited with complete medium and the cells were detached, homogenised and collected. A fraction of the cell suspension was then cultured in a new plate containing fresh medium.

3.2.6. Creation of stable cell lines

For the generation of stable cell lines (3.1.1), CHO cells were seeded the evening before transfection at a density of 1×10^6 cells per $10\,cm$ Petri dish to achieve a confluence of $70 - 80\%$. On the next morning, the cells were transfected via Lipofectamine® 2000 (refLipo) with $12\,\mu g$ plasmid DNA and $36\,\mu l$ Lipofectamine® 2000. In parallel a control plate was transfected with the empty expression vector (pcDNA). After $24\,h$, the medium was replaced with fresh medium containing the selection antibiotic, in this cases gentamicin (G418) at a final concentration of $500\,ng/ml$. The following day, the cells were split and after 4-6 hours the selection antibiotic was added to the transfected stable cell line as well to the control plate again. After a few days all cells of the control plate died. Depending on the transfection efficiency also $5 - 10\%$ of cells from the transfected plates died. The surviving cells, which contained the resistance, were routinely passaged using the medium containing the selection antibiotic. This selection pressure of the antibiotic was kept for 2-3 weeks, until the new cell line could be considered 'stable'. Then, aliquots were frozen and stored. For the purpose of some experiments the stable cells were diluted and plated in a 96-well plate in order to obtain single clones. The wells were checked each day and those containing more than one cell were not considered. The single clones were then cultured and checked for expression level by fluorescent labelling and TIRF microscopy, before aliquots of them got frozen and stored.

3.2.7. Transfection

Via Lipofectamine® 2000

The evening before the transfection, CHO cells were seeded on $24\,mm$ superclean coverslips (3.2.4) at a density of $170,000$ cells per well of a 6-well plate. The next morning, for each well, $0.5\,ml$ of Opti-MEM medium was incubated with $2\,\mu g$ of plasmid DNA and in parallel $0.5\,ml$ of Opti-MEM medium was incubated with $3\,\mu l$ of Lipofectamine® 2000. After 5 minutes of incubation, the mixtures were pooled and incubated for 20 minutes at room temperature.
Before the transfection, cells were washed once with PBS and then with $1\,ml$ of DMEM/F-12 medium supplemented with FBS was added. After the 20 minutes incubation $1\,ml$ of the transfection mixture was added dropwise in a spiral manner on top of the cells.

Via electroporation

Confluent plates of CHO cells were trypsinised, centrifuged and adjusted to a concentration of 5×10^6 cells/ml. For the transfection, 400 μl cell solution, 20 μg plasmid DNA and 0.5 μl dye (each) were added to a 4 mm cuvette. The cuvette was put into the Bio-Rad Gene Pulser II to electroporate with 0.25 V and 960 μFD. After the shock, 800 μl of pre-warmed medium were added slowly and gently and then left for 20 minutes. Before seeding on coverslips, the cell solution was centrifuged for 5 min at 850 rpm and the supernatant was replaced with fresh medium.

Via Effectene

The evening before transfection, HEK 293 AD cells were seeded with a density of 200, 000 on clean 24 mm coverslips. Just before the transfection, the cells were washed with PBS and then 2 ml of fresh phenol red-free medium was added. Per 6-well 1 μg of plasmid DNA was added to 150 μl ECL-buffer, incubated for 2 minutes and followed by the addition of 4 μl of Enhancer and another $2 - 5$ minutes of incubation. Then, 12.5 μl of Effectene were added, the whole mixture was incubated for 20 minutes at room temperature and 150 μl of the mixture was added dropwise in a spiral manner.

Via calcium chloride

HEK293 AD cells were seeded in the morning in 10 cm plates to reach a confluence of 70% 4 hours later. Then, the cells were transfected. Therefore, a mixture of 450 μl sterile H_2O, 10 μl plasmid DNA, 50 μl of $CaCl_2$ 2.5 M and 500 μl 2× BBS were mixed for the transfection of one 10 cm plate. The solution was mixed vigorously before it was incubated for 30 minutes at room temperature. 950 μl of the mixture were added dropwise to the plate and the cells were incubated for 48 hours.

Via Jet-Prime

CHO cells were seeded the evening before at a density of 80, 000 cells in 6-well plates. The next morning, the following transfection mixture was prepared. First, per well of a 6-well plate, 1 μg of plasmid DNA was added to 100 μl of Jet-Prime buffer and the mixture was vortexed. Next, 2 μl of Jet-Prime reagent were added, the solution was vortexed again and incubated for 10 min at room temperature before it was added slowly

and dropwise to the cells. [106]
If the plasmid coding for the tRNA/synthetase for the incorporation of an unnatural amino acid was transfected, a second mixture was prepared additionally. For this purpose, $2.5\,\mu l$ of $100\,mM$ trans-Cyclooctene (TCO) was mixed with $7.5\,\mu l$ of $1\,M$ HEPES buffer. This mixture was added very slowly on the edge to minimize stress for the cells. [106]

3.2.8. Preparation of supported membranes

The preparation of supported membranes was performed following the protocol from Perez et al. ([113]). CHO cells were seeded at a density of $250,000$ cells on Poly-L-Lysine (PLL) coated superclean glass coverslips with a diameter of $24\,mm$. Glass slides were coated with PLL just before the experiment. A coverslip was taken and the remaining medium was removed by touching the edge of the coverslip on a paper tissue. The coverslip was turned with the cells facing the object plate and placed on the glass slide with a small part of the coverslip standing over the edge of the object plate as illustrated in figure 3.1. The thus assembled "sandwich" was turned upside down and pressed on a paper tissue. Manual pressure was applied directly above the coverslip and on its sides (area 1 and 2 shown in figure 3.1). This assembly was left at room temperature for about one minute. The coverslip was then released by pushing the overlapping edge with a tweezers and pulling up the object plate gently to avoid breaking it. The coverslip was placed with the cell side up again in medium and was gently washed two times with PBS before proceeding with labelling.

3.2.9. Labelling

Via SNAP- and CLIP-tag

Transfected cells or membranes containing a SNAP- and/or a CLIP-tag were labelled accordingly before imaging. First, the cells were washed with PBS. Then the dye was solubilised in culture medium with a final concentration of $1\,\mu M$. The samples were incubated with the labelling solution for 20 minutes at $37°\,C$. Afterwards, the cells were washed twice with fresh medium and incubated for 5 minutes. This washing was repeated three times before imaging of the cells.

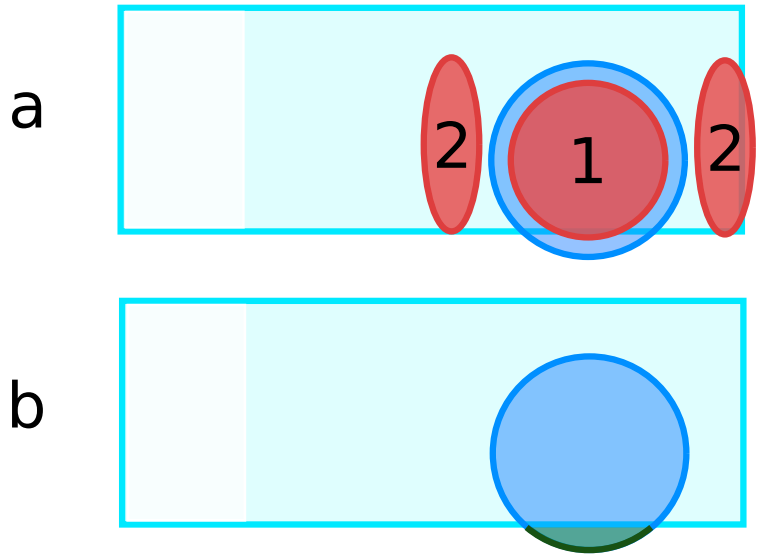

Figure 3.1.: Illustration of supported membrane preparation. a) red zones 1 and 2 show where to apply pressure; b) the green area indicates how to release the coverslip again

Via click chemistry

Click labelling was performed according to the protocol of Nikić et al.. [106] For this reason, tetramethylrhodamine (TAMRA) was diluted in complete medium. The freshly prepared mixture was added and the cells were incubated for 10 minutes at $37°\,C$. Afterwards, the coverslip was washed once with fresh medium and mounted directly in a microscopic chamber with $400\,\mu l$ medium. The protocol was later changed to three additional washing steps with 5 minutes incubation in-between, to reduce unspecific labelling.

3.2.10. Single-molecule TIRF microscopy

After labelling, the coverslip was mounted into an imaging chamber and $400\,\mu l$ of medium were added. Imaging was performed on a customised Nikon Eclipse Ti TIRF microscope. For the excitation a $561\,nm$ and a $638\,nm$ diode laser by Coherent were used, along with a quadruple band filter. If not stated otherwise, the imaging chamber was mounted on a $100\times$ oil-immersion objective (CFI Apo TIRF $100\times$, NA 1.49) and the fluorescence emission was detected by EMCCD cameras (iXon DU897, Andor). The objective was kept at $20°\,C$ via a water-cooling system (Julabo). Movies were acquired using NIS-

Elements AR imaging software (Nikon). The powers of the lasers were adjusted according to the type of experiment. The images were cropped to 448 × 448 pixels and acquired in frame transfer, resulting in a frame rate of 35 frames per second.

Binding curves of fluorescent ligands

CHO cells were transfected via Lipofectamine® 2000 for 24 hours with the respective wild-type receptor. For labelling, the fluorescent ligand was diluted in culture medium, spanning several logs of concentration to obtain a full binding curve. The cells were incubated with the ligand solution for 20 minutes and then mounted into an imaging chamber with fresh medium. Imaging was performed at $20° C$ using a 60× objective of a TIRF microscope. That way, several cells could be imaged within one frame. Pictures or short movies of at least 60 cells were obtained for each ligand concentration.
For each binding curve, negative controls were performed, either transfection of the empty expression vector or transfection of a different subtype of the receptor family, to check for unspecific binding.

Wash resistance test

CHO cells were transfected via Lipofectamine® 2000 for 24 hours with the respective wild-type receptor. The fluorescent ligand was diluted in culture medium. The cells were washed with PBS before being incubated for 20 minutes, with a concentration of ligand $\approx 100 \times k_D$ value, and then mounted into the imaging chamber with $400\,\mu l$ of medium. Imaging was performed using a 60× objective at a TIRF microscope. A frame with several labelled cells was recorded with a laser power of 15%. The cells were then carefully washed once with medium while mounted at the microscope. At this step care was taken to avoid touching of the chamber and coverslip. After washing, the focus was adjusted again on the cells using low laser intensity (2-3%) and then one frame was recorded every minute at 15% laser power.
As a bleaching control a movie was obtained without washing using the same laser power (15%).

3.2.11. Single-molecule FRET experiments

After the preparation of supported membranes (section 3.2.8), the cells were washed once with PBS and then treated for 30 minutes with apyrase to degrade all nucleotides. Next,

the supported membranes were labelled with the fluorescent dyes, as described above. To prevent bleaching and blinking in the smFRET experiments, an oxygen scavenging system was used. The smFRET buffer was prepared fresh by addition of glucose oxidase and catalase to a final concentration of $25\,U/ml$ and $250\,U/ml$ respectively. From this mixture, $200\,\mu l$ were added in the centre of an object plate. The coverslip with the labelled supported membranes was inverted and shortly touched on the edge of a tissue paper to get rid of surplus medium. Then, by approaching with the coverslip to the drop of smFRET buffer, the buffer spread below the coverslip, and the coverslip was centred on the glass slide. The excess of buffer was removed by shortly touching with a paper tissue on the edge of the "sandwich". Last, nail polish was used to seal the sample (preferably fast drying nail polish). In this way, the probe was shielded from new oxygen entering and the oxygen scavaging system could work effectively. When the nail polish dried, imaging started immediately.
The imaging was performed with the same Nikon TIRF set-up as described above. A laser power of 15% was used for SNAP549 and CLIP647 each. Supported membranes with a single-molecule level were searched for using the $639\,nm$ laser, with the laser power at 3% to minimize photo bleaching. If a cell patch was found, first a movie was recorded, imaging both acceptor and donor channel simultaneously, while exciting the donor, SNAP 549. Second, a control movie of the acceptor excitation was acquired.
When apyrase treatment was performed, nucleotides (GTP, GTPγS or GDP) or ligands (Noradrenalin or Yohimbine) were added to the smFRET buffer.

3.2.12. Ensemble FRET

HEK293 AD cells were seeded on PLL coated clean glass coverslips with a diameter of $24\,mm$. After a transfection via effectene for 48 hours, the cells were prepared for imaging. If they contained SNAP- and CLIP-tags, they were labelled accordingly. Before imaging, the cells were washed with PBS and then fresh complete medium was added. The coverslip was mounted in an imaging chamber and washed 3 times with FRET buffer. The such prepared sample was mounted on the FRET set-up described at section 6.1.2, after a drop of immersion oil was dispensed on the objective. The cells were focused using dim bright light. Long flashes of the excitation wavelength were used to search cells with a high expression level on the membrane, which were then centred on the assembled screen. The perfusion tip was carefully placed, so that the flow was not wash

away the cell before the measurement was started using an excitation of $10/100\,ms$. During the experiment, different solutions were perfused to the cell using the perfusion system controlled by a key board.
At the end of each measurement, a bleed through control was added by switching to the excitation wavelength and filter set for the acceptor.

3.2.13. GTPγS assay

Cells were cultured in 10-cm plates and co-transfected via calcium chloride with plasmids for the receptor of interest, G_i, G_β and G_γ. As a negative control, additional plates were transfected with the empty expression vector using pcDNA. As a positive control, the wild-type receptor was also transfected with the G-proteins. In addition, a general control to estimate the transfection efficiency for the calcium transfection, one plate was transfected with EYFP, which was checked after 48 hours at a fluorescence microscope. If the transfection efficiency was above 30-40%, cells were put on ice and lysed by adding $5\,ml$ lysate buffer per plate. The cells were collected with the help of a rubber policeman and collected in a Falcon tube, where they were homogenised using a blade homogeniser (Ultra Turrax). The lysates were centrifuged for 3 minutes at $850\,rpm$ and $4°\,C$. The supernatant was centrifuged again with a ultracentrifuge for 40 minutes at $37,000\,rpm$ and $4°\,C$. The pellet was solubilised in $1\,ml$ binding buffer and grinded 5 to 10 times using a glass potter. The protein quantification was performed using the Biorad protein assay.
Each transfection was divided into 3 groups: one unstimulated, one with $100\,\mu M$ GTP and one stimulated with $100\,\mu M$ norepinephrin (NE). For each group, triplicates for 6 different reaction times were measured: $0\,s$, $15\,s$, $30\,s$, $60\,s$, $120\,s$ and $300\,s$, resulting in 18 samples per group. For each sample $10\,\mu g$ of membranes were used and GTPγS with an average radioactivity of $120,000\,cpm$. This amount corresponds to $0.0545\,\mu Ci$ giving the relation:

$$2.2\ \times\ 10^6\,cpm \mathrel{\widehat{=}} 1\,\mu Ci \tag{3.1}$$

Glass fibre prefilters were soaked in MilliQ water. The calculated amount of radioactive GTPγS was solubilised in binding buffer. The sample tubes were filled with binding buffer beforehand. The reaction was started in a separate tube by adding the GTPγS and mixing. At the respective time points, samples were taken and put on ice to stop the reaction. Afterwards, the samples were transferred onto a pump assembly to run

through the filters. The filters were then washed 3 times with binding buffer before they were put into scintillation tubes. The tubes were filled with $8\,ml$ of scintillation oil and the radioactive samples were measured in a liquid scintillation analyzer (Tri-Carb® 2910 TR Perkin Elmer) each for 5 minutes.

3.2.14. Lysis

Confluent plates of the transfected cells were taken and incubated for 10 minutes with $1\,ml$ of fresh RIPA buffer. Then, the cells were scraped and the lysate was filled into an Eppendorf tube. After three pulses of sonification, each of 15 seconds, the lysate was centrifuged for 30 minutes at $10,000\,rpm$ at $4°\,C$.

3.2.15. Western blotting

For western blotting, 10 % SDS gels were mounted in an electrophoresis chamber filled with running buffer. Before loading, the samples were mixed with $5\times$ Laemli buffer. The electrophoresis was started at $80\,V$ for 20 minutes, and then increased to $150\,V$ and run until the blue Laemli reached the lower end of the gel. The PVDF membrane was activated for blotting by an incubation in methanol for 10 minutes. While building the blotting casette, care was taken to have the correct order and orientation of gel, PVDF membrane and electric poles.

The assembled blotting cassette was mounted in the blotting chamber filled with transfer buffer, and an additional cooling akku. Blotting was done at $100\,V$ at $4°\,C$ for 50 minutes. Next, the membrane was blocked for 1 hour in 2.5% dry milk followed by an incubation overnight with the primary antibody. The following morning , the membrane was washed three times for 10 minutes each with washing buffer. Then it was incubated for 1 hour with the secondary antibody and again washed 3 times for 10 minutes each with washing buffer. A luminol mixture was prepared and spread on the membrane incubating for 1 minute. Finally, the membrane was developed.

3.2.16. Data processing

Single-molecule movies

Movies from single-molecule experiments were sorted for low expressions levels, good focus and high signal-to-noise ratio. The thus selected movies were prepared for the

automated particle detection and tracking in Matlab. Therefore, a mask was drawn in Fiji is just ImageJ (FIJI) around the cell or membrane patch that should be tracked. The movies were then analysed with customised scripts, based on the tracking algorithm developed by Jaqaman et al. [75]. If further analysis was performed, this will be described in the corresponding results section.

Ensemble FRET

The data from ensemble FRET experiments was analysed in Origin (from OriginLab Corporation). For each measurement the direct excitation peak for the acceptor was taken to correct the overall measurement for bleed through and false direct excitation by calculating:

$$F_{\text{trueAcc}} = F_{\text{Acc}} - F_{\text{Don}} \cdot b - d \cdot E_{\text{Acc}} \tag{3.2}$$

Where F_{trueAcc} is the corrected acceptor fluorescence emission, F_{Acc} is the measured fluorescence acceptor emission, F_{Don} is the measured donor fluorescence emission, b is the bleed through correction factor, d the direct excitation correction factor and E_{Acc} the fluorescence emission measured for the acceptor control in each experiment.
The correction factors were determined previously for the FRET set-up. For the FRET ratio, the acceptor emission is divided by the donor emission. The ratio was then normalised and plotted over time. The changes according to stimulation could be determined directly.

Binding curves

To obtain the mean intensity for each cell, a mask of the cell shape was created in FIJI. The background intensity was subtracted. At least 50 cells per condition from three independent experiments were taken. Per concentration, all cells were averaged and the standard error of the mean (SEM) was calculated. Intensity values were normalized to those obtained with the highest concentration ($10\,\mu M$). Data were fitted to a one site ligand binding model with Hill slope of 1 in Prism 6 (GraphPad Software Inc.).

Washout curves

The acquired image sequences of the washout experiments were analysed using FIJI. A region of interest (ROI) was manually defined for each cell and its background-subtracted average intensity was measured. The intensity values were normalised to the starting intensity. Data were plotted and fitted to a one-phase exponential decay in Prism 6. The curve for Cy5 was corrected for bleaching as it showed 21 % photo bleaching in 20 frames. For this reason the intensities from the bleaching control movie were fitted linearly in Origin, and the values were added to the measured intensities of the washout experiment.

Part I.

Part I - Characterisation and application of novel fluorescent ligands for opioid receptors

4. Results

As mentioned above (section 1.6.3), fluorescent ligands can be used to label and investigate GPCRs. A set of fluorescent ligands was generated by Prof. Michael Decker's group. Two sub-type selective MOR ligands, containing 14β-(p-nitro-cinnamoylamino)-7,8-dihydrocodeinone (CACO), were synthesised by Christian Gentzsch and a pair of fluorescent ligands for DOR was synthesised by Antonios Drakopoulos, based on the antagonist naltrindole. The respective structures are shown in 4.1.

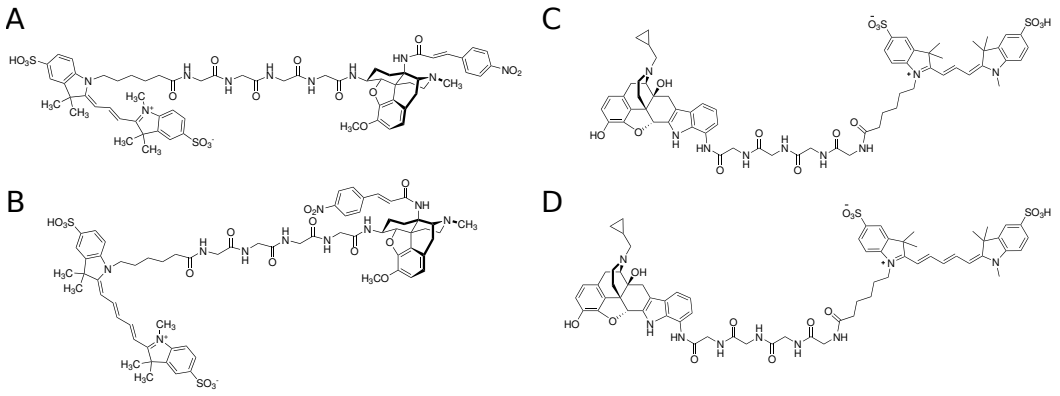

Figure 4.1.: The structures of the synthesised fluorescent ligands. A and B compounds from Christian Gentzsch for μOR. Both have as parent compound CACO. A tetraglycin functions as linker to A) a Cy3 and B) a Cy5. C and D compounds from Antonios Drakopoulos for δOR. Both have as parent compound naltrindole. A tetraglycin functions as linker to C) a Cy3 and D) a Cy5.

4.1. Investigating the binding affinity of the new ligands

The compounds provided by Prof. Decker's group all showed a good selectivity and high signal-to-noise ratio in first tests. This made them applicable for investigations using fluorescent microscopy techniques. A crucial question, when applying changes to the structure of a ligand, is whether or in which regards the structural changes translate into pharmacological changes. Hence I performed binding experiments to determine the affinity of the ligands.

CHO cells were transiently transfected with wild-type MOR or DOR for 24 h and afterwards incubated for 20 min each with 8 different concentrations of the fluorescent compounds. The concentrations were chosen to cover a range that would allow to reach a plateau for low binding and a saturation plateau for 100 % binding. For each concentration at least 40 cells were measured. Three individual experiments were acquired for each compound, each normalised to the highest concentration, and all three thus obtained binding curves were averaged and fitted with a logarithmic dose response curve in Prism. The results are shown in figure 4.2. The fitting gave a k_D of 87.29 ± 49 nM for Caco-Gly4-Cy3 and of 295.2 ± 141 nM for the Cy5 variant with $R^2 = 0.8573$ and 0.9149 respectively.

The same analysis was performed for the compounds for the DOR giving $k_D = 2.265 \pm 0.753$ nM and $k_D = 5.673 \pm 1.931$ nM for Anti-Delta-Cy3 and Anti-Delta-Cy5 respectively with R^2 of 0.9595 and 0.9644.

Thus, the attachment of the fluorophores via a linker indeed leads to changes in the pharmacological properties compared to the parent compounds.

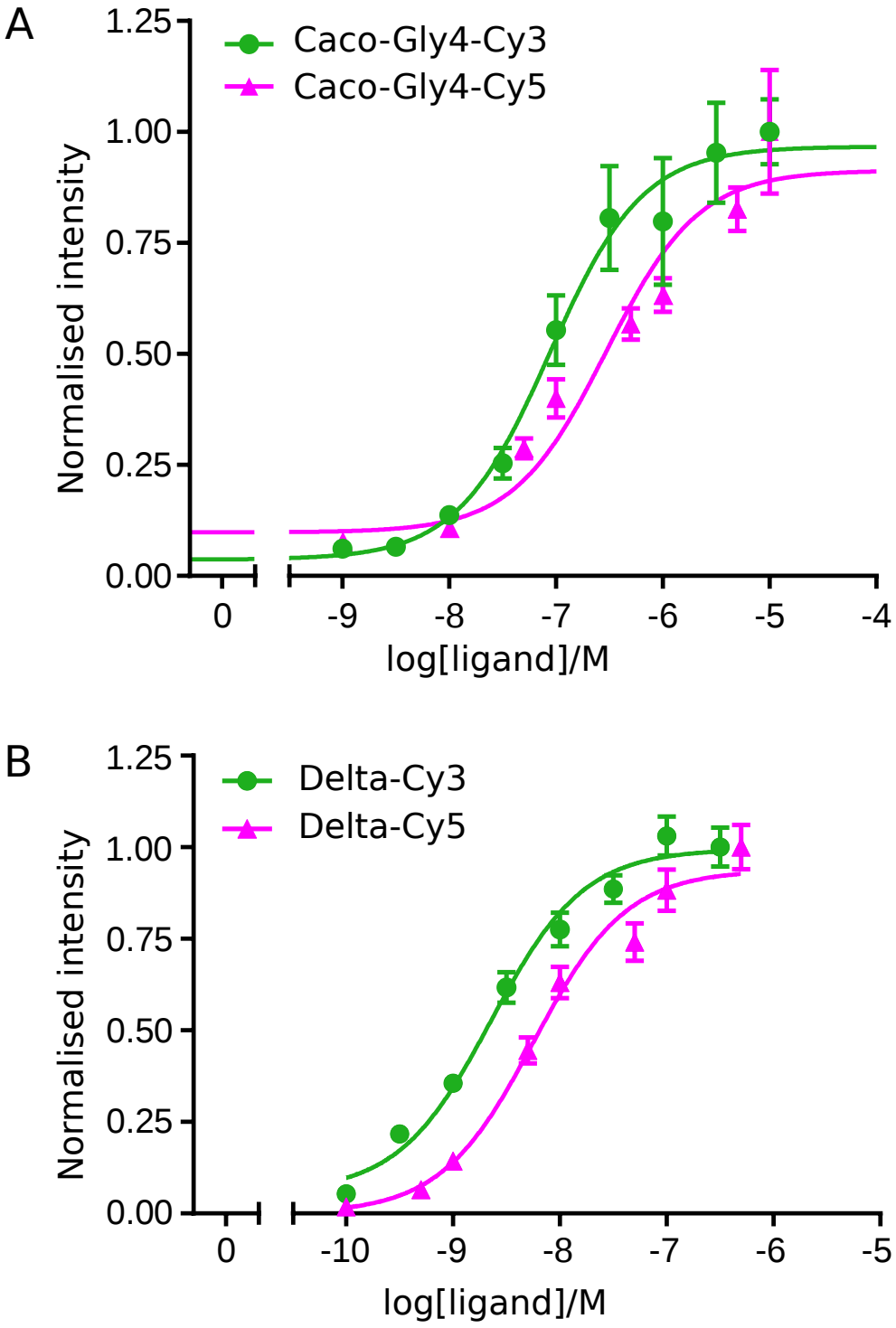

Figure 4.2.: Binding curves of the fluorescent ligands. A) shows the compounds for the μOR, the Cy3 variant in green, Cy5 in magenta. B) are the binding curves for the δOR compounds, Cy3 again in green and Cy5 in magenta. All curves are fitted with a sigmoidal curve and the SEM are shown for all concentrations. The mean represents three independent binding experiments for all curves.

4.2. Do the ligands possess wash resistance?

As the parent compounds were reported to show some wash resistance, I wanted to assess how the chemical modifications changed this property. The experiments were performed with transiently transfected CHO cells. One picture was taken before the cells were washed while mounted on the microscope and then another picture was taken once every minute. As a control for bleaching a movie of 20 frames was obtained using the same laser power. In case of Caco-Gly4-Cy5, the wash-out curve was corrected for the bleaching derived from the control movie, as it contributed significantly. The average intensity of the same cells was normalised to the initial intensity and fitted with a one-exponential decay in Prism as shown in figure 4.3. It was observed that the compounds wash out fast in the first few minutes and then slow down reaching a plateau. The loss of fluorescence intensity can be seen already by eye in panel A of figure 4.3, showing the same cells over the course of 12 minutes. In the case of Caco-Gly4-Cy3, $34 \pm 4\,\%$ of the ligand stays bound ($R^2 = 0.9932$) and for Caco-Gly4-Cy5 $54 \pm 3\,\%$ ($R^2 = 0.9805$).
From the two compounds for DOR the ligand linked to Cy3 was tested for wash resistance in this work. Anti-Delta-Cy3 reaches a plateau at $69 \pm 3\,\%$ with a $R^2 = 0.9884$ as shown in figure 4.4. The Cy5 variant was measured by the collaboration partner Antonios Drakopoulos and he could obtain a wash resistance of $93 \pm 1\,\%$ with $R^2 = 0.8095$ (data not shown).
This proves that the chemical modifications also lead to changes in the wash resistance, while still preserving the overall property. Interestingly in both cases the compound containing Cy5 shows a significant higher wash resistance than the compounds with Cy3.

4.3. Single-Molecule experiments to unravel the diffusion behaviour

Since all the different compounds showed a good signal-to-noise ratio and suitable photophysical properties, I applied and used them for single-molecule imaging. Transiently transfected CHO cells with wild-type MOR or DOR, respectively with an average receptor density of approximately 0.85 receptors/μm^2 for MOR and 1.18 receptors/μm^2 for DOR were used. Thus, the expression level was low enough to perform automated

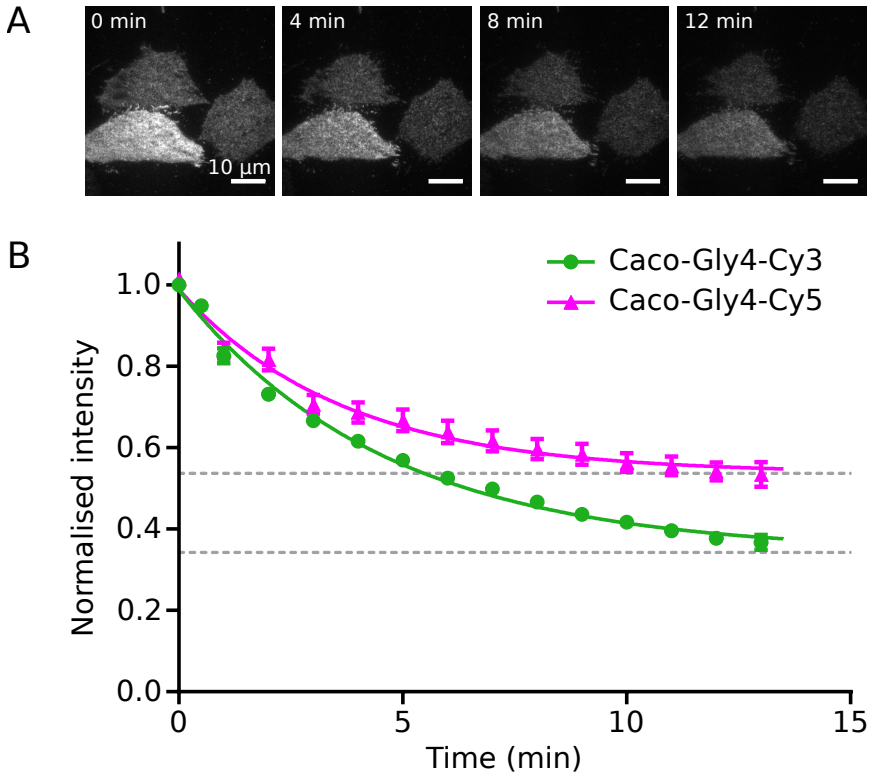

Figure 4.3.: Wash resistance of the μ OR ligands. A) shows labelled cells after one wash. The decrease of fluorescence intensity was clearly observable by eye. B), washout curves. The values are fitted to a one exponential decay showing that both compounds reach a plateau. The plateau for the Cy3 compound (shown in green) is 34 % whereas Caco-Gly4-Cy5 (magenta) reaches a plateau at 54 %. Points are averaged over 12 cells out of 4 individual experiments, shown with SEMs.

particle detection and tracking. The scripts used in our lab are based on the algorithm presented by Jaqaman et al. in [75] and customised for our purposes. After tracking, the obtained trajectories were analysed for the time-averaged mean squared displacement (TAMSD), allowing to categorise the particles into the different classes of motion. In the case of MOR, the cells were incubated with Caco-Gly4-Cy3. Even though the compound showed less wash resistance, Cy3 is more photostable allowing longer observations of individual particles. Due to wash-out of the ligand over time (the compound possesses a wash resistance of only 34 %), the cells were just imaged in the first $4-5$ min after mounting in the imaging chamber. The analysis revealed that 22 % of MOR are virtually immobile, 34 % show sub-diffusive behaviour, another 34 % diffuse normally and 10 % show super-diffusion.

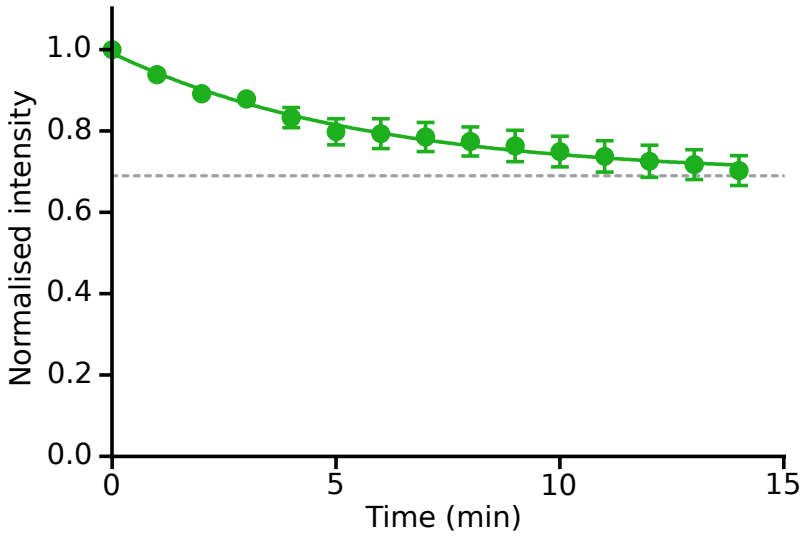

Figure 4.4.: Wash resistance of the δ OR ligand with Cy3. The values are fitted to a one exponential decay showing that the compounds reaches a plateau of wash resistance at 69 %. Points are averaged over 12 cells out of 4 individual experiments, shown with SEMs.

The fluorescent ligands for DOR exhibits a higher wash resistance, nevertheless the samples were not imaged longer than 10 min. Else, the number of trajectories that are prematurely ended by ligand dissociation or bleaching would be to high. Again, the variant with Cy3 was chosen for the same reasons mentioned above. The DOR shows heterogeneous diffusion behaviour as well, with 27 % being virtually immobile, 38 % being sub-diffusive, 27 % normally diffusing and 9 % of receptors being super-diffusive.
The novel fluorescent ligands were successfully applied to investigate the diffusion of the two subtypes on a single-molecule level. In both cases, the diffusion behaviour is heterogeneous but similar amongst the subtypes.

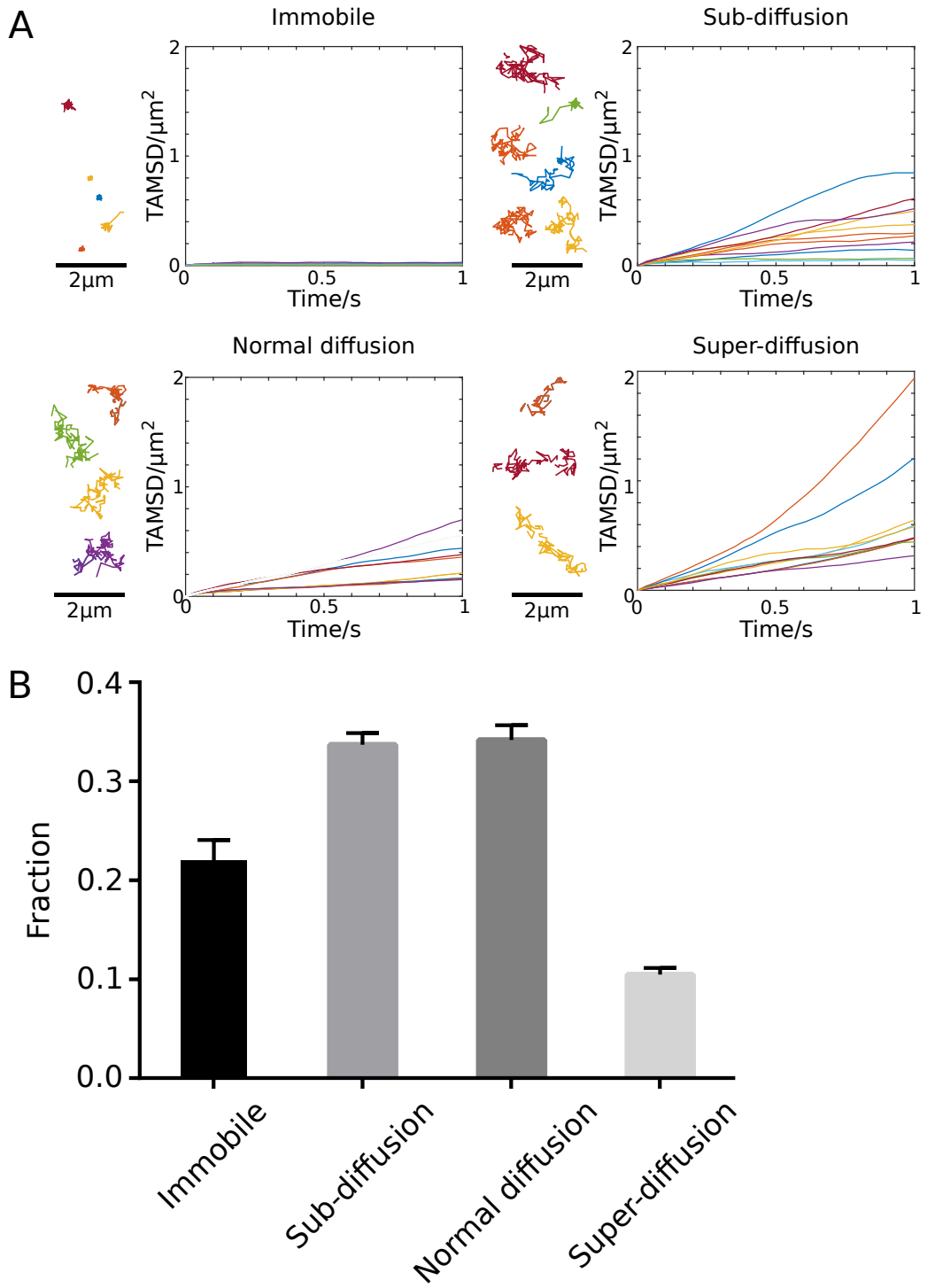

Figure 4.5.: Time-averaged mean squared displacement analysis for μOR. A) shows example trajectories and the corresponding TAMSD curves for the four categories of diffusive behaviour. B) shows the fractions of all four categories. 2225 individual particle trajectories were analysed from 29 different cells.

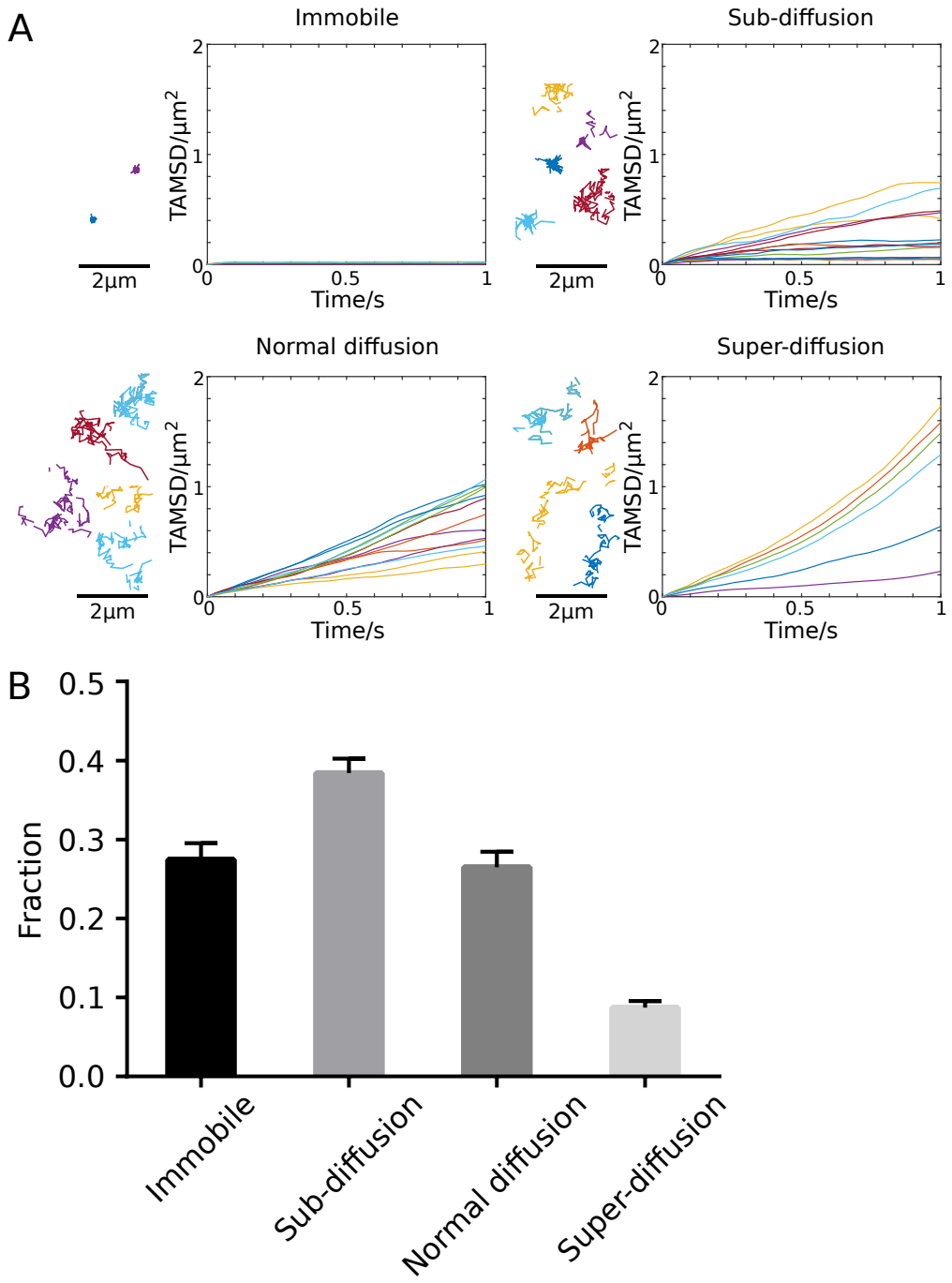

Figure 4.6.: Time-averaged mean squared displacement analysis for δOR. A) shows example trajectories for the four categories of diffusive behaviour and the corresponding TAMSD curves. B) shows the fractions of all four categories. The TAMSD was calculated from over 1103 individual trajectories taken from 31 different cells.

4.4. Investigation of dimerisation

To look at possible homodimers of μ opioid receptors, CHO cells were transiently transfected with the wild-type receptor and after $5 - 6$ h labelled with a mixture of both fluorescent MOR ligands, Caco-Gly4-Cy3 and Caco-Gly4-Cy5. To achieve roughly similar labelling for both colours, the concentrations were adjusted to 1 μM for Caco-Gly4-Cy3 and 0.5 μM for Caco-Gly4-Cy5. The detected density for the Cy3 channel was on average 0.9 ± 0.08 receptors per μm^2 and for Cy5 0.8 ± 0.05 receptors per μm^2. As for the one colour experiment, care was taken to only image within the first minutes after mounting, to reduce the effect of wash-out. TIRF imaging movies were acquired simultaneously in both emitting channels.

The thus acquired movies were analysed using automated particle detection and tracking. After tracking, of both channels individually, further analysis was employed to check for colocalisation using a customised Matlab script. The colocalisation and all following analysis were performed in collaboration with Dr. Yann Lanoiselée (AG Calebiro, Institute of Metabolism and Systems Research, University of Birmingham). Both channels were aligned correctly using images of fluorescent beads, which were imaged before each experiment, allowing corrections of possible distortions or translations later on. The result of the colocalisation script is an interaction matrix for all colocalisations, as there is no possibility to distinguish between random colocalisation or 'real' colocalisation due to protein-protein interaction. In mathematical terms the true interactions are convolved with random colocalisations, and the end result is a mixture containing all colocalisations.

To separate between random colocalisations and true interactions, to 'deconvolve' them, a monomeric control was measured using CD86. [38, 114, 115] This monomeric membrane protein is not expected to interact with MOR. CD86 was co-transfected with wild-type MOR bearing a N-terminal SNAP-tag. For two colour TIRF imaging the receptors were labelled with SNAP 647 and Caco-Gly4-Cy3 respectively. Imaging and analysis was done as described for the MOR-MOR cases. The interactions derived from CD86-MOR are random, as no productive interactions should occur. Thus it is now known what a colocalisation matrix looks like, if only random colocalisations are observed. In the next step, the interaction matrix obtained from MOR-MOR was deconvolved with the one from the control, CD86-MOR, using the Lucy-Richardson deconvolution. [116] This gives an estimate of colocalisations that are due to real interactions. The raw and

deconvolved data are shown in figure 4.7 A. In 4.7 B an exponential decay was fitted to the fraction of true interactions, $F_r(t)$, using

$$F_r(t) = F_{\text{true}} e^{-(k_{\text{off}}+k_{\text{loss}})t} \tag{4.1}$$

it was thus possible to derive $k_{\text{off}} = 0.557 \pm 0.207\, s^{-1}$. Furthermore, the exponential time constant τ was calculated to be $1.797 \pm 0.487\,\text{s}$. The association rate can be expressed as

$$\frac{d[D]_\rho}{dt} \cdot F_{\text{true}} = k_{\text{on}}[\mu_1]_\rho[\mu_2]_\rho \tag{4.2}$$

where $[\mu_1]_\rho$ and $[\mu_2]_\rho$ are the monomer densities in each channel and $d[D]_\rho/dt$ the rate of new colocalisations per area unit of area.
Assuming that at a long time scale, the formation and the dissociation rates reach an equilibrium, the dimer density can be calculated as:

$$[D]_\rho = \frac{1}{k_{\text{off}}} \frac{d[D]_\rho}{dt} \cdot F_{\text{true}} \tag{4.3}$$

giving a fraction of dimers of $4.45\,\%$. The association rate k_{on} was then calculated using:

$$k_{\text{on}} = \frac{\frac{d[D]_\rho}{dt} \cdot F_{\text{true}}}{\left([Ch1]_\rho - \frac{1}{k_{\text{off}}} \frac{d[D]_\rho}{dt} \cdot F_{\text{true}}\right)\left([Ch2]_\rho - \frac{1}{k_{\text{off}}} \frac{d[D]_\rho}{dt} \cdot F_{\text{true}}\right)} \tag{4.4}$$

where $k_{\text{on}} = 0.020 \pm 0.004\,\mu\text{m}^2\text{molecule}^{-1}s^{-1}$. Here the monomer densities are not measured directly but calculated using the estimated dimer density from eq. 4.3

As a lot of receptors seem to stop while colocalising with another receptor, I checked the possibility of colocalisation with clathrin coated pits (CCPs). To that end, I performed the same set of experiment as described above but with co-transfection of GFP-clathrin. The 200 frames recorded of the clathrin channel were stacked and the CCPs were automatically located and fitted with a 2D Gaussian giving an estimated width L for each individual pit. All receptor-receptor interactions that lasted longer than 20 frames (560 ms) were checked for colocalisation with a CCP. If one of the interacting receptors was localised once within the L of a pit, the whole receptor-receptor interaction was counted as 'inside' a pit. If the interacting receptors were never localised within any L of any pit, then the interaction was attributed to be 'outside' of CCPs. Because

CCPs are diffraction limited, the length L is larger than the actual size of the pits, therefore the fraction of inside pits was over-estimated, rather than under-estimated. Still the analysis showed that $77 \pm 9\,\%$ of receptor-receptor interactions happened outside of CCPs, whereas $23 \pm 9\,\%$ colocalise with a CCP, shown in figure 4.8.
Taken together, it could be determined that at a single-molecule level a small but persistent fraction of MOR is present as homodimers. Furthermore, the majority of those homodimers is present outside of CCP. It can be concluded from the analysis, that those interactions are true and not an artefact of random colocalisation or internalisation processes.

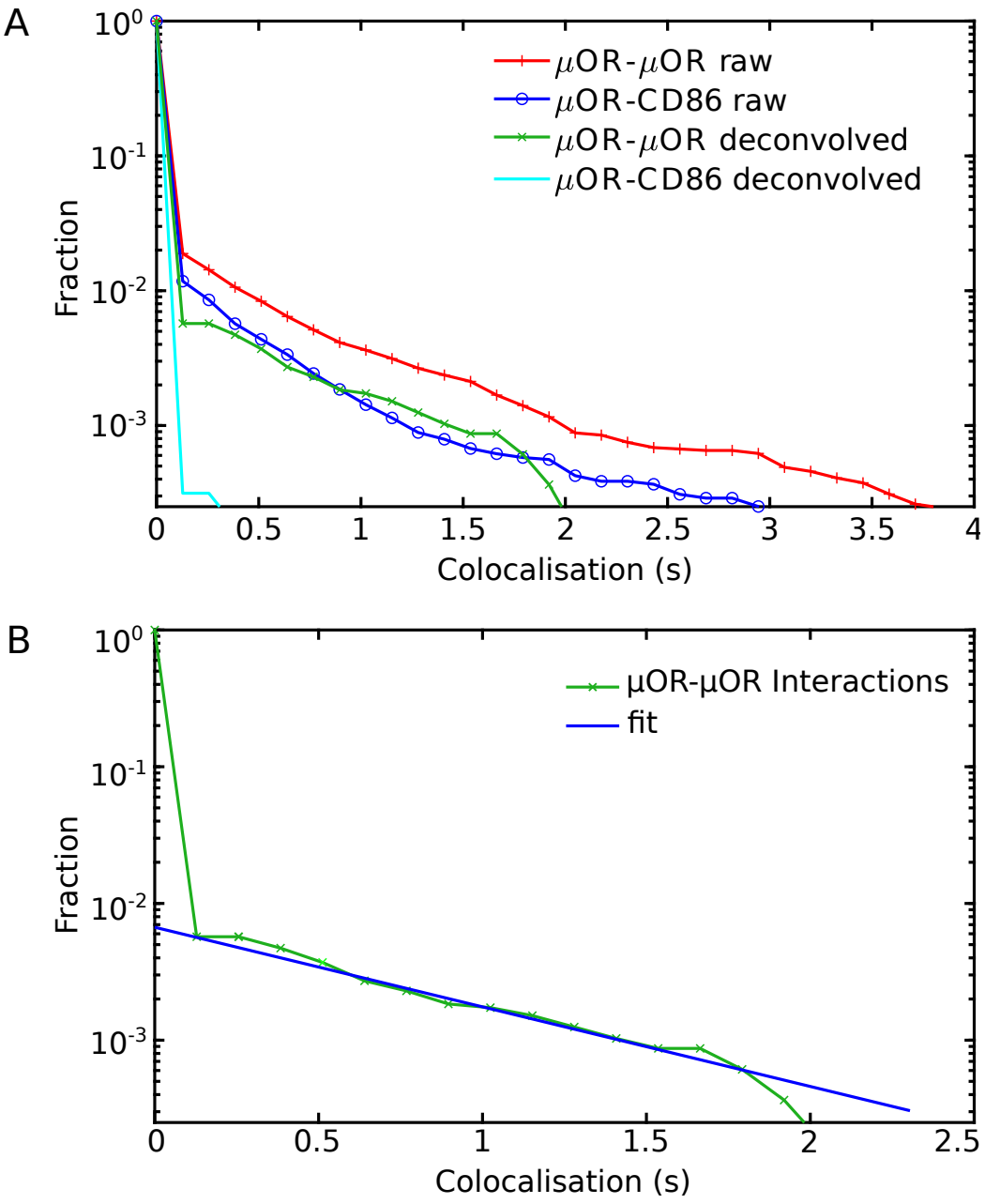

Figure 4.7.: Results of the deconvolution. In A) the raw data of colocalisations of μOR with μOR is shown (red). As a control the colocalisations of CD86 with μOR was measured (blue). The raw data of μOR-μOR deconvolved with the CD86 control is shown (green). The control deconvolved with itself should give in the optimal case a single peak at 0 (cyan), here it is close enough. B) shows the deconvolved, meaning 'true' interactions, which were fitted giving a tau of $1.797 \pm 0.487\,\mathrm{s}$

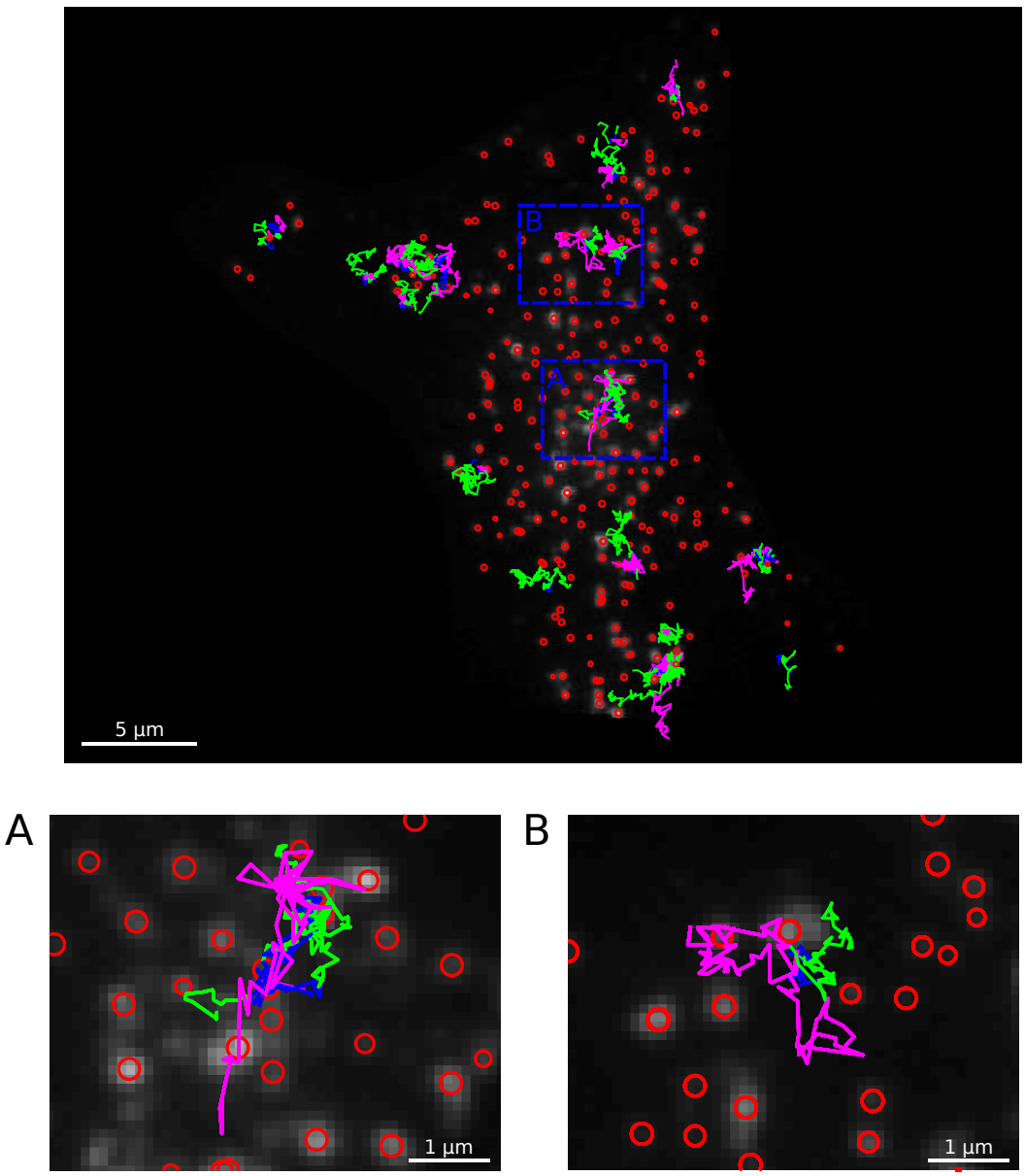

Figure 4.8.: Shown is a representative cell with tracked interactions overlaid on the clathrin channel. Receptor-receptor interactions are shown in blue, receptors bound to Caco-Gly4-Cy3 are depicted in green and bound to the CY5 variant in magenta. The clathrin channel is represented in a heat map in grey scale with lighter colour corresponding to higher amounts of GFP-clathrin. The red circles indicate the located and fitted CCP. Inset A) shows very long receptor-receptor interactions which colocalise even with several pits. In B), a typical interaction is visualised, where the monomers diffuse normally and stop while interacting, but in this case outside of CCPs.

5. Discussion

5.1. The set of new fluorescent ligands is specific and easily detectable

The new fluorescent ligands for MOR and DOR were designed to be applicable for fluorescent microscopy methods and to be sub-type selective. In a first test, CHO were transiently transfected with wild-type MOR or DOR . With TIRF imaging it was possible to achieve a high signal-to-noise ration so that the ligands attached to either Cy3 or Cy5 are easily detectable.
For the sub-type selectivity, both,the CACO and the naltrindole compounds were tested on untransfected cells, as well as CHO cells transfected with the other sub-type. The CACO fluorescent ligands only bound to cells expressing MOR while the naltrindole compounds only labelled cells expressing DOR. Saturation binding experiments by a collaboration partner in Montpellier (group of Sébastien Granier) confirmed the high sub-type selectivity as well.
Thus, it was confirmed that the chemically modified ligands retain properties of the parent compounds, like the high sub-type selectivity, but also that the attached fluorophores, Cy3 and Cy5, make them suitable for TIRF imaging.

5.2. Conjugation of linker and fluorophore changes properties of the pharmacophore

CACO was previously reported by others as a sub-type selective, high affinity MOR ligand with a k_D of 0.52 ± 0.14 nM. [117] After the conjugation of tetraglycin as a linker and Cy3 as fluorophore, not only the structure is changed, but also pharmacological

properties. In figure 4.2 A both compounds, with either Cy3 or Cy5, show a loss in affinity. With k_D values of 87.29 ± 49 nM and 295.2 ± 141 nM respectively, the compounds loose some of the affinity but retain a dissociation constant in the nM range.
Furthermore, McLaughlin et al. reported a wash resistance of 50 % for CACO using [D-Ala^2, *N*-MePhe^4, Gly-ol]-enkephalin (DAMGO) for inhibition binding experiments. [117] For the new ligands, the compound attached to Cy3 shows a small loss in wash resistance to 34 ± 4 %, whereas CACO attached to Cy5 retains it's property with 54 ± 3 %. The differences to the parent compound CACO can be explained through the chemical modifications - the Cy3 and Cy5 dyes both increase the size of the compounds. Nevertheless, the pharmacophores show decent pharmacological and photophysical properties, making them suitable for single-molecule microscopy applications.
The same conclusion is true for the compounds designed for the DOR. They display very high affinity with a k_D in the one digit nM range for both, the Cy3 and the Cy5 compound. Thus, they experienced only a minor loss in comparison to the parent compound naltrindole with $k_D \approx 0.2$ nM. [118] Similar to the MOR compounds the naltrindole ligands possess wash resistance and as for MOR the Cy3 derivative has a lower wash resistance (69 %) than the Cy5 compound with outstanding 93 %. With such a high wash resistance, the ligand is nearly comparable with covalent labelling systems such as the SNAP-tag.[38]

In general, it seems that wash resistance is a neglected property of fluorescent ligands, as it is not expected to occur. To the best of my knowledge, the BODIPY derivative of CACO is the only fluorescent MOR ligand reported to show wash resistance with 95 %. [119] This could be due to several factors. First, the ligands are not tested for wash resistance, as it is not expected and might not show any relevance for the design of the respective method, that the ligand is designed and used for (e.g. if the downstream signalling is investigated, GTPγS binding for example). Second, wash resistance could prove disadvantageous in competition binding assays or other dynamic comparisons of ligands, and thus only fluorescent ligands without wash resistance properties, and that are fully reversible, are reported. Third, there could be a problem in quantification of the wash resistance, as it is often observed qualitatively and not quantitatively. [117, 120, 121] Fourth, the wash resistance may be observed, but the advantage is not. Therefore, this property is not reported and no efforts are made to improve the wash resistance of fluorescent ligands.

For single-molecule imaging and tracking, it is advantageous to have wash-resistant fluorophores, as most labelling protocols include washing steps before the actual imaging. This led, for example, to the development of labelling tags like SNAP and HALO (see section 1.6). Those tags form irreversible covalent binding and lead to an extreme high wash resistance. The disadvantage of those tags, however, lies in their need to be encoded with the protein of interest, therefore differing from the wild-type receptor. In contrast, wash-resistant fluorescent ligands have the advantage of not needing chemical modifications of the protein itself while only the ligand is changed.

5.3. The opioid receptors show a heterogeneous diffusion behaviour

After proving that the two sets of selective fluorescent ligands possess suitable properties, they were applied in single-molecule imaging. As Cy3 is more photostable than Cy5, the compound Caco-Gly4-Cy3 was chosen for one colour experiments to investigate the diffusion behaviour of wild-type MOR in CHO cells. The results show that 22 % of receptors are virtually immobile. This means that a substantial fraction of receptors does not show high mobility, as their movement is negligible in comparison to other diffusive behaviours or is even so small that it cannot be resolved with our application. [74, 78, 122] One reason could be that the particle stops for interactions with other proteins, or that the receptors are trapped in a CCP and will be internalised soon. Some receptors in the virtually immobile fraction may also be due to false detection, for example if spots from the background are detected as receptors by the automated detection and tracking scripts. For DOR labelled with naltrindole-Cy3, the fraction of receptors showing nearly no diffusion was even higher, at 27 %.
Sub-diffusive motion was observed for 34 % of MOR and 38 % of DOR. Sub-diffusive behaviour can arise from different effects, and means that over long periods of time the particle is exploring less space than expected for normal diffusion, hence it's a form of anomalous diffusion. This can for example be due to interactions with the environment, or because the membrane is too crowded. 34 % of the MOR and 27 % of the DOR showed normal diffusion with an average diffusion coefficient of $0.12\,\mu m^2 s^{-1}$ and $0.15\,\mu m^2 s^{-1}$ respectively.

This leaves a fraction of 10 % for the MOR and 9 % for the DOR being super-diffusive. Super-diffusion is also a form of anomalous diffusion and could for example be directed motion. The results are comparable to previous findings from our lab for the α_{2A} adrenergic receptor with 6 % of the receptors being super-diffusive. [74]
Important to note is that the ligand might influence the diffusion behaviour of the receptor. Tabor et al. demonstrated that different ligands influence the fraction of dimers formed, as well as the diffusion coefficient of the receptors. [37] In the case of the dopamine receptor, an antagonist increased the fraction of dimers and at the same time slowed down the receptors, resulting in a lower diffusion coefficient. For both sub-types of the opioid receptors, the fluorescent ligands were, at least long-term, antagonistic. This could explain the higher fractions for virtually immobile and sub-diffusive motion in comparison to the α_{2A} AR reported by Sungkaworn et al., as the receptors could be involved in dimer formation and dissociation. [74] In addition, the difference in ligands can explain the difference between MOR and DOR - naltrindole is a pure antagonist, whereas CACO is a short-term agonist and a long-term antagonist.
In a very recent study, Metz et al. investigated the mobility of MOR in AtT20 cells stably expressing FLAG-tagged MORs labelled with quantum dots. [123] In the basal state, Metz et al. observed that 33 % of receptors were virtually immobile, which is significantly higher than the 22 % of the present study. [123] This can be explained by the usage of quantum dots, which were proven to slow down the diffusion of receptors. [124, 125] As described above, the presence of a ligand can also alternate the diffusion behaviour. This was confirmed in the study of Metz et al., as they measured the mobility under basal condition, after 1 minute treatment with DAMGO or morphine, and after 10 minutes treatment with those agonists. In the case of DAMGO, the fraction of immobile receptors decreases significantly after 1 minute treatment, and then increases above the basal level after 10 minutes. This is a good indicator, that the mobility is strongly dependent on the ligand, as well as on the time the receptor is exposed to the ligand. Morphine on the other hand did not change the fraction of immobile receptors after 1 minute but increased it after 10 minutes. It thus clearly indicates that the nature of the ligand, and which signalling pathway it triggers, has an influence on the diffusion behaviour. This was highlighted before by Melkes et al. using fluorescence recovery after photobleaching (FRAP) on MOR in the presence of different biased ligands. [126]
A further explanation for the higher fractions of virtually immobile receptors in the study of Metz et al. could be the different cell model. The mobility of receptors strongly

depends on the membrane and how compact it is - the more densely packed, the slower the particles, and the more sub-diffusion or even confined and immobile receptors can be observed.

5.4. The mu opioid receptor is mostly monomeric

As discussed in the introduction (section 1.3 and 1.4), dimerisation plays an important role and is widely discussed for opioid receptors. Many studies were performed using diverse techniques and different models which lead on the one hand to findings favouring dimers [65, 66, 51, 67, 45, 68, 69] and on the other hand to findings favouring opioid receptors as monomers [63, 64]. The level of dimers can have an effect on the downstream signalling or even trigger different pathways or internalisation processes, and thus influence the pharmacological response. A better understanding of dimerisation, especially for the MOR, could lead to the development of pain killers with less side effects.
To investigate the possibility of MOR dimers, the Cy3 and Cy5 compounds of CACO were used in two colour TIRF microscopy experiments on CHO cells expressing transiently MOR. I found that most receptors are monomeric with a small, but persistent, fraction of dimeric receptors. These receptor dimers likely arise from transient interactions among MORs as implicated by the k_{on} and k_{off} times. The automated computational analysis gave k_{on}, k_{off} and τ values which are comparable to other studies. [74, 34, 37] With the receptor densities, k_{on} ,and k_{off}, the fraction of dimers was calculated to be 4.45 %. Sungkaworn et al. found values in the same range for $\alpha_{2\text{A}}$AR and $G_{\alpha i}$ interactions after stimulation. [74] Together with the relatively long interaction times, my findings indicate that the found fraction of dimers for MOR could be biologically relevant. On a technical level, I was cautious to get a realistic estimation of dimer populations and association rate k_{on}. The experimental design allowed only the direct observation of dimers labelled with two different ligands. Based on the direct observations, the fraction of dimers would have been underestimated. To also include dimers consisting of two times the same colour (Cy3-Cy3 or Cy5-Cy5), k_{off} was calculated from the distribution of dissociation times (eq. 4.1). Likewise, k_{on} (eq. 4.4) and the final dimer density (eq. 4.3) were calculated based on measurable variables. However, the assumption has been made that dimers cannot interact with further receptors to form higher order oligomers.
The observed small fraction of dimers and the dissociation rate of $0.557 \pm 0.207\, s^{-1}$ are in

good agreement with the majority of the literature. Provasi et al. found no dissociation events after dimer formation within their 10 μs simulations. [68] The resulted k_{off} from my investigations is indeed several magnitudes larger than the time window of normal CG MD simulations. However, it is important to note that it would not be feasible to resolve a dissociation rate in the μs range with a frame rate of 35 μs. Meral et al. used MD simulations in their recent study as well, and claimed that the fraction of homo-dimers at physiological conditions is 'negligible'. [64] In their simulations, the dimer lifetime does not exceed ~ 0.3 ms which is significantly smaller from the $\tau = 1.797 \pm 0.487$ s in my experiments. My findings differ from studies using BRET and co-immunoprecipitation. This may be due to the different methods, using either cell destruction or far higher expression levels. [35, 66, 51] Only the study of Wang et al. is contradicting my results in part. In their study they found dimerisation happens before the trafficking of the receptor to the cell membrane. [45] However, my study clearly exhibited dynamic formation and dissociation of receptors within the membrane.

In my experiments, the majority of the particles seem to stop while interacting. To check if the found dimers are artefacts from internalisation processes, the receptor-receptor interactions were analysed for colocalisation with CCPs. As explained above, the presence of CCPs was slightly overestimated. Thus, the fraction of dimers colocalising with CCPs is probably smaller than the estimated 23 %. This is in agreement with a resent study by Metz et al. where they report that 5 % of receptors under basal condition and 12 % after 10 minutes stimulation with DAMGO colocalise with CCPs. [123]

It is possible that the formation of the dimer itself requires the receptors to stop. Thus, it would be easier to find the right orientation and do conformational adjustments as observed in some MD simulations. [64] It may also be due to interactions with other proteins and effectors, as the study of Sungkaworn et al. also showed how receptors stop within hot spots while signalling. [74] The presence of signalling hot spots could also explain the discrepancies between MD simulations and results from in vitro experiments. Accordingly, it would be worthwhile to investigate the nature of the dimer formation further using different, and including biased ligands, ranging from full agonists to partial agonists and antagonist, to reveal possible effects. This could give more insights into the role of different signalling pathways in dimer formation.

Part II.

Part II - smFRET on α_{2A} AR

6. Results

In this project, I wanted to look at the activation process of GPCRs. Especially of interest is the number of substates the receptor has, as recent studies suggested that there could be more than just an active and inactive state. [1, 2, 3, 4] The α_{2A}AR was chosen as prototypical GPCR model and fluorescent single-molecule TIRF microscopy as method. Investigations on a single-molecule level are advantageous to capture also short lived or rare events. In ensemble experiments, those short or rare events get masked by the more prominent states.

6.1. α_{2A} AR with SNAP- and CLIP-tag

6.1.1. smFRET experiments

Testing dye combinations for smFRET

The chosen α_{2A}AR has a CLIP-tag in the third intracellular loop and a SNAP-tag at the C-tail. Thus, it was suitable for FRET studies as well as fluorescent single-molecule microscopy. In order to perform smFRET, different dye combinations were tested to select the most promising FRET pair for measurements at the TIRF microscope. This means clear signals, low background and good labelling properties. The pair needed to contain one SNAP dye and one CLIP dye for orthogonal labelling of α_{2A}AR-SNAP-CLIP mutant. Furthermore, emission in red and far red were preferable for TIRF measurements. These requirements led to the selection of 6 potential pairs:

- CLIP-Surface 647 + SNAP-Surface 549[1]
- CLIP-Surface 647 + SNAP-Surface Alexa 546
- SNAP-Surface Alexa 647 + CLIP-Surface 547
- SNAP-Surface 649 + CLIP-Surface 547

[1] In the text shorter names will be used like 'SNAP 549'

- CLIP-Surface 547 + SNAP-Surface 488
- CLIP-Surface 647 + SNAP-Surface 488

CHO cells were transiently transfected for 24 h with a CD86 construct bearing a N-terminal SNAP- and CLIP-tag. This insured that both dyes are close enough for FRET to occur once they are labelled, with the FRET distance up to 10 nm. The cells were labelled sequentially with the dyes, washed and then imaged at the TIRF microscope. Both, acceptor and donor channel were checked for successful labelling. Images were acquired by only illuminating the donor with a laser power of 15 % with either a 488 nm or a 561 nm diode laser.
The signal detected in the acceptor channel is a mixture of direct excitation, bleed through from the donor channel and FRET. The results of all 6 pairs tested are shown in figure 6.1. Using CLIP 647 as acceptor dye and either SNAP 549 or SNAP Alexa 546 as donor gave the best results, with respect to high signal-to-noise ratio, labelling efficiency and specificity. For those combinations, dynamic behaviour of single-particles was observed in the acceptor channel. With SNAP 488 as donor nearly no signal was observed for CLIP 647. In combination with CLIP 547 as acceptor for SNAP 488, the signal was very dim and not as sharp and bright as seen for the red/far red combinations. Taking CLIP 547 as donor and SNAP 649 as acceptor gave acceptable results, but CLIP 547 showed a higher background than other dyes. This was also observed in combination with SNAP Alexa 647, which gave better results than SNAP 649, but still the background from CLIP 547 was too high and the acceptor signal lower than for SNAP 549/CLIP 647. Thus, SNAP 549 as donor and CLIP 647 as acceptor dye were chosen for further experiments.

Detection of smFRET events

To investigate the activation process of a prototypical GPCR, the α_{2A}AR mutant with a CLIP-tag in the 3ICL and a N-terminal SNAP-tag was chosen, as mentioned before. This receptor was chosen as it showed high FRET efficiencies with CFP and YFP. [23] Replacing the FPs with labelling tags at the intracellular side of the receptor presented a challenge. Therefore, different approaches were tested. A first way to achieve intracellular labelling was to electroporate CHO cells for transfection and simultaneously adding the acceptor and donor dyes. Thus, the cells would incorporate the plasmid and the

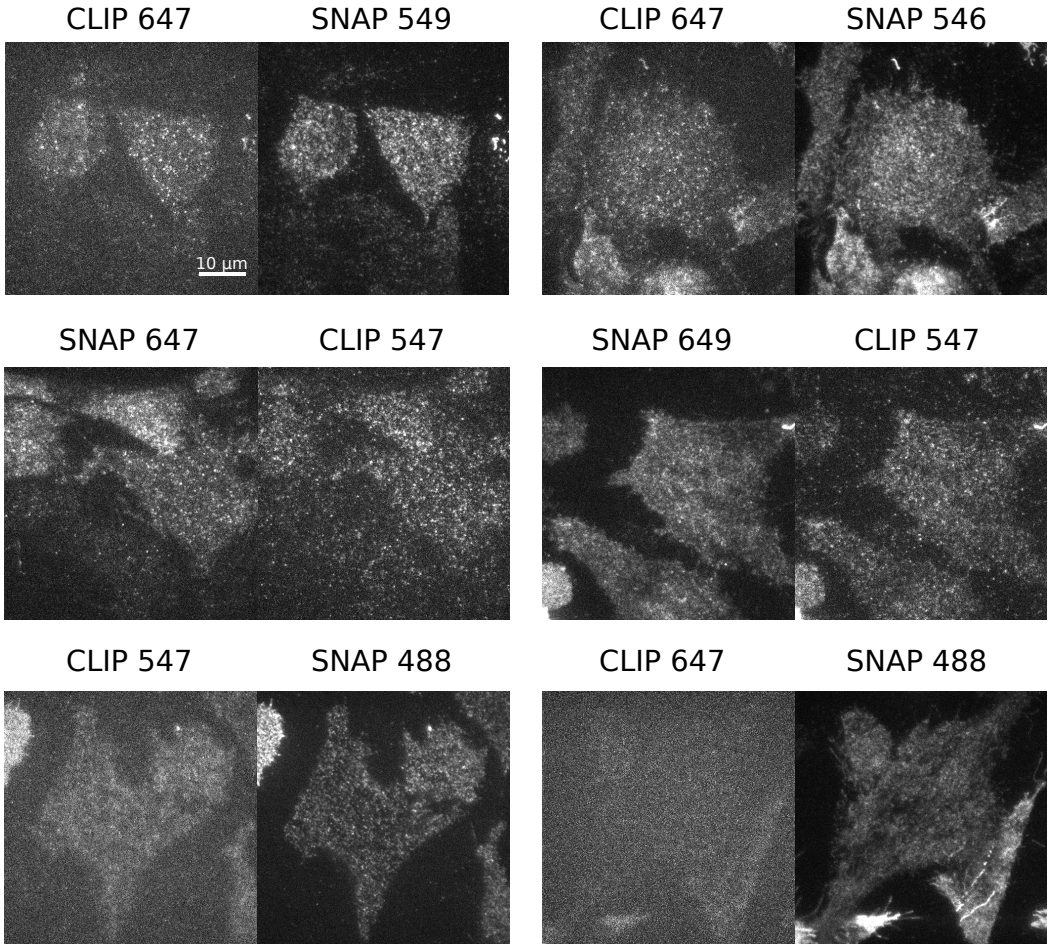

Figure 6.1.: Comparison of different dye combinations. For each possible FRET pair the acceptor channel is shown to the left and the donor channel on the right. For all images only the donor was excited.

dyes. Once the cell starts the expression, the dyes could label the receptors. However, this approach turned out to be too stressful for the cells and not efficient enough. Too less dye was taken up during electroporation, resulting in very poor labelling.
At the beginning of this project, the number of commercially available cell-permeable dyes was limited. In this case two good cell-permeable dyes would have been needed for orthogonal labelling and emission in red and far red.
Another approach of labelling the intracellular side of the receptor was the preparation of supported membranes (see section 3.2.8). [113] Therefore, the glass coverslips were coated with PLL before seeding CHO cells. The transfection was performed as before using Lipofectamine and after 4 h supported membranes were prepared as described in sec-

tion 3.2.8. Such a short transfection time did not allow to obtain supported membranes. To overcome this limitation, a stable cell line was created with the α_{2A}AR construct containing the CLIP- and SNAP-tag, which I called 'Altair'. Altair cells showed different expression levels ranging from very low, suitable for single-molecule experiments, to very high expression. The preparation of supported membranes with Altair cells was successful and reproducible. Before TIRF imaging, receptors were labelled with SNAP 549 and CLIP 647. The acceptor dye CLIP 647 was tested for direct excitation with the 561 nm diode laser as well as for the bleed through from the donor SNAP 549 into the acceptor channel. Both effects were very low and negligible in comparison to the signals acquired in experiments.

To reduce receptor bleaching and blinking, a special smFRET buffer with an oxygen scavenging system was used. To prevent new oxygen leak into the buffer, the coverslips were placed on top of 200 μm thick double sided tape and sealed with nail polish. In figure 6.2 a supported membrane from Altair cells labelled with SNAP 549 and CLIP 647 excited at 561 nm is shown. In the merged image, particles that are present in both channels simultaneously appear yellow. The acceptor in this case is excited by radiationless energy transfer from the excited donor, meaning that FRET occurs.

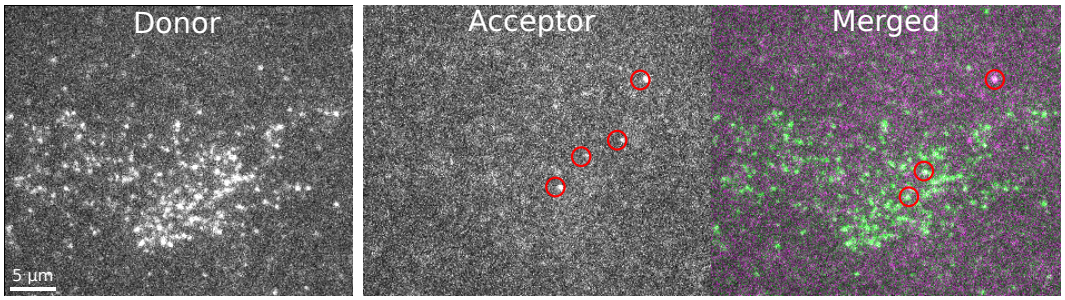

Figure 6.2.: Supported membrane of Altair cells showing smFRET events. On the left is the donor channel, with a directly excited supported membrane of Altair cells. In the middle is the corresponding acceptor channel with single receptors being clearly distinguishable above the background. On the right a merged figure is shown with donor depicted in green, acceptor in magenta. Receptor emitting in both channels, due to FRET, appear white in the merged image.

A zoom-in of a smFRET event is shown in figure 6.3. In the beginning, the particle appears red, which represents acceptor emission. The particle moves some time before it switches to green, which represents donor emission. In this event, the loss of the red signal and smFRET event is likely due to the photobleaching of the acceptor dye.

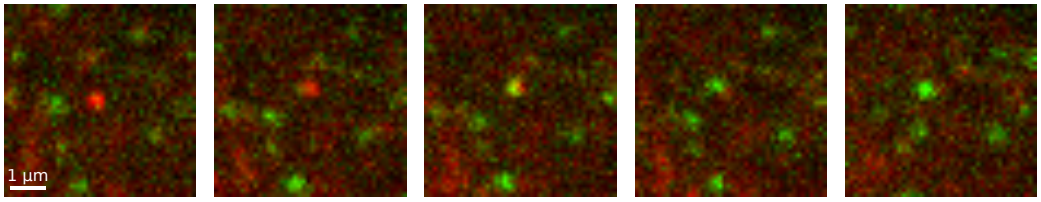

Figure 6.3.: Switching of smFRET event. Shown are frames of an α_{2A}AR switching between FRET states. First two frames the receptor is in a high FRET state emitting mainly far red (acceptor), here depicted in red. In the third frame the receptor switches the FRET state exhibiting a mixture of donor and acceptor emission, green and red, appearing in this merge yellow. Afterwards the receptor continues moving and emitting mainly in the donor channel, green.

Different environments to shift the receptor into different substates

The receptor activation process depends on the presence of ligands and nucleotides. Thus, the environment of the receptor has direct impact on the activation process. As described in the introduction, 1.2, nucleotides, agonists or antagonists can shift the free energy landscapes for the different substates of the receptor. I wanted to use those different conditions to push the system into different substates and to investigate how many there are. To this aim, supported membranes of Altair cells were imaged under different conditions: basal without nucleotides, stimulated without nucleotides, basal with nucleotides and stimulated with nucleotides. As an agonist for α_{2A}AR norepinephrine was used at a saturating concentration of 100 μM, while yohimbine (100 μM) was used as an antagonist, and as nucleotide 10 μM GTPγS. To control the presence of nucleotides, the membranes were treated for 30 minutes before imaging with apyrase, an enzyme that hydrolyses nucleotides.

The single-molecule movies were tracked and analysed. Therefore, a script was written to sort detected particles and to identify particles that are present in acceptor and donor

channel simultaneously at the same area. For those particles, emitting in red and far red, the intensities were plotted over time like shown in figure 6.4. The signal-to-noise ratio was too low for further analysis of smFRET events.
After apyrase treatment, a further decrease in the signal-to-noise ratio was observed, hence no further analysis was pursued.

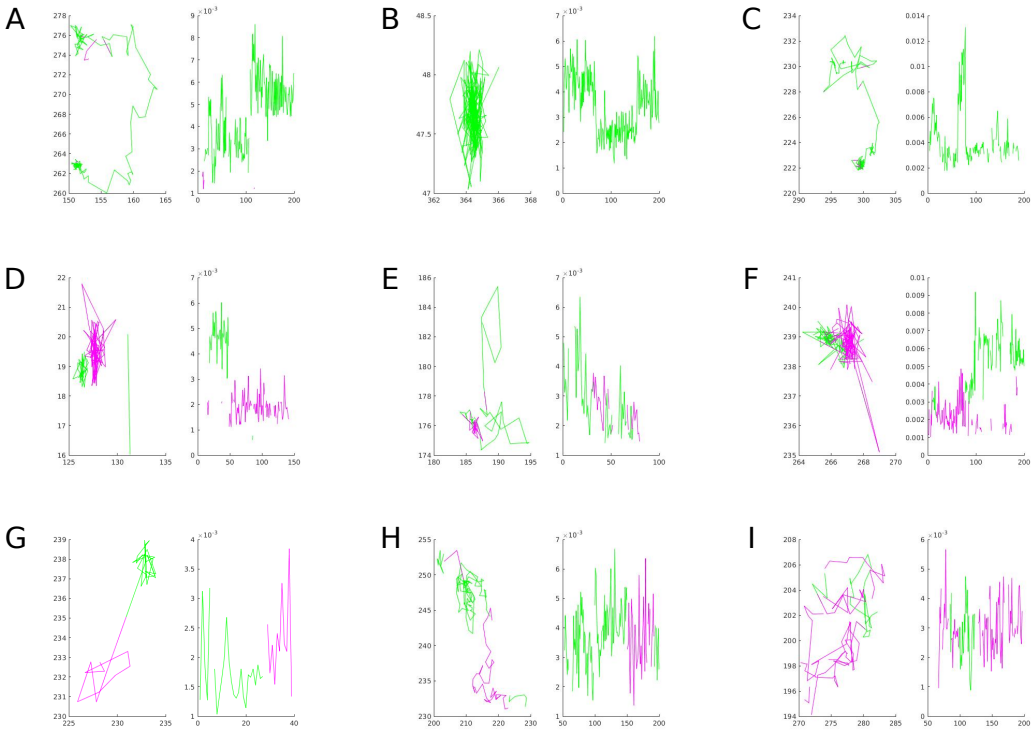

Figure 6.4.: Trajectories and intensities of smFRET events. Shown are nine different smFRET events observed after apyrase treatment and yohimbine stimulation. Always on the left are the trajectories depicted, on the right the fluorescent intensities.The donor is shown in green, the acceptor in magenta. A to C show events of donor emission with stepwise changes in intensity. In D to I examples of switches between donor and acceptor excitation are represented. From the trajectories it can be seen how the receptors in both channels got assigned as the same receptor. Especially in G and H the trajectories are continued by the acceptor channel (magenta) when the donor emission (green) stops.

6.1.2. Testing the functionality of the construct

Setting up a FRET set-up with exchangeable filter sets

To test the α_{2A}AR construct with SNAP- and CLIP-tag in ensemble FRET measurements, and to be able to compare the results with those obtained with smFRET at the TIRF set-up, a new FRET set-up was needed. At the TIRF microscope smaller, brighter and stable organic fluorophores are used, mainly emitting in the red and far-red spectrum of the visible spectrum. However, the FRET set-ups available at the institute were only equipped for measurements using CFP, YFP and GFP. Hence, the new FRET set-up needed to be equipped with filters, that match our requirements and to be easily exchangeable to allow a more flexible choice of fluorophores. Therefore, an Axiovert 200 from Zeiss was reassembled and modified. The light path for the emission was extended and a holder for exchangeable filter cubes was installed in front of the two detectors. The excitation filter-sets were already easily exchangeable as they can be mounted into a filter wheel. A scheme of the set-up is shown in figure 6.5.

The filters and beam splitters were chosen deliberately, taking into account the excitation and emission profiles of donor and acceptor dyes to achieve a balance between efficient donor excitation, maximum read-out of the emission and limiting bleed through, direct acceptor excitation and cross-talk. The thus assembled filter-sets can be found in table 6.1.2.
Furthermore, an old perfusion system was cleaned, re-assembled and put in place to enable dynamic measurements with ligand stimulations and washing steps.

Table 6.1.: Filter-sets for the re-assembled FRET set-up

Name filter-set	Filter 1	Beam splitter	Filter 2
CFP-YFP Donor-Set	436/20	455	-
CFP-YFP Acceptor-Set	504/12	515	535/30
488-546 Donor-Set	472/30	495	-
488-546 Acceptor-Set	546/10	555	595/40
546-647 Donor-Set	542/20	555	-
546-647 Acceptor-Set	635/18	649	-

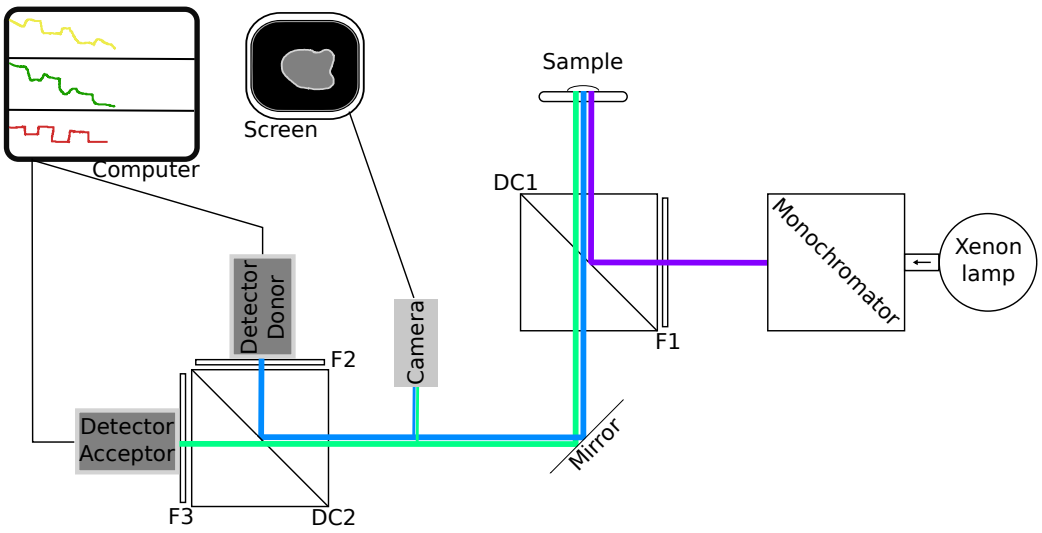

Figure 6.5.: Scheme of the FRET set-up. A xenon lamp is used as a white light source from which a monochromator is used for wavelength selection. A clean-up excitation filter (F1) is placed before a dichroic mirror (DC1). The excitation light for the donor is reflected to the specimen from which emitted light from donor and acceptor can transmit through the DC1. A small part of the emitted light is deviated to a camera for visualisation and region selection for experiments. The majority of the emitted light is divided by a second dichroic mirror (DC2) specific for the donor-acceptor couple in use. The thus divided light passes through acceptor filters (F2 and F3) before it is detected. The signals are simultaneously visualised at a computer from which the experiment can be controlled.

Ensemble FRET measurements with SNAP-CLIP-construct

The smFRET events qualitatively observed in TIRF experiments could be due to artefacts. To test if those events were relevant, the construct was tested in ensemble FRET. In ensemble measurements a change in FRET signal should be observable after stimulation, comparable to the responses observed with CFP and YFP as FRET pair. [23]

HEK T cells were transfected using effectene for 48 hours with the same construct stably expressed in Altair cells. As a control α_{2A}AR with CFP and YFP was transfected. The SNAP-CLIP construct was labelled with CLIP TMR and SNAP SiR. At the newly reconstructed FRET set-up, this dye combination proved to be challenging. High signals could be observed for the donor channel, emitting red light, but nearly no signal could

be measured for far red (SNAP SiR). Tests with HEK T cells overexpressing CD86 with N-terminal SNAP- and CLIP-tag were used as control. Overexpression and successful labelling was confirmed at the TIRF microscope but the signal in the FRET set-up still remained absent. Different dyes emitting in far red were tested but no promising candidate was identified. Thus, the experiment performed at the TIRF microscope could not be tested directly with ensemble FRET.

Functional testing with G_i-Sensor

To overcome the limitations of the far red in ensemble FRET measurements, a different approach was chosen to test the functionality of the α_{2A}AR construct. Therefore, the activation of G_i protein was investigated using a G_i sensor. [127, 74, 24] Wild-type α_{2A}AR was used as positive control. G_i sensor and α_{2A}AR constructs were co-transfected via effectene in HEK T cells and imaged after 48 hours at the above described FRET set-up. Cells expressing the G_i sensor at the cell surface were stimulated with increasing concentrations of norepinephrine ($10\,\text{nM} - 100\,\mu\text{M}$). The wild-type α_{2A}AR showed increasing activation of G_i proteins with increasing concentration of norepinephrine. For the mutant with SNAP- and CLIP-tag even for saturating concentration no FRET signal could be observed (figure 6.6). These tests with G_i sensor were performed by Dr. Marie-Lise Jobin (AG Calebiro, Institute of Pharmacology, University of Würzburg).

Functional testing with GTPγS binding assay

Another approach to test the functionality of GPCRs is the GTPγS binding assay with the radioactive sulphur isotope ^{35}S. This assay requires larger amounts of sample and several controls need to be included. Furthermore, different constructs were planned to compare. In addition, those samples should be tested under different conditions, basal and stimulated either with agonist or antagonist. Activated G-proteins bind GTP and are inactivated upon hydrolysis of the nucleotide to GDP. The GTPγS cannot be hydrolysed, at least not at a detectable rate, thus trapping the G-protein in an activated state. The G-protein can just be activated and bind GTPγS if the receptor is functional. Accordingly, if bound GTPγS can be detected by a scintillator, it indicates that the G-protein got activated by an activated receptor. [128, 129, 130, 131]
Several trials were performed but the results were not as promising to justify the effort in comparison to other methods like the G_i sensor, described above.

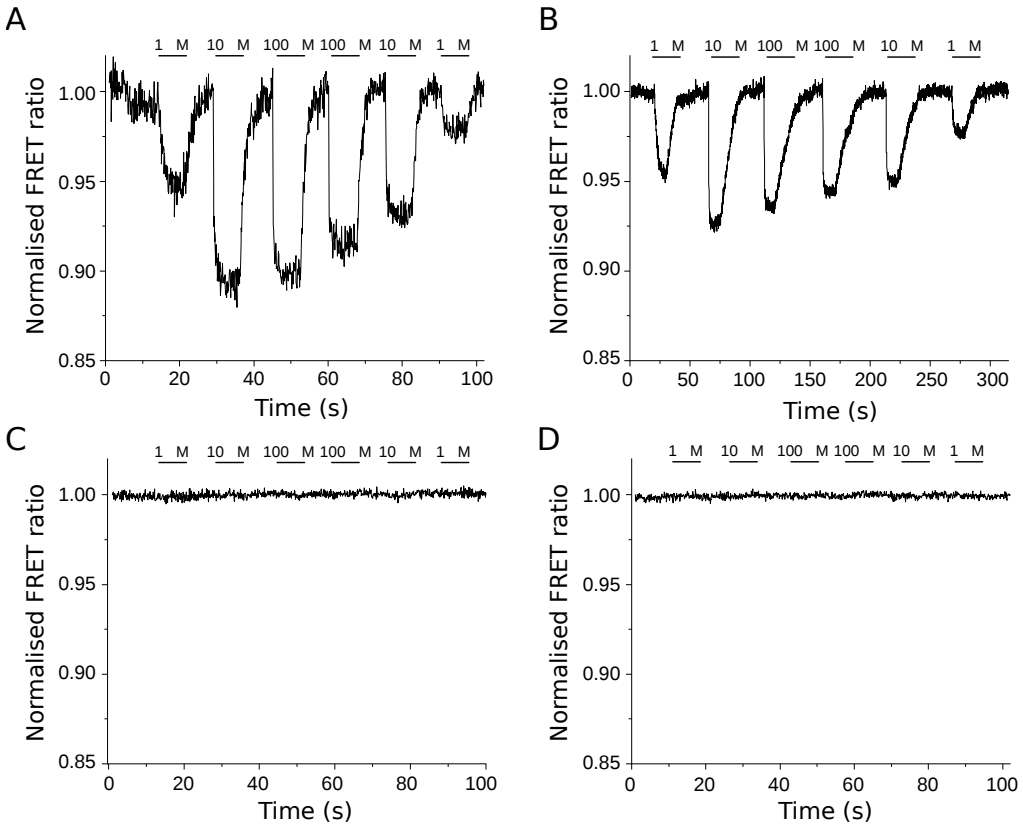

Figure 6.6.: Results of the functional testing with G_i sensor. A) α_{2A}AR with CFP and YFP with norepinephrine stimulation. B) the wild-type α_{2A}AR G_i response after norepinephrine stimulation as positive control, showing that the G_i sensor works. C) negative control with pcDNA and G_i sensor. D) α_{2A}AR construct with SNAP and CLIP tag showing no G_i activation after stimulation. The traces are representative of three independent experiments.

6.2. α_{2A} AR with SNAP-tag and an unnatural amino acid

6.2.1. Generation of 5 different mutants with unnatural amino acid

The α_{2A}AR with SNAP- and CLIP-tag did not show any functionality, neither in ensemble FRET experiments nor in tests with the G_i sensor. For this reason, an alternative labelling strategy was explored. To minimise the effect of the incorporated tag on the functionality of the receptor I tried to replace the tag in the 3ICL with an unnatural amino acid. The unAA could later be fluorescently labelled via click chemistry (section 1.6). The selected insertion site should not affect the G protein binding or destabilise the structure of the receptor. Previous experiences from the Sauer group (Biotechnology and Biophysics, Biocenter, University of Würzburg) showed lysine and serine residues are preferable to be replaced with an unAA (unpublished data). For this reason, 5 different possible sites were selected. One at the beginning of the 3ICL (lysine 327), one relatively in the middle of the loop (serine 347), and three towards the end, close to helix 6 (serine 360, lysine 370 and threonin 373). The SNAP-tag in the C-tail was kept. Thus, it served as a reliable control to check the proper expression of the full length receptors and later on as the labelling site for the second fluorophore for smFRET studies. The cloning was performed as described in section 3.2.3 by Ulrike Zabel (Institute of Pharmacology, University of Würzburg).
Both tags are on the intracellular side. Consequently, the labelling has to be performed with either two efficient cell permeable dyes or on supported membranes (section 3.2.8). As of today, there are no efficient cell permeable dyes for click labelling yet available, hence it was evident that supported membranes would be needed. As seen before, the development and use of stable cell lines facilitates the preparation of supported membranes and improves their reproducibility (section 6.1.1). Thus, five stable cell lines were created expressing each one of the constructs in CHO cells and all five were successfully generated (see table 6.2.1). Without the additional transfection of tRNA and synthetase, the protein synthesis will stop at the amber codon, resulting in a truncated receptor. In this work, a receptor that successfully incorporated the unAA is referred to as full length receptor. There was the concern, that stable cell lines expressing truncated receptor could be unhealthy. However, all new cell lines grew as untransfected CHO cells, only the cell shape slightly differed as the cells grew more long than wide.

Table 6.2.: Overview of stable cell lines and which plasmid they contain.

Name of the cell line	Construct
Bellatrix	α2A-K327amb-SNAP
Capricorni	α2A-S347amb-SNAP
Deneb	α2A-S360amb-SNAP
Enif	α2A-K370amb-SNAP
Fafnir	α2A-T373amb-SNAP

6.2.2. Comparison of constructs via SNAP labelling

The different mutants in the stable cell lines needed to be tested. On the one hand it needed to be checked, if they can express the full length receptor. On the other hand, I also wanted to compare the different mutants to choose the most promising construct for further experiments. For this purpose, the stable cell lines were transfected with the tRNA and synthetase construct and the medium was supplemented with TCO as unAA to express the full length receptor containing the unAA. To check whether the transfection worked and to compare the different cell lines, the cells were then labelled with SNAP silicon-rhodamine (SiR), a cell permeable dye. Only if the unAA was incorporated successfully the full length receptor is synthesised including the SNAP-tag at the C-terminus. The C-terminal labelled cells were imaged at a TIRF microscope.
The different stable cell lines showed different transfection efficiencies. Bellatrix displayed the highest transfection efficiency and the cells also showed different expression levels among themselves (see figure 6.7 A). For Capricorni and Deneb (B and C in figure 6.7 respectively) it appeared that less cells were expressing the full length receptor and comparably more 'ghost' cells were seen. This means that the cells were internalising the dyes without labelling the receptors. Thus, the dye was diffusing freely in the cytosol, which is an indicator that the cells are unhealthy. This was even more eminent for Enif cells (figure 6.7 D). For the Fafnir cell line no cells with full length receptor could be found. These results showed that Bellatrix is the most promising candidate and was in consequence chosen for the experiments thereafter.

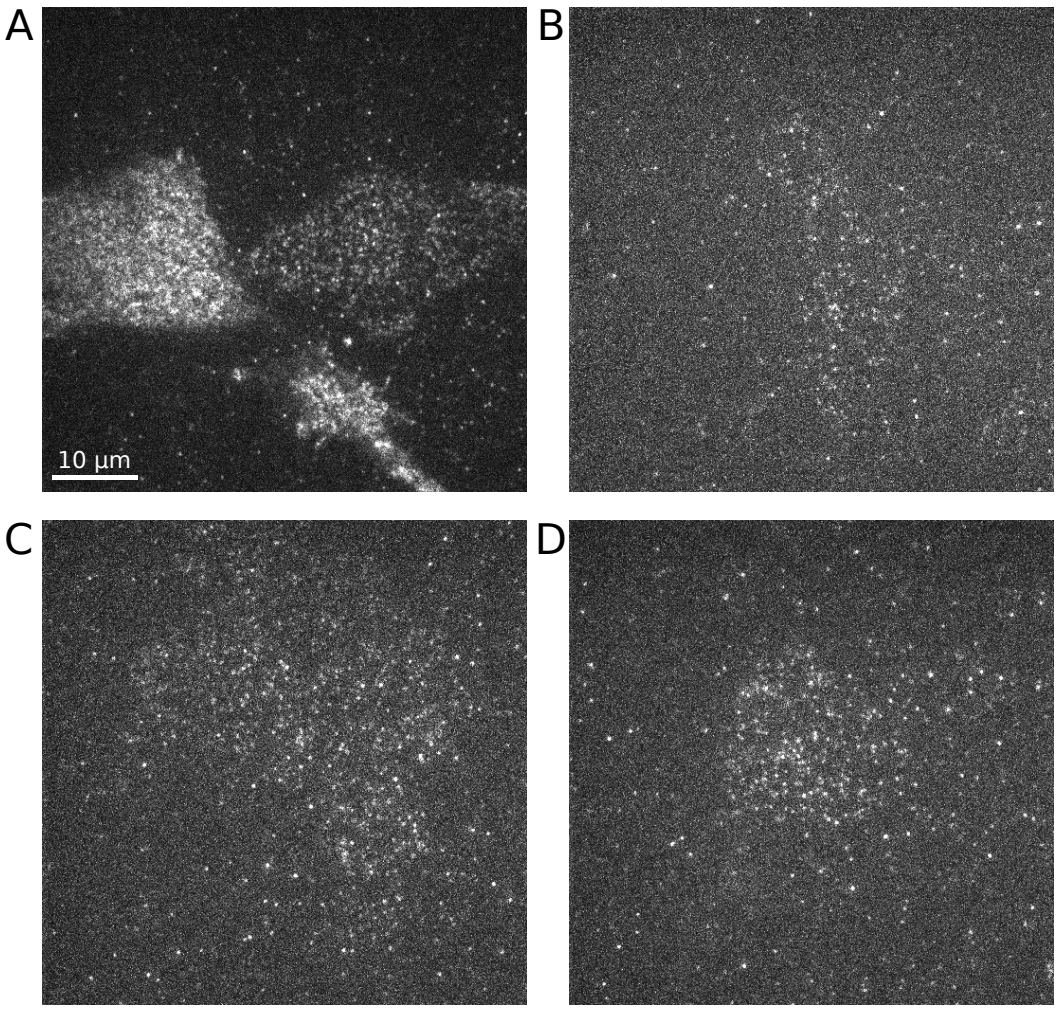

Figure 6.7.: Stable cell lines expressing full length receptors labelled with SNAP SiR. Shown are four of the five stable cell lines with amber mutation. In A) Bellatrix cells are shown with different expression levels. B) shows a Capricorni cell with very low expression level. C) is a cell from the Deneb cell line whereas D) shows a labelled Enif cell. Both Deneb and Enif had a similar expression level as Capricorni. For Fafnir no cells with full length receptor were found.

6.2.3. Comparison of expression levels of truncated and full length receptors via western blotting

To check the expression levels of the stable cell lines for truncated and full length receptor (after addition of tRNA/synthetase and TCO), western blots were performed.

First, the stable cell lines were stained with an HA-tag primary antibody without transfection for full length receptor, to just compare the expression of truncated receptors. This served as a second control to check whether the creation of the stable cell lines was successful. As the western blot in figure 6.8 shows, the stable cell lines all express truncated receptors and even though their lengths differ just in a few amino acids, the difference in size can be seen.

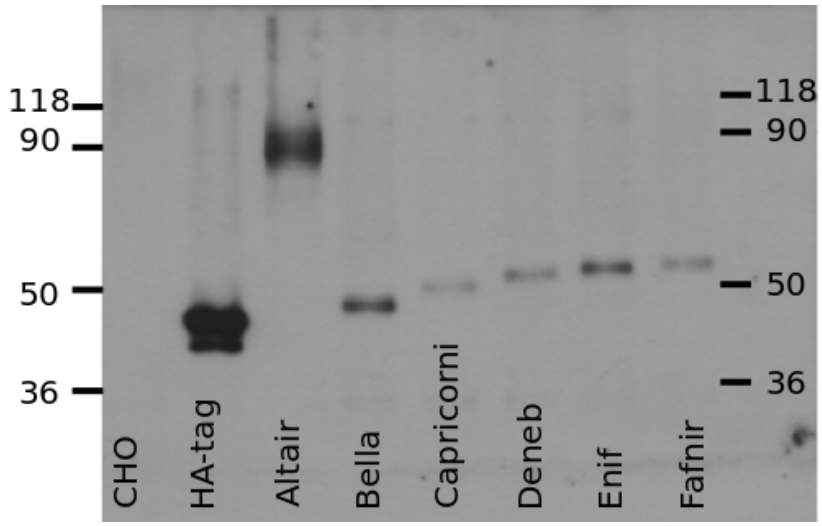

Figure 6.8.: Western blot of the different stables cell lines. Lysates of untransfected CHO cells, a positive HA-tag control, Altair, Bellatrix, Capricorni, Deneb, Enif and Fafnir were loaded and detected with an HA-tag antibody.

From the tests with SNAP labelling, the stable cell line 'Bellatrix' was chosen as most promising candidate. Accordingly, those cells were taken for further tests to optimise the transfection protocol with Jet-Prime (section 3.2.7) and the plasmid for the tRNA and synthetase. In figure 6.9 it can be seen, that with transfection and addition of TCO the lanes with Bellatrix get additional signal contributions at bigger molecular weight going up to the size of Altair cells, which corresponds to the full length receptor with SNAP- and CLIP-tag. However, for none of the tested conditions a clear second band was observed. Without transfection of tRNA and synthetase, those signals are absent (compare figure 6.8) and also for Enif with transfection, those contributions are not present. Those contributions seen in transfected Bellatrix cells could be an indication for longer fragments of the receptor, meaning that the protein synthesis progresses beyond the stop codon but terminates at different positions before the full length receptor.

To better distinguish the full length receptor from the truncated one in western blots, a SNAP antibody was tested. Unfortunately, this antibody provided a western blot with high amount of unspecific bands even in untransfected CHO cells, hence I did not proceed experiments with this antibody.

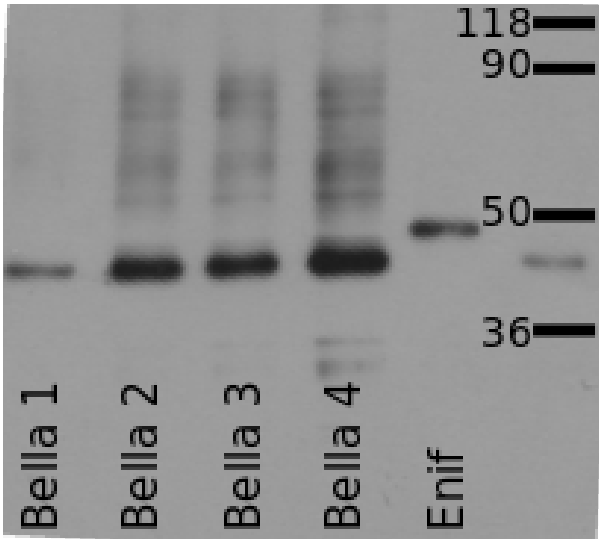

Figure 6.9.: Western blot of different transfections of Bellatrix (Bella) and Enif. Bellatrix cells were seeded at increasing densities and then transfected with tRNA/synthetase to express the full length α_{2A}AR. In the last lane transfected Enif cells were loaded.

6.2.4. Click labelling of unnatural amino acid

An important and necessary step is the successful click labelling of the unAA, to introduce the second dye. Before attempting click labelling on transfected Bellatrix cells, coverslips from the same transfection were labelled with SNAP SiR to check for sufficient transfection levels of full length receptors. If transfection proved satisfactory, supported membranes were prepared and labelled afterwards with click TAMRA before imaging at a TIRF microscope. In figure 6.10 Bellatrix cells expressing the full length receptor are shown labelled with click TAMRA. All cells were very bright, showing a high expression level of the receptor containing the unAA. Regions outside of cells showed a high background as well, indicating unspecific binding. Furthermore, the cells appeared to be more intact than supported membranes, which means TAMRA is cell permeable to a significant degree and the preparation of supported membranes did not work properly.

As high background from unspecific binding was observed, it was not possible to distinguish cells with a lower expression level, and several washing steps did not improve the signal-to-noise ratio.
Due to overall low transfection efficiency and time limitation, no further improvements could be made.

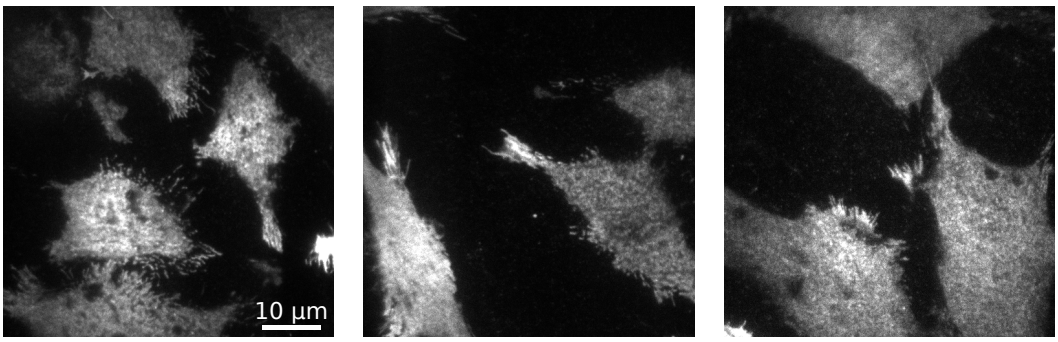

Figure 6.10.: Three representative images of click labelled Bellatrix cells. Bellatrix cells transfected with tRNA/synthetase for the incorporation of an unAA into α_{2A}AR click labelled with TAMRA.

7. Discussion

7.1. Is the SNAP/CLIP-tag construct for α_{2A} AR good enough?

7.1.1. Detection of smFRET experiments with SNAP/CLIP-tag construct

For the investigation of the activation process of GPCRs the α_{2A}AR was chosen with SNAP- and CLIP-tag. Thus, it was suitable to perform two colour labelling and test for smFRET events. Looking at a single-molecule level would help to capture short-lived or rare events, which are obscured in ensemble measurements.
Before testing smFRET on α_{2A}AR in cells, different SNAP- and CLIP-dyes were tested to select the most promising combination. With a CD86 with N-terminal SNAP- and CLIP-tag next to each other, a control was chosen that assures that donor and acceptor fluorophore are in a proximity, that allows for FRET to occur. From the tested combinations SNAP 488 plus CLIP 647 gave the least acceptor signal. This can be explained by the big gap between the spectra, all other combinations had a more significant spectral overlap. Even though differences could be observed CLIP 547 showed comparably high background, indicating poorer labelling specificity. SNAP 488 plus CLIP 547 gave less sharp images compared to red/far red combinations. Thus, the decision was made to either use SNAP 549/CLIP 647 or SNAP 546/CLIP 647. Both gave very similar results with just a slight advantage for SNAP 549 over SNAP 546. In addition, SNAP 549 was more commonly used at the lab. As a result, SNAP 549 and CLIP 647 were identified as most promising dye pair for smFRET experiments at our TIRF microscope.

One major challenge was to achieve high labelling efficiencies for the α_{2A}AR construct with intracellular SNAP- and CLIP-tag. To this aim, a stable cell line was created with

this construct, Altair cells, from which supported membranes could be prepared. Supported membranes served as a solution for the intracellular labelling problem, but their preparation was not always successful. In successful experiments also just $\approx 10 - 20\,\%$ of cells were turned into supported membranes. This was a limiting factor, as it reduced the number of cells with appropriate receptor density per coverslip further. Additionally, supported membranes are not as stable as intact cells. After preparation, the next steps, including imaging, needed to be fast and efficient.

In addition to solving the intracellular labelling problem, supported membranes enabled the manipulation of the environment of the receptor. As described before, the environment with ligands and nucleotides plays an important role. Ligands, can shift the probabilities of different receptor conformations. In addition, nucleotides can help trapping the receptor in a specific conformation. To have control over the nucleotides present, apyrase was used before experiments. Apyrase is an enzyme that hydrolyses nucleotides.
The working hypothesis was to shift/trap the receptor to different conformational states using different ligands or nucleotides. This was shown before successfully by [6, 132, 18]. However, the apyrase treatment was another stressful experimental step for the delicate supported membranes. Additionally, it was a time consuming step further prolonging the protocol. Afterwards, the coverslip with the sample was mounted on a sample slide with smFRET buffer containing an oxygen scavenging system. The whole sample was sealed with nail polish. Those treatments increased the stress on the sample even more. While imaging, one could observe by eye that the membrane patches become more stiff, and the movements slower, until the patches became static. For the experiment only the intact membrane patches with moving single receptors were acquired. Due to the toxicity of the smFRET buffer, the sample had to be exchanged fast.

Having identified and selected a suitable dye pair, succesfully prepared supported membranes, and utilised an oxygen scavenging system, a protocol was thus established for smFRET imaging. With that protocol smFRET movies could be acquired at the TIRF microscope. With labelled membrane patches from Altair cells, clear single receptors could be observed moving in the acceptor channel upon donor excitation. Those signals were more prominent and stood out in comparison to what was seen in the controls for bleed through or direct excitation (acceptor excitation by the donor laser).

These results were reproducible. However, just very few receptors were very bright in the acceptor channel. This can be due to different reasons. On the one hand, it could be, that most of the receptors were in a low FRET state. In this case meaning activated as the TM6 and the C-terminus are far apart. Only receptors with a closed G-protein binding site would exhibit high FRET states. It is likely that the lower FRET state, as expected for the activated receptor, is not bright enough to be distinguished by eye. On the other hand, it could be possible that the receptor mutant has an impaired functionality. In this case, it would be hard to see any changes in FRET. However, this would also depend on the type of problem. It could still be that just a few receptors function normally whereas the majority is dead and not undergoing any conformational changes any more.
To test the existence of different substates and if their equilibrium can be shifted, different conditions were employed to the membranes. The first step was an apyrase treatment to hydrolyse all nucleotides. Next, samples were measured in the presence of different ligands. Norepinephrine was chosen as agonist and yohimbine as antagonist. The antagonist was hypothesised to shift the equilibrium to the higher FRET state, corresponding to an inactive conformation. With norepinephrine the receptor is activated. Thus, the probability to find the receptor in an open conformation for G-protein coupling is increased. Likewise, the supported membranes were measured with different nucleotides: either GDP or GTPγS. The latter cannot be hydrolysed, hence trapping the G protein in an activated state and coupled to the receptor. This results in a low FRET state. Whereas an abundance of GDP has the opposite effect, trapping the G_α subunit in the inactive form.

The acquired single-molecule movies were analysed using automated particle detection and tracking. Afterwards, a routine was implemented to combine and identify particles that appear in donor and acceptor channel simultaneously. Of those particles the intensities and trajectories were plotted for further analysis. From the first results, it appears that the signal-to-noise ratio is not high enough to distinguish between several substates. If the quality of the data would have been better, a Hidden Markov model would have been applied. This would allow to identify the number of substates present without a priori estimations. Yet, the data acquisition needs to be improved before the data processing can be improved and further customised.

7.1.2. SNAP/CLIP-tag construct does not have any functionality

The qualitatively observed smFRET events in TIRF experiments needed to be confirmed. Else, it could be that the events were artefacts and not relevant for the investigation of receptor activation. The functionality of the receptor can be tested in ensemble FRET measurements. Only if the receptor can be activated by ligands and displays conformational rearrangements, can changes in the FRET signal be observed. In order to perform those tests, a set-up was needed suitable for the FRET pair emitting in red and far red.
As described in section 6.1.2, an old FRET microscope was modified and adapted. The set-up is equipped now with exchangeable filter sets for different FRET pairs, expanding the freedom of choice of fluorophores. The new FRET set-up is routinely used in the lab for different projects, amongst which one contributed already to a publication (Sungkaworn et al., [74]). With the external emission filter cubes in combination with the filter wheel for excitation filters, the set-up is easily and quickly adaptable to different fluorophores that are used. Furthermore, the perfusion system with 8 different reservoirs allows for dose-response curves over a wide range of concentrations or to compare different ligands within one experiment. The projections of the region of interest to a screen served advantageous while searching cells with high surface expression and additionally in testing the flow from the perfusion system. The whole set-up was fully functional within a few months.

The signals observed at the TIRF microscope, which look like smFRET events, needed to be confirmed. Therefore, the functionality of the α_{2A}AR construct with SNAP and CLIP-tag was tested in ensemble FRET experiments. If FRET could be observed in receptor-overexpressing cells, than the probability is high, that the observed events at TIRF are smFRET events. To achieve a maximal signal, the receptor was overexpressed for 48 hours in HEK T cells. These cells were chosen because they exhibit a high membrane expression. CLIP TMR and SNAP SiR were chosen as fluorophore combination. Both are cell-permeable and thus offer the advantage of bypassing the preparation of supported membranes. Preparation of supported membranes in transiently transfected cells has proven before already to be not feasible. With CLIP TMR and SNAP SiR the absorption and emission spectra were still very close to the smFRET pair SNAP 549 and CLIP 647.

Even though the new filter sets for the FRET set-up were planned for FRET pairs emitting in red and far red, no signal could be detected in far red. To rule out a labelling problem, control cells overexpressing the receptor and labelled with SNAP SiR were imaged at the TIRF microscope, which is significantly more light sensitive. The TIRF images confirmed that the receptor was overexpressed and also labelled succesfully. Accordingly, the detection at the FRET set-up must have been the problem. Thus, it was not possible to perform ensemble FRET experiments and to look at the direct activation under norepinephrine stimulation.

To overcome this limitation, the G_i sensor was chosen. The sensor shows a drop in FRET upon G_i activation. G_i is activated by the activated receptor, thus requiring the conformational changes, that we wanted to look at initially. Showing that the G-protein activation is still working, would prove that the receptor did not lose its functionality.
The G_i sensor contains a CFP and YFP as FRET pair and could be used without further modifications at the new FRET set-up. Wild-type α_{2A}AR was co-transfected with the G_i sensor as a control. Upon stimulation the FRET signal decreased, confirming that the sensor works reliably at this set-up. It was even possible to distinguish differences in the FRET signal with increasing norepinephrine concentration. However, with α_{2A}AR SNAP and CLIP-tag no FRET signals were observed.
This is a concerning indication, that the SNAP and CLIP-tag construct lost its functionality. Still, other explanations could be possible, too. Even though the expression of the sensor was directly observed by CFP and YFP emission, there was no control for co-expression of the sensor and α_{2A}AR . Even though the control with wild-type α_{2A}AR worked well, it is not necessarily the case, that both plasmids express comparably. The plasmid for wild-type α_{2A}AR can have higher (co-) transfection efficiency. Thus, the chance of measuring a cell co-expressing sensor and receptor would be higher. If the plasmid with the inserted SNAP- and CLIP-tag performs weaker for co-transfection, it is possible that only cells expressing the sensor were imaged. Thus, the sensor could not show FRET changes, as it could not be activated by a receptor.
After all, the functionality of the SNAP- CLIP-tag α_{2A}AR construct could not be confirmed, neither with ensemble FRET nor with the G_i sensor. This might be the result of technical problems, especially for the ensemble FRET. Nevertheless, a solution to recover the functionality of the receptor was needed.

7.2. Does the insertion of an unAA solve the problems of the SNAP/CLIP construct?

7.2.1. Successful insertion of amber codon

The α_{2A}AR construct with CLIP- and SNAP-tag did not show any functionality. Former publication using CFP and YFP demonstrate, that the insertion of tags in the third ICL and the C-tail are possible without loosing the functionality. Nevertheless, a tag is always a change in the receptor and the effect of the insertion should be minimised. One way to achieve this is to minimise the size of the tag itself. Another way, to try different insertion sites. Accordingly, I tried to use an unAA instead of the CLIP-tag in the third ICL. Thus, minimising the size of the tag dramatically to just one amino acid. In addition, I tried five different insertion sites.

Five stable cell lines were created, each expressing one of the five different amber mutants. A first indication, that the creation was successful was the acquired gentamicin resistance. This could just be observed, if the cells stably express the truncated α_{2A}AR with a stop codon in the third ICL. The new cell lines grow like CHO cells, only the shape differs slightly. This indicates that the over expression of a truncated receptor does not affect the health of the cells, as far as can be seen by the morphology. Furthermore, it was proven in western blots, that the different cell lines are expressing the truncated receptor, bearing a HA-tag, and that the length of the truncated receptor differs between the cell lines. Even the difference of a few amino acids in length could be observed in western blots. Moreover, the different cell lines show similar expression levels. This, however, can just serve as an indicator as cells are pooled together for the lysate preparation and amongst those cells the variability of expression levels can still be high.

The creation of a stable cell line expressing the full length receptor was not considered as this would require orthogonal antibiotic resistances for the plasmid of the receptor and the plasmid encoding for the tRNA and synthetase. Thus, only one transfection was needed for further experiments. However, as the transfection with Jet Prime for the tRNA and synthetase construct lasts 48 hours, the cells have enough time to rest and recover before the preparation of supported membranes. In addition, co-transfection together with the receptor constructs was expected to lead to a high over expression, which is not desirable for single-molecule experiments.

The new stable cell lines were tested for the expression efficiency of full length receptors after transfection with tRNA/synthetase and the addition of TCO to the medium. After SNAP labelling, the cell lines showed differences amongst each other. The cells with the best transfection efficiency and also different expression levels were Bellatrix. Only a few ghost cells were detected but their level was minor and in most cases even lower than for the other cell lines. Interestingly, the efficiency decreases the later the amber codon is introduced in the receptor. For Bellatrix, the stop codon is at the beginning of the 3ICL. In the case of Enif and Fafnir, the point mutation was introduced at the very end, close to the sixth αhelix. In comparison to the location within the loop, the type of amino acid, that got replaced, seems to have a lesser influence. In both, Bellatrix and Enif, a Lysine was replaced with an amber codon. Bellatrix shows clearly better transfection efficiencies. For Capricorni and Deneb, a Serine was mutated, both show comparable efficiencies and expression levels. For Fafnir, it remains unclear why it showed negative results. It could be the position close to TM6 or it could be the threonine, that got replaced, probably both had an influence on the expression. Furthermore, it is important to note that Eason et al. showed that parts of the ICL3 is necessary for G-protein coupling. [133] In their study, they changed complete domains. Still, changing one amino acid within the domain could lead to the impairment of G^s coupling. The mutation sites of Deneb, Enif and Fafnir are in this domain. coupling to G^i should not be effected according to the finding of Eason et al.. [133]

To test the ratio between truncated and full length receptor, western blots were performed. For this reason, Bellatrix and Enif cells were transfected with tRNA/synthetase to get expression of the full length receptor. The western blot shows clear bands for the truncated receptor at the same level seen before for the untransfected cell lines. Additionally to this clear signal, the Bellatrix cells show signals for bigger protein fractions. This might be an indication, that receptor synthesis in the ribosomes continues beyond the introduced stop codon. Those contributions are totally absent for Enif. This observation is in good agreement with the results from the SNAP labelling. At the TIRF microscope Bellatrix cells demonstrated a higher probability to express the full length receptor than Enif cells. This strengthened the choice of Bellatrix as the most promising candidate for further experiments.

7.2.2. Bellatrix expression levels are still not high enough for smFRET experiments

The amber mutant expressed in Bellatrix cells was chosen as most promising candidate. In TIRF imaging it exhibits the highest transfection efficiency and different expression levels. Furthermore, it displayed bands in western blotting bigger than the truncated receptor. Based on those results, Bellatrix cells were chosen for further experiments. On the one hand, FRET experiments to test the functionality with the G_i sensor, on the other hand the preparation of supported membranes and click labelling. In ensemble FRET experiments no signal was detected for G_i activation. As seen by TIRF experiments before, the expression level and transfection efficiency could greatly differ. Furthermore, it was not possible to check the cells simultaneously for co-expression of G_i sensor and the full length receptor. For this reason, ensemble FRET experiments were repeated with HEK cells transfected with G_i sensor, the Bellatrix plasmid and the tRNA/synthetase. The expression of full length receptor was checked again by SNAP labelling with SNAP SiR. SNAP SiR was chosen as control labelling because it exhibits the lowest spectral overlap with the CFP/YFP FRET pair of the G_i sensor. If the transfection efficiency was high enough, cells were measured at the FRET set-up for G_i activation after stimulation with noradrenalin. A few cells showed very small responses but nothing comparable to the positive control of the wild-type α_{2A}AR . At the FRET set-up it was not possible to check each cell individually for co-expression of the full length receptor and the G_i sensor. This could explain why just a few cells showed any response. The comparably small response might be due to the low expression levels of the full length receptor. The positive control with wild-type α_{2A}AR had far higher expression levels. Additionally, the western blot showed that the majority of receptors are truncated even after transfection of tRNA/synthetase. A high over-expression, which is needed for ensemble FRET experiments, was not achieved.

The low expression levels of full length receptor could serve as an advantage for the smFRET experiments. Accordingly, click labelling was tested on supported membranes. The preparation of supported membranes is on a normal coverslip successful for around 10 % of the cells, thus being a limiting factor for further experiments. As a consequence, cells were tested beforehand for high transfection efficiencies. The transfection efficiency turned out to be another limiting factor as only one transfection reached an efficiency of $10 - 20\,\%$. From this experiment supported membranes were prepared and immediately

click labelled with TAMRA. The dye caused a high background because of unspecific binding. Moreover, the dye labelled several intact cells, not supported membranes, indicating that the dye is cell-permeable, at least to a certain degree. Interestingly, the fraction of cells labelled with TAMRA via click chemistry was higher than the fraction observed with SNAP SiR before. This is in agreement with the findings from the western blot, showing several fragments longer than the truncated receptor. It seems that the receptor is translated beyond the introduced amber codon in the 3ICL but only rarely until the C-terminal SNAP-tag.

To confirm this hypothesis, further experiments would be needed as well as further improvements in the transfection efficiency for the full length receptor. Parameters that could be tested for better transfection efficiency include the timing as well as the coating. The cell density and the amount of plasmid was tested and optimised already. Further perspectives for this project will be developed in the outlook, chapter 8.

8. Outlook

Opioid receptors play a key role as analgesic drug targets. However, the current drugs have major side effects which also led to the so called 'opioid crisis' in the US. A better understanding of the receptor function is essential for the development of new, and improvements of current drugs. In order to achieve this, a better understanding of receptor dimerisation is needed. Single-molecule microscopy has previously proven to serve as a good measure to address dynamic dimerisation for different GPCRs. In this study a novel set of fluorescent ligands targeting the MOR or the DOR was used to investigate the diffusion behaviour of those receptors at a single-molecule level. In the case of the MOR homodimerisation was examined.

Accordingly, it would be logical to continue this investigation by using the DOR ligands to explore the dimerisation of the δ subtype. The results of such a study could be compared to the findings of MOR. Our collaboration partner Antonios Drakopoulos has used the same approach to study the KOR using fluorescent antagonists. Interestingly, in the case of KOR no dimerisation beyond random colocalisation was observed (unpublished data). With such a different behaviour for two different subtypes it would be intriguing to compare the behaviour of the third subtype as well.
On the long-term, it would be fascinating to expand the set of fluorescent ligands to have different types of ligands, e.g. full agonist, partial agonist and antagonist. Thus, it would allow to directly compare the effect on the diffusion and also on a possible dimer formation.

Likewise, it would be useful to use this new characterised set of subtype specific fluorescent ligands, available for all three subtypes, to also investigate heterodimerisation at a single-molecule level. A study by He et al. showed that heterodimerisation influences the internalisation and trafficking of opioid receptors. [53] Gomes et al. showed that heterodimerisation also alters the pharmacological response to ligands. [66] Thus, single-

molecule approaches can help to characterise the effects of homo- and heterodimerisation and to understand the different pathways that are triggered. With this understanding it could be feasible to reduce unwanted side effects, paving the way for safer pain killers. Heterodimerisation could be investigated with two different approaches. First, one could use the set of fluorescent ligands at hand and choose different fluorophore for the different sub-type. This way one would compare obtained colocalisations with random colocalisations, as this study did for MOR homodimers. A second approach would require the synthesis of dual ligands that combine two ligands, each for one sub-type. However, with dual ligands it could be more critical to conclude if the heterodimerisation is elevated by their nature, meaning that once one side of the ligand binds to one receptor, the second moiety recruits a second receptor.

In addition, the use of fluorescent ligands has the advantage that the targeted receptor does not need to be genetically changed. Accordingly, the ligands could be used for studies on wild-type opioid receptors in brain slices or primary cell cultures like neurons. Especially helpful in this case is the high subtype selectivity and affinity of the presented ligands. It would be worthwhile to compare the applicability of the fluorescent ligands to methods using antibodies for fluorescent staining (especially for imaging). For fluorescent ligands only one labelling step is needed in comparison to two steps with the use of primary and secondary antibodies.
On the long term, if the fluorescent ligands can be further improved and the application to primary cells or even tissue samples is successful, they could be used as reporter for cancer detection. Singleton et al. have shown an elevation of MOR expression in metastatic lung cancer. [134] As fluorophores have a low penetration depth in tissues, the fluorophore moiety might need to be replaced in this case.

In the case of the smFRET project on α_{2A}AR , some questions need to be solved and improved. A first step would be the improvement of expression of the full length receptor in Bellatrix cells, as this will be needed for all further experiments. The first trials for the incorporation of the unAA were promising, and labelling of the full length receptor was successful on several occasions. However, it was still too low to pursue preparation of supported membrane, or for functional tests using ensemble FRET or the G_i sensor. Both an increased transfection efficiency and higher expression levels of full length receptor, could improve the detection in western blots. In the best case, two distinct bands can be detected, corresponding to the truncated receptor (stopped at the amber codon) and the second band for the full length receptor.
For the smFRET protocol further improvements in the signal-to-noise ratio would be desirable. Different possibilities arise.
i) The smFRET buffer could be improved to be less toxic for the cells or supported membranes.
ii) More time could be dedicated to attempt further improvements and shorten the whole protocol. The preparation of supported membranes, apyrase treatment, labelling with two dyes, washing, mounting and sealing with smFRET buffer takes a long time. However, supported membranes are not very stable for a long time period.
iii) It was suggested to add a small amount of ethanol to the imaging buffer, as this could improve the signal-to-noise-ratio, even though this would increase the toxicity.
iv) Since the beginning of my PhD project, more dyes for SNAP and CLIP labelling became commercially available. Accordingly, new combinations of FRET pairs could be tested.
Last but not least, the extraction of smFRET intensities was achieved but the signal-to-noise ratio was too low for further analysis. If the signal-to-noise ratio could be improved, more elaborate data processing would be needed. In this regard, the use of a Hidden Marcov Model was envisioned. This would allow to determine the number of substates without making *a priori* assumptions, reducing the bias.

If the method becomes reliably established, it will help to improve our understanding of the activation process of α_{2A}AR . Additionally, it could be applied to other receptors, leading to more general knowledge. The effect of different ligands can be investigated more directly, not just at a downstream level. It might be that different substates of the receptor favour different pathways. Accordingly, different substates could be specifically

targeted in the drug development. It is important to note that smFRET experiments were until now performed on purified or reconstituted receptors, but not in their native environment. Consequently, the results found with purified receptors could be validated by smFRET on supported membranes or even living cells.

9. Appendix

9.1. Plasmid maps

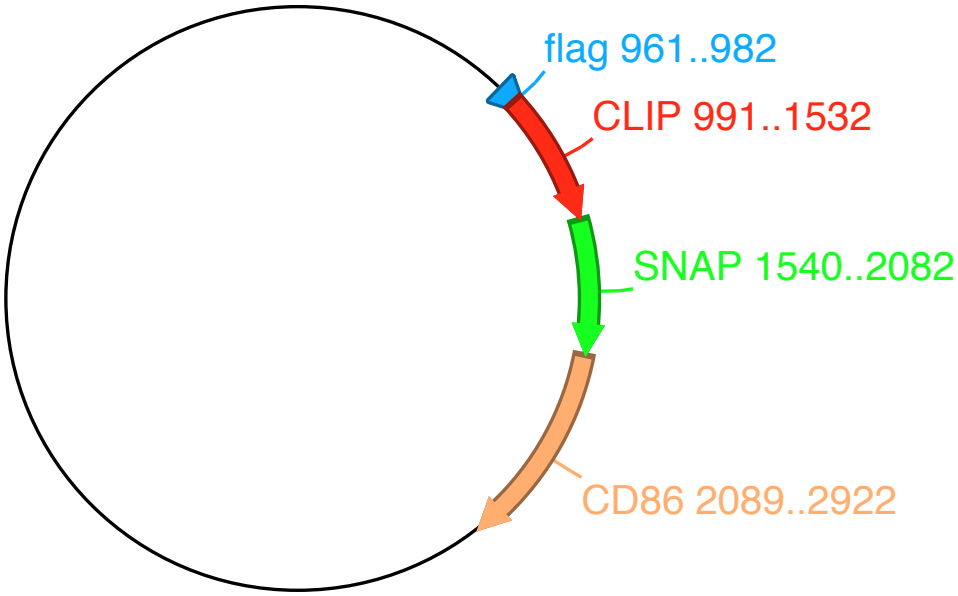

Figure 9.1.: Plasmid map of CD86 with N-terminal SNAP- and CLIP-tag.

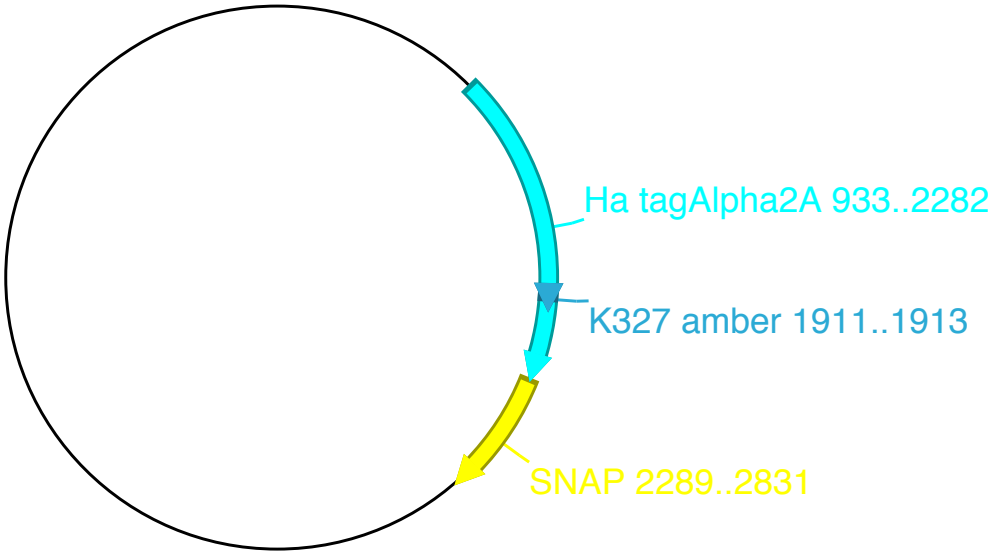

Figure 9.2.: Plasmid map of the K327amber mutation of α_{2A}AR. The stable cell line bearing this plasmid is called 'Bellatrix'.

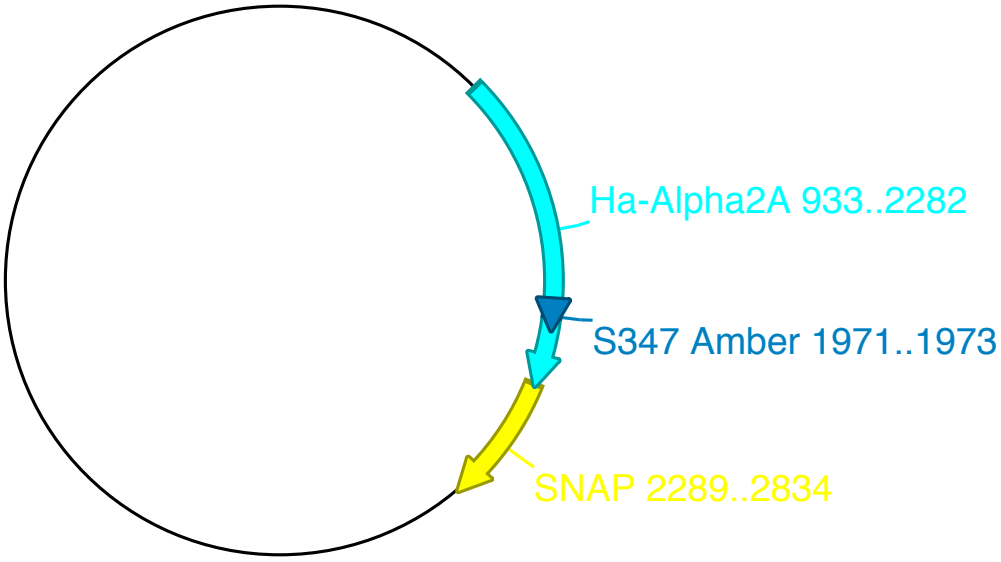

Figure 9.3.: Plasmid map of the S347amber mutation of α_{2A}AR. The stable cell line bearing this plasmid is called 'Capricorni'.

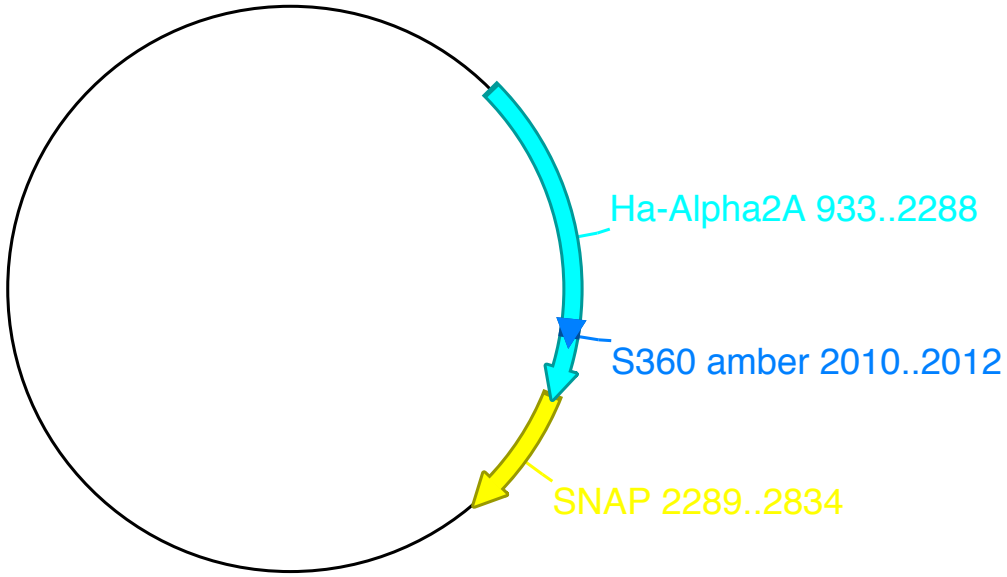

Figure 9.4.: Plasmid map of the S360amber mutation of α_{2A}AR. The stable cell line bearing this plasmid is called 'Deneb'.

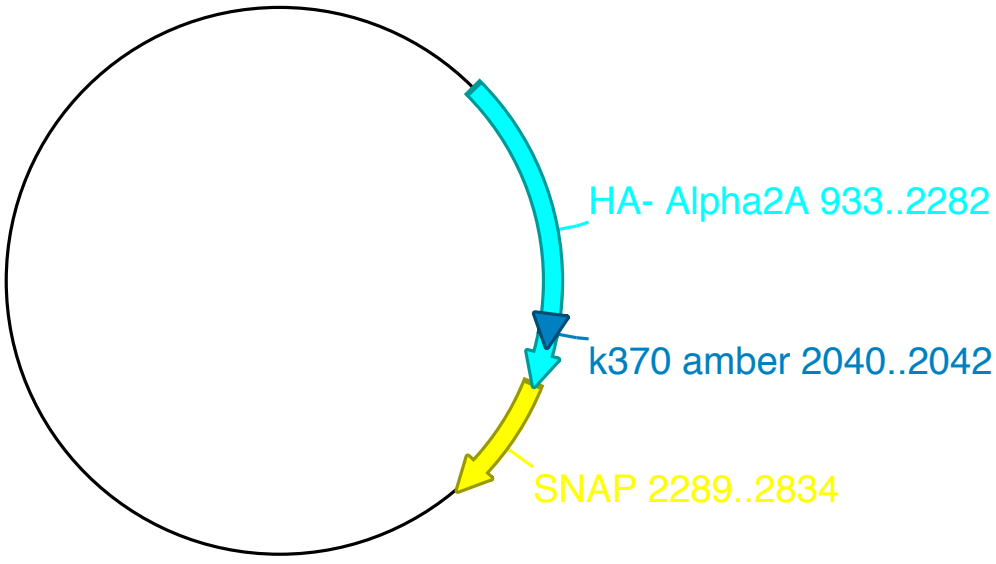

Figure 9.5.: Plasmid map of the K370amber mutation of α_{2A}AR. The stable cell line bearing this plasmid is called 'Enif'.

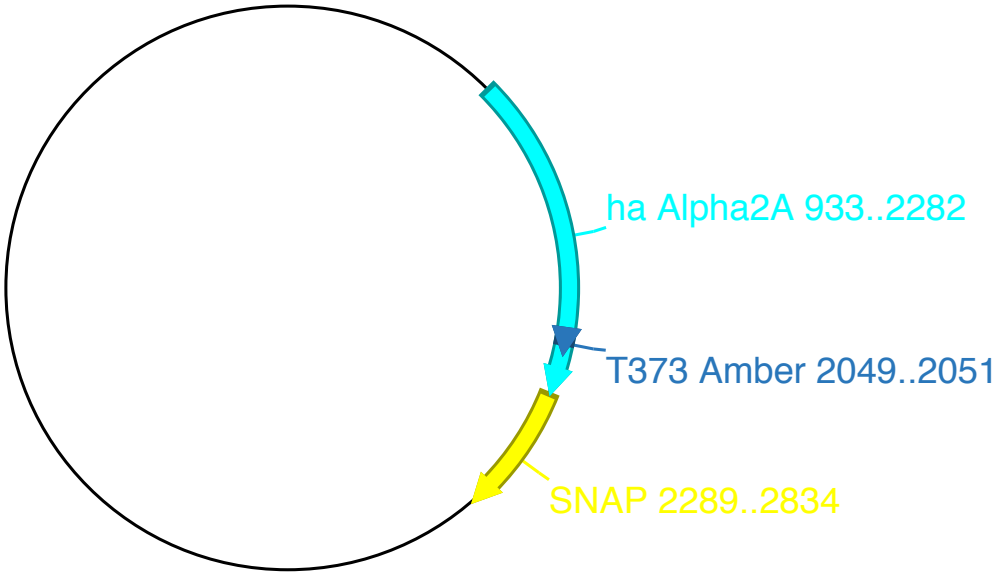

Figure 9.6.: Plasmid map of the T373amber mutation of α_{2A}AR. The stable cell line bearing this plasmid is called 'Fafnir'.

Bibliography

[1] Roland Seifert, Ulrik Gether, Katharina Wenzel-Seifert, and Brian K Kobilka. Effects of Guanine, Inosine, and Xanthine Nucleotides on β2-Adrenergic Receptor/Gs Interactions: Evidence for Multiple Receptor Conformations. *Molecular pharmacology*, 56(2):348–358, 1999.

[2] Aashish Manglik, Tae Hun Kim, Matthieu Masureel, Christian Altenbach, Zhongyu Yang, Daniel Hilger, Michael T. Lerch, Tong Sun Kobilka, Foon Sun Thian, Wayne L. Hubbell, R. Scott Prosser, and Brian K. Kobilka. Structural insights into the dynamic process of β<inf>2</inf>-adrenergic receptor signaling. *Cell*, 161(5):1101–1111, 2015.

[3] Rémy Sounier, Camille Mas, Jan Steyaert, Toon Laeremans, Aashish Manglik, Weijiao Huang, Brian K. Kobilka, Héléne Déméné, and Sébastien Granier. Propagation of conformational changes during μ-opioid receptor activation. *Nature*, 524(7565):375–378, 2015.

[4] Linnea Olofsson, Suren Felekyan, Etienne Doumazane, Pauline Scholler, Ludovic Fabre, Jurriaan M. Zwier, Philippe Rondard, Claus a. M. Seidel, Jean-Philippe Pin, and Emmanuel Margeat. Fine tuning of sub-millisecond conformational dynamics controls metabotropic glutamate receptors agonist efficacy. *Nature Communications*, 5:5206, 2014.

[5] Alexander S. Hauser, Misty M. Attwood, Mathias Rask-Andersen, Helgi B. Schiöth, and David E. Gloriam. Trends in GPCR drug discovery: New agents, targets and indications. *Nature Reviews Drug Discovery*, 16(12):829–842, 2017.

[6] Søren G F Rasmussen, Brian T DeVree, Yaozhong Zou, Andrew C Kruse, Ka Young Chung, Tong Sun Kobilka, Foon Sun Thian, Pil Seok Chae, Els Pardon,

Diane Calinski, Jesper M Mathiesen, Syed T A Shah, Joseph A Lyons, Martin Caffrey, Samuel H Gellman, Jan Steyaert, Georgios Skiniotis, William I Weis, Roger K Sunahara, and Brian K Kobilka. Crystal Structur of the β2Adrenergic Receptor-Gs protein complex. *Nature*, 477(7366):549–555, 2011.

[7] Christopher J Draper-Joyce, Maryam Khoshouei, David M Thal, Yi-lynn Liang, Anh T N Nguyen, Sebastian G B Furness, Hariprasad Venugopal, Jo-anne Baltos, Jürgen M Plitzko, Radostin Danev, and Wolfgang Baumeister. Structure of the adenosine-bound human adenosine A 1 receptor– G i complex. *Nature*, 2018.

[8] Antoine Koehl, Hongli Hu, Shoji Maeda, Yan Zhang, Qianhui Qu, Joseph M. Paggi, Naomi R. Latorraca, Daniel Hilger, Roger Dawson, Hugues Matile, Gebhard F. X. Schertler, Sebastien Granier, William i. Weis, Ron O. Dror, Aashish Manglik, Georgios Skiniotis &, and Brian K. Kobilka. Structure of the μ-opioid receptor-Gi protein complex. *Nature*, 2018.

[9] Aashish Manglik, Andrew C. Kruse, Tong Sun Kobilka, Foon Sun Thian, Jesper M. Mathiesen, Roger K. Sunahara, Leonardo Pardo, William I. Weis, Brian K. Kobilka, and Sébastien Granier. Crystal structure of the mu-opioid receptor bound to a morphinan antagonist. *Nature*, 485(7398):321–326, 2012.

[10] Dandan Zhang, Qiang Zhao, and Beili Wu. Structural studies of G protein-coupled receptors. *Molecules and Cells*, 38(10):836–842, 2015.

[11] Steven M Foord, T O M I Bonner, Richard R Neubig, Edward M Rosser, Jean-phillipe Pin, Anthony P Davenport, Michael Spedding, and Anthony J Harmar. International Union of Pharmacology. XLVI. G Protein-Coupled Receptor List. *Pharmacological Reviews*, 57(2):279–288, 2005.

[12] C. Harrison and J. R. Traynor. The [35S]GTPγS binding assay: Approaches and applications in pharmacology. *Life Sciences*, 74(4):489–508, 2003.

[13] Kristen L. Pierce, Richard T. Premont, and Robert J. Lefkowitz. Signalling: Seven-transmembrane receptors. *Nature Reviews Molecular Cell Biology*, 3(9):639–650, 2002.

[14] William I Weis and Brian K Kobilka. The Molecular Basis of G Protein - Coupled Receptor Activation. 2018.

[15] Benjamin G. Tehan, Andrea Bortolato, Frank E. Blaney, Malcolm P. Weir, and Jonathan S. Mason. Unifying Family A GPCR Theories of Activation. *Pharmacology and Therapeutics*, 143(1):51–60, 2014.

[16] Aashish Manglik and Andrew C. Kruse. Structural Basis for G Protein-Coupled Receptor Activation. *Biochemistry*, 56(42):5628–5634, 2017.

[17] Rajan Lamichhane, Jeffrey J. Liu, Goran Pljevaljcic, Kate L. White, Edwin van der Schans, Vsevolod Katritch, Raymond C. Stevens, Kurt Wüthrich, and David P. Millar. Single-molecule view of basal activity and activation mechanisms of the G protein-coupled receptor β 2 AR. *Proceedings of the National Academy of Sciences*, page 201519626, 2015.

[18] G. Glenn Gregorio, Matthieu Masureel, Daniel Hilger, Daniel S. Terry, Manuel Juette, Hong Zhao, Zhou Zhou, Jose Manuel Perez-Aguilar, Maria Hauge, Signe Mathiasen, Jonathan A. Javitch, Harel Weinstein, Brian K. Kobilka, and Scott C. Blanchard. Single-molecule analysis of ligand efficacy in β2AR-G-protein activation. *Nature*, 2017.

[19] Zara Y Weinberg and Manojkumar A Puthenveedu. Regulation of G protein-coupled receptor signaling by plasma membrane organization and endocytosis, 2019.

[20] Viacheslav O. Nikolaev, Moritz Bünemann, Lutz Hein, Annette Hannawacker, and Martin J. Lohse. Novel single chain cAMP sensors for receptor-induced signal propagation. *Journal of Biological Chemistry*, 279(36):37215–37218, 2004.

[21] Tetsuji Okada, Krzysztof Palczewski, Oliver P Ernst, and Klaus Peter Hofmann. Activation of rhodopsin:new insights from structural and biochemical studies. *TRENDS in Biochemical Sciences*, 26(5):318–324, 2001.

[22] He Tian, Thomas P. Sakmar, and Thomas Huber. The Energetics of Chromophore Binding in the Visual Photoreceptor Rhodopsin. *Biophysical Journal*, 113(1):60–72, 2017.

[23] Jean Pierre Vilardaga, Moritz Bünemann, Cornelius Krasell, Mariàn Castro, and Martin J Lohse. Measurement of the millisecond activation switch of G protein-coupled receptors in living cells. *Nature Biotechnology*, 21(7):807–812, 2003.

[24] Carsten Hoffmann, Guido Gaietta, and Moritz Bünemann. A FlAsH-based FRET approach to determine G protein-coupled receptor activation in living cells. *Nature Methods*, 2(3):171–176, 2005.

[25] Monika Maier-Peuschel, Nadine Frölich, Christian Dees, Leif G. Hommers, Carsten Hoffmann, Viacheslav O. Nikolaev, and Martin J. Lohse. A fluorescence resonance energy transfer-based M2 muscarinic receptor sensor reveals rapid kinetics of allosteric modulation. *Journal of Biological Chemistry*, 285(12):8793–8800, 2010.

[26] Nicole Ziegler, Julia Bätz, Ulrike Zabel, Martin J. Lohse, and Carsten Hoffmann. FRET-based sensors for the human M1-, M3-, and M 5-acetylcholine receptors. *Bioorganic and Medicinal Chemistry*, 19(3):1048–1054, 2011.

[27] R. K. Sunahara and P. A. Insel. The molecular pharmacology of G protein signaling then and now: A tribute to Alfred G. Gilman. *Molecular Pharmacology*, (May):585–592, 2016.

[28] Nguyen Minh Duc, Hee Ryung Kim, and Ka Young Chung. Structural mechanism of G protein activation by G protein-coupled receptor. *European Journal of Pharmacology*, 763:214–222, 2015.

[29] Louis M. Luttrell. Transmembrane signaling by G protein-coupled receptors. *Methods in molecular biology (Clifton, N.J.)*, 332:3–49, 2006.

[30] A. De Lean, J. M. Stadel, and R. J. Lefkowitz. A ternary complex model explains the agonist-specific binding properties of the adenylate cyclase-coupled β-adrenergic receptor. *Journal of Biological Chemistry*, 255(15):7108–7117, 1980.

[31] Kou Qin, Chunmin Dong, Guangyu Wu, and Nevin A. Lambert. Inactive-state preassembly of Gq-coupled receptors and Gqheterotrimers. *Nature Chemical Biology*, 7(10):740–747, 2011.

[32] M. Nobles, A. Benians, and A. Tinker. Heterotrimeric G proteins precouple with G protein-coupled receptors in living cells. *Proceedings of the National Academy of Sciences*, 102(51):18706–18711, 2005.

[33] R. A.John Challiss and Jürgen Wess. Receptors: GPCR-G protein preassembly? *Nature Chemical Biology*, 7(10):657–658, 2011.

[34] Jonathan A Hern, Asma H Baig, Gregory I Mashanov, Berry Birdsall, John E T Corrie, Sebastian Lazareno, Justin E Molloy, and Nigel J M Birdsall. Formation and dissociation of M1 muscarinic receptor dimers seen by total internal reflection fluorescence imaging of single molecules. *Proceedings of the National Academy of Sciences of the United States of America*, 107(6):2693–8, 2010.

[35] Bryen A. Jordan and Lakshmi A. Devi. G-protein-coupled receptor heterodimerization modulates receptor function. *Nature*, 399(6737):697–700, 1999.

[36] Rinshi S. Kasai, Shuichi V. Ito, Ryo M. Awane, Takahiro K. Fujiwara, and Akihiro Kusumi. The Class-A GPCR Dopamine D2 Receptor Forms Transient Dimers Stabilized by Agonists: Detection by Single-Molecule Tracking. *Cell Biochemistry and Biophysics*, 76(1-2):29–37, 2018.

[37] Alina Tabor, Siegfried Weisenburger, Ashutosh Banerjee, Nirupam Purkayastha, Jonas M. Kaindl, Harald Hübner, Luxi Wei, Teja W. Grömer, Johannes Kornhuber, Nuska Tschammer, Nigel J. M. Birdsall, Gregory I. Mashanov, Vahid Sandoghdar, and Peter Gmeiner. Visualization and ligand-induced modulation of dopamine receptor dimerization at the single molecule level. *Scientific Reports*, 6(1):1–16, 2016.

[38] Davide Calebiro, Finn Rieken, Julia Wagner, Titiwat Sungkaworn, Ulrike Zabel, Alfio Borzi, Emanuele Cocucci, Alexander Zürn, and Martin J Lohse. Single-molecule analysis of fluorescently labeled G-protein-coupled receptors reveals complexes with distinct dynamics and organization. *Proceedings of the National Academy of Sciences of the United States of America*, 110(2):743–8, 2013.

[39] Julie Kniazeff, Laurent Prézeau, Philippe Rondard, Jean Philippe Pin, and Cyril Goudet. Dimers and beyond: The functional puzzles of class C GPCRs. *Pharmacology and Therapeutics*, 130(1):9–25, 2011.

[40] Josée-France Villemure, Lynda Adam, Nicola J Bevan, Katy Gearing, Sébastien Chénier, and Michel Bouvier. Subcellular distribution of GABA(B) receptor homo- and hetero-dimers. *The Biochemical journal*, 388(Pt 1):47–55, 2005.

[41] J-P Pin, L Comps-Agrar, D Maurel, C Monnier, M L Rives, E Trinquet, J Kniazeff, P Rondard, and L Prézeau. G-protein-coupled receptor oligomers: two or more

for what? Lessons from mGlu and GABAB receptors. *The Journal of physiology*, 587(Pt 22):5337–5344, 2009.

[42] Kenichi Kawano, Tetsuya Yagi, Nozomu Fukada, Yoshiaki Yano, and Katsumi Matsuzaki. Stoichiometric analysis of oligomeric states of three class-A GPCRs, chemokine-CXCR4, dopamine-D2, and prostaglandin-EP1 receptors, on living cells. *Journal of Peptide Science*, 23(7-8):650–658, 2017.

[43] Graeme Milligan, Richard J. Ward, and Sara Marsango. GPCR homo-oligomerization. *Current Opinion in Cell Biology*, 57:40–47, 2019.

[44] Patricia M Dijkman, Oliver K Castell, Alan D Goddard, Juan C Munoz-garcia, Chris De Graaf, Mark I Wallace, and Anthony Watts. Dynamic tuneable G protein-coupled receptor monomer-dimer populations. *Nature Communications*, pages 1–14, 2018.

[45] Danxin Wang, Xiaochun Sun, LM Bohn, and W Sadee. Opioid receptor homo- and heterodimerization in living cells by quantitative bioluminescence resonance energy transfer. *Molecular pharmacology*, 67(6):2173–2184, 2005.

[46] Urszula Golebiewska, Jennifer M. Johnston, Lakshmi Devi, Marta Filizola, and Suzanne Scarlata. Differential response to morphine of the oligomeric state of μ-opioid in the presence of δ-opioid receptors. *Biochemistry*, 50(14):2829–2837, 2011.

[47] Lakshmi A Devi. Heterodimerization of G-protein-coupled receptors: Pharmacology, signaling and trafficking, 2001.

[48] Muzeyyen Ugur, Lyes Derouiche, and Dominique Massotte. Heteromerization modulates mu opioid receptor functional properties in vivo. *Frontiers in Pharmacology*, 9(NOV):1–10, 2018.

[49] S. Ferre, V. Casado, L. A. Devi, M. Filizola, R. Jockers, M. J. Lohse, G. Milligan, J.-P. Pin, and X. Guitart. G Protein-Coupled Receptor Oligomerization Revisited: Functional and Pharmacological Perspectives. *Pharmacological Reviews*, 66(2):413–434, 2014.

[50] Samuel M. Walsh, Signe Mathiasen, Sune M. Christensen, Jonathan F. Fay, Christopher King, Davide Provasi, Ernesto Borrero, Søren G.F. Rasmussen, Juan Jose Fung, Marta Filizola, Kalina Hristova, Brian Kobilka, David L. Farrens, and Dimitrios Stamou. Single Proteoliposome High-Content Analysis Reveals Differences in the Homo-Oligomerization of GPCRs. *Biophysical Journal*, 115(2):300–312, 2018.

[51] Ivone Gomes, Achla Gupta, Julija Filipovska, Hazel H Szeto, John E Pintar, and Lakshmi A Devi. A role for heterodimerization of mu and delta opiate receptors in enhancing morphine analgesia. *Proceedings of the National Academy of Sciences of the United States of America*, 101(14):5135–9, 2004.

[52] Graeme Milligan. G Protein-Coupled Receptor Dimerization: Function and Ligand Pharmacology. *Molecular Pharmacology*, 66(1):1–7, 2004.

[53] Li He, Jamie Fong, Mark Von Zastrow, and Jennifer L. Whistler. Regulation of opioid receptor trafficking and morphine tolerance by receptor oligomerization. *Cell*, 108(2):271–282, 2002.

[54] Alistair D. Corbett, Graeme Henderson, Alexander T. McKnight, and Stewart J. Paterson. 75 Years of opioid research: The exciting but vain quest for the Holy Grail. *British Journal of Pharmacology*, 147(SUPPL. 1):153–162, 2006.

[55] Craig W Stevens. The evolution of vertebrate opioid receptors Craig, 2009.

[56] Fabien Decaillot, Noura Abul-Husn, and Lakshmi Devi. Delta Opioid Peptide Receptor. *xPharm: The Comprehensive Pharmacology Reference*, pages 1–12, 2007.

[57] Jean Luc Butour, Christiane Moisand, Honoré Mazarguil, Catherine Mollereau, and Jean Claude Meunier. Recognition and activation of the opioid receptor-like ORL1 receptor by nociceptin, nociceptin analogs and opioids. *European Journal of Pharmacology*, 321(1):97–103, 1997.

[58] Matthias Seefelder. *Opium - Eine Kulturgeschichte*. DTV Deutscher Taschenbuch, Landsberg, 1993.

[59] UNODC. *World Drug Report 2019 -Depressants*. 2019.

[60] HHS. The opioid epidemic. (293):2019, 2019.

[61] Holly Hedegaard, Margaret Warner, and Arialdi M. Minino. Drug Overdose Deaths in the United States, 1999-2015. *NCHS data brief*, (273):1–8, 2017.

[62] Cobin D. Soelberg, Raeford E. Brown, Derick Du Vivier, John E. Meyer, and Banu K. Ramachandran. The US Opioid Crisis: Current Federal and State Legal Issues. *Anesthesia and Analgesia*, 125(5):1675–1681, 2017.

[63] Adam J. Kuszak, Sethuramasundaram Pitchiaya, Jessica P. Anand, Henry I. Mosberg, Nils G. Walter, and Roger K. Sunahara. Purification and functional reconstitution of monomeric mu-opioid receptors. Allosteric modulation of agonists binding by Gi2. *Journal of Biological Chemistry*, 284(39):26732–26741, 2009.

[64] Derya Meral, Davide Provasi, Diego Prada-gracia, Jan Möller, Kristen Marino, Martin J Lohse, and Marta Filizola. Molecular details of dimerization kinetics reveal negligible populations of transient μ -opioid receptor homodimers at physiological concentrations. *Scientific Reports*, 8(February):1–13, 2018.

[65] Svetlana Cvejic and Lakshmi A Devi. Dimerization of the δ opioid receptor: Implication for a role in receptor internalization. *Journal of Biological Chemistry*, 272(43):26959–26964, 1997.

[66] I Gomes, B A Jordan, A Gupta, N Trapaidze, V Nagy, and L A Devi. Heterodimerization of mu and delta opioid receptors: A role in opiate synergy. *The Journal of neuroscience : the official journal of the Society for Neuroscience*, 20(22):RC110, 2000.

[67] Ivone Gomes, Julija Filipovska, Bryen A. Jordan, and Lakshmi A. Devi. Oligomerization of opioid receptors. *Methods*, 27(4):358–365, 2002.

[68] Davide Provasi, Mustafa Burak Boz, Jennifer M. Johnston, and Marta Filizola. Preferred Supramolecular Organization and Dimer Interfaces of Opioid Receptors from Simulated Self-Association. *PLoS Computational Biology*, 11(3):1–21, 2015.

[69] Chuan Li Xi Zhang, Yuan Yuan, Longrong Wang, Yanzhi Guo, Menglong Li and Xuemei Pu. Use multiscale simulation to explore the effects of the homodimerizations between different conformation states on the activation and allosteric pathway for the μ-opioid receptor. *Physical Chemistry Chemical Physics*, 20:13485–13496, 2018.

[70] F. M. Decaillot, R. Rozenfeld, A. Gupta, and L. A. Devi. Cell surface targeting of - opioid receptor heterodimers by RTP4. *Proceedings of the National Academy of Sciences*, 105(41):16045–16050, 2008.

[71] Davide Calebiro and Titiwat Sungkaworn. Single-Molecule Imaging of GPCR Interactions. *Trends in Pharmacological Sciences*, 39:1–14, 2017.

[72] He Tian, Alexandre Fürstenberg, and Thomas Huber. Labeling and Single-Molecule Methods To Monitor G Protein-Coupled Receptor Dynamics. *Chemical Reviews*, pages A–BH, 2016.

[73] Kenichi Suzuki, Ken Ritchie, Eriko Kajikawa, Takahiro Fujiwara, and Akihiro Kusumi. Rapid hop diffusion of a G-protein-coupled receptor in the plasma membrane as revealed by single-molecule techniques. *Biophysical Journal*, 88(5):3659–3680, 2005.

[74] Titiwat Sungkaworn, Marie-Lise Jobin, Krzysztof Burnecki, Aleksander Weron, Martin J. Lohse, and Davide Calebiro. Single-molecule imaging reveals receptor-G protein interactions at cell surface hot spots. *Nature*, 2017.

[75] Khuloud Jaqaman, Dinah Loerke, Marcel Mettlen, Hirotaka Kuwata, Sergio Grinstein, Sandra L Schmid, and Gaudenz Danuser. Robust single-particle tracking in live-cell time-lapse sequences. *Nature Methods*, 5(8):695–702, 2008.

[76] Donald B. Raid. An algorithm for tracking multiple targets. *IEEE Transactions on Automatic Control*, 24(6):843–854, 1979.

[77] Michael J. Saxton and Ken Jacobson. SINGLE-PARTICLE TRACKING:Applications to Membrane Dynamics. *Annual Review of Biophysics and Biomolecular Structure*, 26(1):373–399, 1997.

[78] Ralf Metzler, Jae-Hyung Jeon, Andrey G. Cherstvy, and Eli Barkai. Anomalous diffusion models and their properties: non-stationarity, non-ergodicity, and ageing at the centenary of single particle tracking. *Phys. Chem. Chem. Phys.*, 16(44):24128–24164, 2014.

[79] Kim C. Jonas, Francesca Fanelli, Ilpo T. Huhtaniemi, and Aylin C. Hanyaloglu. Single molecule analysis of functionally asymmetric G protein-coupled receptor

(GPCR) oligomers reveals diverse spatial and structural assemblies. *Journal of Biological Chemistry*, 290(7):3875–3892, 2015.

[80] Seamus J. Holden, Stephan Uphoff, Johannes Hohlbein, David Yadin, Ludovic Le Reste, Oliver J. Britton, and Achillefs N. Kapanidis. Defining the limits of single-molecule FRET resolution in TIRF microscopy. *Biophysical Journal*, 99(9):3102–3111, 2010.

[81] Marko Sustarsic and Achillefs N Kapanidis. Taking the ruler to the jungle: single-molecule FRET for understanding biomolecular structure and dynamics in live cells. *Current Opinion in Structural Biology*, 34:52–59, 2015.

[82] David W Piston and Gert-Jan Kremers. Fluorescent protein FRET: the good, the bad and the ugly. *Trends in biochemical sciences*, 32(9):407–414, 2007.

[83] Bryce T. Bajar, Emily S. Wang, Shu Zhang, Michael Z. Lin, and Jun Chu. A guide to fluorescent protein FRET pairs. *Sensors (Switzerland)*, 16(9):1–24, 2016.

[84] Dibyendu Kumar Sasmal, Rajeev Yadav, and H. Peter Lu. Single-Molecule Patch-Clamp-FRET-Anisotropy Microscopy Studies of NMDA Receptor Ion Channel Activation and Deactivation under Agonist Ligand Binding in Living Cells. *Journal of the American Chemical Society*, page jacs.6b03496, 2016.

[85] John J Sakon and Keith R Weninger. Detecting the conformation of individual proteins in live cells. *Nature Publishing Group*, 7(3):203–205, 2010.

[86] R Vafabakhsh, J Levitz, and E Y Isacoff. Conformational dynamics of a class C G-protein-coupled receptor. *Nature*, 524(7566):497–501, 2015.

[87] Marlon J Hinner and Kai Johnsson. How to obtain labeled proteins and what to do with them. *Current opinion in biotechnology*, 21(6):766–76, dec 2010.

[88] Julia Manhard. *No Title*. Master thesis, Würzburg, Würzburg, 2013.

[89] George G. Holz, Guoxin Kang, Mark Harbeck, Michael W. Roe, and Oleg G. Chepurny. Cell physiology of cAMP sensor Epac. *Journal of Physiology*, 577(1):5–15, 2006.

[90] A. D. Stumpf and C. Hoffmann. Optical probes based on G protein-coupled receptors - Added work or added value? *British Journal of Pharmacology*, 173(2):255–266, 2016.

[91] Martin J. Lohse, Moritz Bünemann, Carsten Hoffmann, Jean Pierre Vilardaga, and Viacheslav O. Nikolaev. Monitoring receptor signaling by intramolecular FRET. *Current Opinion in Pharmacology*, 7(5):547–553, 2007.

[92] Nelson B Cole. Site-Specific Protein Labeling with SNAP-Tags. pages 1–19, 2013.

[93] Antje Keppler, Susanne Gendreizig, Thomas Gronemeyer, Horst Pick, Horst Vogel, and Kai Johnsson. A general method for the covalent labeling of fusion proteins with small molecules in vivo. *Nature biotechnology*, 21(1):86–9, jan 2003.

[94] Helen M O'Hare, Kai Johnsson, and Arnaud Gautier. Chemical probes shed light on protein function. *Current opinion in structural biology*, 17(4):488–94, aug 2007.

[95] Arnaud Gautier, Alexandre Juillerat, Christian Heinis, Ivan Reis Corrêa, Maik Kindermann, Florent Beaufils, and Kai Johnsson. An Engineered Protein Tag for Multiprotein Labeling in Living Cells. *Chemistry and Biology*, 15(2):128–136, 2008.

[96] Georgyi V. Losâ ,*, Lance P. Encellâ , Mark G. McDougallâ¡, Danette D. Hartzellâ , Natasha Karassinaâ , Chad Zimprichâ , Monika G. Woodâ , Randy Learishâ , Rachel Friedman Ohanaâ , Marjeta Urhâ , Dan Simpsonâ , Jacqui Mendezâ , Kris Zimmermanâ , Paul Ottoâ , Gediminas and Keith V. Wood. HaloTag: A Novel Protein Labeling Technology for Cell Imaging and Protein Analysis. *ACS Chemical Biology*, 3(12):765–775, 2008.

[97] Antje Keppler, Claudio Arrivoli, Lucia Sironi, and Jan Ellenberg. Fluorophores for live cell imaging of AGT fusion proteins across the visible spectrum. *BioTechniques*, 41(2):167–175, 2006.

[98] Richard J. Ward, Tian Rui Xu, and Graeme Milligan. *GPCR oligomerization and receptor trafficking*, volume 521. Elsevier Inc., 1 edition, 2013.

[99] Howard M. Goodman, John Abelson, Arthur Landy, S. Brenner, and J. D. Smith. Amber suppression: A Nucleotide change in the anticodon of a tyrosine transfer RNA. *Nature*, 217(5133):1019–1024, 1968.

[100] Caroline Köhrer, Eric L. Sullivan, and Uttam L. RajBhandary. Complete set of orthogonal 21st aminoacyl-tRNA synthetase-amber, ochre and opal suppressor tRNA pairs: Concomitant suppression of three different termination codons in an mRNA in mammalian cells. *Nucleic Acids Research*, 32(21):6200–6211, 2004.

[101] J Christopher, J Spencer, C Michael, and G Peter. A General Method for Site-Specific Incorporation of Unnatural Amino Acids into Proteins. *Science*, 244:182–188, 1989.

[102] Shixin Ye, Caroline Köhrer, Thomas Huber, Manija Kazmi, Pallavi Sachdev, Elsa C Y Yan, Aditi Bhagat, Uttam L. RajBhandary, and Thomas P. Sakmar. Site-specific incorporation of keto amino acids into functional G protein-coupled receptors using unnatural amino acid mutagenesis. *Journal of Biological Chemistry*, 283(3):1525–1533, 2008.

[103] Li Yin Huang, George Umanah, Melinda Hauser, Cagdas Son, Boris Arshava, Fred Naider, and Jeffrey M. Becker. Unnatural amino acid replacement in a yeast G protein-coupled receptor in its native environment. *Biochemistry*, 47(20):5638–5648, 2008.

[104] R. Serfling and I. Coin. *Incorporation of Unnatural Amino Acids into Proteins Expressed in Mammalian Cells*, volume 580. Elsevier Inc., 1 edition, 2016.

[105] Thomas Huber, Saranga Naganathan, He Tian, Shixin Ye, and Thomas P. Sakmar. *Unnatural amino acid mutagenesis of GPCRs using amber codon suppression and bioorthogonal labeling*, volume 520. Elsevier Inc., 1 edition, 2013.

[106] Ivana Nikić, Jun Hee Kang, Gemma Estrada Girona, Iker Valle Aramburu, and Edward a Lemke. Labeling proteins on live mammalian cells using click chemistry. *Nature protocols*, 10(5):780–91, 2015.

[107] Franziska Neubert, Gerti Beliu, Ulrich Terpitz, Christian Werner, Christian Geis, Markus Sauer, and Sören Doose. Bioorthogonal click chemistry enables site-specific fluorescence labeling of functional NMDA receptors for super-resolution imaging. *Angewandte Chemie*, 2018.

[108] Pablo Mateos-Gil, Sebastian Letschert, Sören Doose, and Markus Sauer. Super-Resolution Imaging of Plasma Membrane Proteins with Click Chemistry. *Frontiers in Cell and Developmental Biology*, 4(September):98, 2016.

[109] Ivana Nikić and Edward A. Lemke. Genetic code expansion enabled site-specific dual-color protein labeling: Superresolution microscopy and beyond. *Current Opinion in Chemical Biology*, 28:164–173, 2015.

[110] Francisco Ciruela, Kenneth A Jacobson, and Victor Fernández-Duenas. Portraying G Protein-Coupled Receptors with Fluorescent Ligands. 2014.

[111] Leigh A. Stoddart, Carl W. White, Kim Nguyen, Stephen J. Hill, and Kevin D.G. Pfleger. Fluorescence- and bioluminescence-based approaches to study GPCR ligand binding. *British Journal of Pharmacology*, 173(20):3028–3037, 2016.

[112] Luca Agnetta, Michael Kauk, Maria Consuelo Alonso Canizal, Regina Messerer, Ulrike Holzgrabe, Carsten Hoffmann, and Michael Decker. A Photoswitchable Dualsteric Ligand Controlling Receptor Efficacy. *Angewandte Chemie - International Edition*, 56(25):7282–7287, 2017.

[113] J.-B. Perez, K. L. Martinez, J.-M. Segura, and H. Vogel. Supported Cell-Membrane Sheets for Functional Fluorescence Imaging of Membrane Proteins. *Advanced Functional Materials*, 16(2):306–312, jan 2006.

[114] Sandra Dorsch, Karl Norbert Klotz, Stefan Engelhardt, Martin J. Lohse, and Moritz Bünemann. Analysis of receptor oligomerization by FRAP microscopy. *Nature Methods*, 6(3):225–230, 2009.

[115] Franziska Fricke, Joel Beaudouin, Roland Eils, and Mike Heilemann. One, two or three? Probing the stoichiometry of membrane proteins by single-molecule localization microscopy. *Scientific Reports*, 5(June):1–8, 2015.

[116] L. B. Lucy. An iterative technique for the rectification of observed distributions. *The Astronomical Journal*, 79(6):745, 1974.

[117] Jay P McLaughlin, Kevin P Hill, Q I Jiang, Alice Sebastian, Sydney Archer, and Jean M Bidlack. Nitrocinnamoyl and Chlorocinnamoyl Derivatives of Dihydrocodeinone : In Vivo and In Vitro Characterization of μ-Selective Agonist and

Antagonist Activity. *The Journal of Pharmacology and Experimental Therapeutics*, 289(1):304–311, 1999.

[118] PS Portoghese, M Sultana, and AE Takemori. Naltrindole, a highly selective and potent non-peptide delta opioid antagonist. *European journal of pharmacology*, 146(1):185–186, 1988.

[119] Paul J Emmerson, Sydney Archer, Wageeh El-hamouly, and Alfred Mansour. Synthesis and Characterization of 4 , 4-Difluoro-4-bora- Ligands for the Mu Opioid Receptor. 54(97):1315–1322, 1997.

[120] Alice Sebastian, Jean M. Bidlack, Qi Jiang, Darlene Deecher, Milton Teitler, Stanley D. Glick, and Sydney Archer. 14beta-[(p-Nitrocinnamoyl)amino]morphinones, 14beta-[(p-Nitrocinnamoyl)amino]-7,8-dihydromorphinones, and Their Codeinone Analogues: Synthesis and Receptor Activity. *Journal of Medicinal Chemistry*, 36(21):3154–3160, 1993.

[121] I Derrick, J W Lewis, H A Moynihan, J Broadbear, and J H Woods. Potential irreversible ligands for opioid receptors. Cinnamoyl derivatives of beta-naltrexamine. *J Pharm Pharmacol*, 48(2):192–196, 1996.

[122] Yann Lanoiselee. *Revealing the transport mechanisms from a single trajectory in living cells*. PhD thesis, 2018.

[123] Marissa J. Metz, Reagan L. Pennock, Diego Krapf, and Shane T. Hentges. Temporal dependence of shifts in mu opioid receptor mobility at the cell surface after agonist binding observed by single-particle tracking. *Scientific Reports*, 9(1):7297, 2019.

[124] Libin Abraham, Henry Y. Lu, Rebeca Cardim Falcão, Joshua Scurll, Timothy Jou, Brian Irwin, Reza Tafteh, Michael R. Gold, and Daniel Coombs. Limitations of Qdot labelling compared to directly-conjugated probes for single particle tracking of B cell receptor mobility. *Scientific Reports*, 7(1):1–13, 2017.

[125] M. Howarth, K. Takao, Y. Hayashi, and A. Y. Ting. Targeting quantum dots to surface proteins in living cells with biotin ligase. *Proceedings of the National Academy of Sciences*, 102(21):7583–7588, 2005.

[126] Barbora Melkes, Lucie Hejnova, and Jiri Novotny. Biased μ-opioid receptor agonists diversely regulate lateral mobility and functional coupling of the receptor to its cognate G proteins. *Naunyn-Schmiedeberg's Archives of Pharmacology*, 389(12):1289–1300, 2016.

[127] Jakobus Van Unen, Anette D. Stumpf, Benedikt Schmid, Nathalie R. Reinhard, Peter L. Hordijk, Carsten Hoffmann, Theodorus W J Gadella, and Joachim Goedhart. A new generation of FRET sensors for robust measurement of Gαi1, Gαi2 and Gαi3 activation kinetics in single cells. *PLoS ONE*, 11(1):1–14, 2016.

[128] Graeme Milligan. Principles: Extending the utility of [35S]GTPγS binding assays. *Trends in Pharmacological Sciences*, 24(2):87–90, 2003.

[129] J R Jasper, J D Lesnick, L K Chang, S S Yamanishi, T K Chang, S a Hsu, D a Daunt, D W Bonhaus, and R M Eglen. Ligand efficacy and potency at recombinant alpha2 adrenergic receptors: agonist-mediated [35S]GTPgammaS binding. *Biochemical pharmacology*, 55(7):1035–1043, 1998.

[130] Marcel Bermudez, Andreas Bock, Fabian Krebs, Ulrike Holzgrabe, Klaus Mohr, Martin J. Lohse, and Gerhard Wolber. Ligand-Specific Restriction of Extracellular Conformational Dynamics Constrains Signaling of the M2Muscarinic Receptor. *ACS Chemical Biology*, 12(7):1743–1748, 2017.

[131] Andreas Bock, Nicole Merten, Ramona Schrage, Clelia Dallanoce, Julia Bätz, Jessica Klöckner, Jens Schmitz, Carlo Matera, Katharina Simon, Anna Kebig, Lucas Peters, Anke Müller, Jasmin Schrobang-Ley, Christian Tränkle, Carsten Hoffmann, Marco De Amici, Ulrike Holzgrabe, Evi Kostenis, and Klaus Mohr. The allosteric vestibule of a seven transmembrane helical receptor controls G-protein coupling. *Nature Communications*, 3, 2012.

[132] Yongping Zhu, Lei Zhang, Xuejun C. Zhang, and Yongfang Zhao. Structural dynamics of G i α protein revealed by single molecule FRET. *Biochemical and Biophysical Research Communications*, 2017.

[133] Margaret G Eason and Stephen B Liggett. Chimeric Mutagenesis of Putative G-protein Coupling Domains of the alpha2A -Adrenergic Receptor. *Journal of Biological Chemistry*, 271(22):12826–12832, 1996.

[134] P. A. Singleton, T. Mirzapoiazova, R. Hasina, R. Salgia, and J. Moss. Increased μ-opioid receptor expression in metastatic lung cancer. *British Journal of Anaesthesia*, 113(SUPPL. 1):i103–i108, 2014.

Acknowledgements

First, I would like to thank my primary supervisor Prof. Davide Calebiro for giving me the opportunity to work on those exciting projects in his lab. Furthermore, I want to thank him for his well-founded and helpful scientific advice over the past years.
My second and third supervisor, Prof. Markus Sauer and Prof. Kristina Lorenz, I thank for the scientific discussions and their help throughout my PhD.

A lot of gratitude goes to AG Calebiro. Everyone was helpful, welcoming and made the lab a nice place to work in. Notamment, merci beaucoup á Marie-Lise Jobin, for scientific help, discussions and a lot of fun and support inside, as well as outside, the lab. Many thanks to Kerstin Bathon, who was always ready to jump in to help and explain. Of course, a lot of thanks go to Titiwat Sungkaworn for teaching me single-molecule microscopy and cell culture. I also thank Christin Misigaiski a lot for all her help and enthusiasm in the lab and especially for keeping all my cell lines happy. Thanks as well to all the technicians, Bianca Klüpfel, Alexandra Bohl and Ines Elsner, for their help and support. I would like to thank Amod Godbole, Sana Siddig, Isabella Maiellaro and Sandra Lyga for their supportive and positive attitude towards lab work and science.
A lot of thanks goes to Birmingham to Zsombor Koszegi and Yann Lanoiselée for all their help and patience with me, especially towards the end.

Thanks to my collaboration partners Christian Gentzsch and Antonios Drakopoulos from the group of Prof. Michael Decker for their work on the 'Mordor' project. Thanks as well to Gerti Beliu for his help and advice with the unnatural amino acid project.

I want to thank the Elitenetzwerk Bayern for the financial support, the interdisciplinary programme and all the scientific events they made possible. Within the network I want to especially thank Theresa, Ilona, Ruiqi, Matze and Luca for support, discussions, Stammtische and a lot of fun.

Ich möchte mich bei meiner Familie für die Unterstützung in den letzten Jahren bedanken. Bei meinen Eltern möchte ich mich vor allem dafür bedanken, dass sie mich darin bestärkt haben für das einzustehen, was mir wichtig ist und dass sie stets meinen Wissensdrang und meine Neugierde gefördert haben.

During a PhD, support is not only needed in the lab but also outside. I am very grateful for all the friends I have outside of work, who where there, supporting me each in their own way. Thus, a lot of thanks goes to Severin and Timothy (especially for the LaTeX support), Gefion and Markus, Josi, Anne, Mariam, Michaela, Jani, Christoph and the rageline.

Last but not least, I would like to thank Wilm. For everything. I hope this work, and the level of LaTeX skills that went into it, would have made him proud.

Affidavit

I hereby confirm that my thesis entitled *Investigation of dynamic processes of prototypical class A GPCRs by single-molecule microscopy* is the result of my own work. I did not receive any help or support from commercial consultants. All sources and / or materials applied are listed and specified in the thesis.

Furthermore, I confirm that this thesis has not yet been submitted as part of another examination process neither in identical nor in similar form.

Place, Date	Kerstin Seier

Eidesstattliche Erklärung

Hiermit erkläre ich an Eides statt, die Dissertation *Untersuchung von dynamischen Prozessen von prototypischen Klasse A GPCR's durch Einzelmolekülmikroskopie* eigenständig, d.h. insbesondere selbständig und ohne Hilfe eines kommerziellen Promotionsberaters, angefertigt und keine anderen als die von mir angegebenen Quellen und Hilfsmittel verwendet zu haben.

Ich erkläre außerdem, dass die Dissertation weder in gleicher noch in ähnlicher Form bereits in einem anderen Prüfungsverfahren vorgelegen hat.

Ort, Datum	Kerstin Seier